AD

USAAVLABS TECHNICAL REPORT 68-21

COMPARATIVE PERFORMANCE STUDY OF PROPELLER, DUCTED PROPELLER, AND TURBOFAN PROPULSION SYSTEMS

By

D. S. Douglas
S. Mills
E. Kisielowski

June 1968

U. S. ARMY AVIATION MATERIEL LABORATORIES
FORT EUSTIS, VIRGINIA

CONTRACT DA 44-177-AMC-437(T)
DYNASCIENCES CORPORATION
BLUE BELL, PENNSYLVANIA

Disclaimers

The findings in this report are not to be construed as an official Department of the Army position unless so designated by other authorized documents.

When Government drawings, specifications, or other data are used for any purpose other than in connection with a definitely related Government procurement operation, the United States Government thereby incurs no responsibility nor any obligation whatsoever; and the fact that the Government may have formulated, furnished, or in any way supplied the said drawings, specifications, or other data is not to be regarded by implication or otherwise as in any manner licensing the holder or any other person or corporation, or conveying any rights or permission, to manufacture, use, or sell any patented invention that may in any way be related thereto.

Disposition Instructions

Destroy this report when no longer needed. Do not return it to originator.

DEPARTMENT OF THE ARMY
HEADQUARTERS US ARMY AVIATION MATERIEL LABORATORIES
FORT EUSTIS, VIRGINIA 23604

IN REPLY REFER TO:

This report was prepared by Dynasciences Corporation under the terms of Contract DA 44-177-AMC-437(T). It describes analytical methods for evaluating performance and general design parameters of propeller, ducted propeller, and concentric front fan propulsion systems using a typical V/STOL aircraft mission. As such, the report is offered for the stimulation and exchange of ideas.

Task 1M121401D14415
Contract DA 44-177-AMC-437(T)
USAAVLABS Technical Report 68-21

June 1968

COMPARATIVE PERFORMANCE STUDY OF PROPELLER, DUCTED PROPELLER, AND TURBOFAN PROPULSION SYSTEMS

FINAL REPORT

Dynasciences Report No. DCR-248

By

D. S. Douglas
S. Mills
E. Kisielowski

Prepared by

Dynasciences Corporation
Blue Bell, Pennsylvania

for

U.S. ARMY AVIATION MATERIEL LABORATORIES
FORT EUSTIS, VIRGINIA

SUMMARY

Presented in this investigation are analytical methods for evaluating performance of open propellers, ducted propellers, and turbofans for the purpose of selecting the most suitable propulsion system for Army aircraft mission requirements. Techniques are presented for trade-off analyses and optimization of the basic design parameters of each propulsion system. These techniques utilize specially developed nomographs, which can effectively be applied for preliminary design purposes. The nomographs and other numerical results presented in this report are based on the available performance data for the three propulsion systems.

FOREWORD

The work reported herein was sponsored by the U.S. Army Aviation Materiel Laboratories (USAAVLABS), Fort Eustis, Virginia, and was performed by the Dynasciences Corporation, Blue Bell, Pennsylvania, under Contract DA 44-177-AMC-437(T), during the period from June 1966 through October 1967.

Mr. James Gomez, Jr., was the Army technical representative. His contributions to this work are gratefully acknowledged. Recognition is given to Mr. H. V. Borst of the Boeing Company, Vertol Division, Morton, Pennsylvania, for his comments regarding this program. Acknowledgement is made to Mr. G. Rosen of Hamilton Standard, Division of United Aircraft Corporation, Windsor Locks, Connecticut, for his help and cooperation in supplying the additional ducted propeller data. The following Dynasciences Corporation personnel contributed to this work:

Mr. D. S. Douglas - Aeronautical Engineer
Mr. S. Mills - Sr. Aeronautical Engineer
Mr. T. Fukushima - Sr. Aeronautical Engineer
Mr. E. Kisielowski - Manager, Aeronautics
Mr. H. G. Somerson - Director, Applied Sciences

TABLE OF CONTENTS

LIST OF ILLUSTRATIONS

LIST OF TABLES

LIST OF SYMBOLS

A	area, ft.^{2}
a_o	lift curve slope of a two-dimensional wing per radian
AF	activity factor, $\frac{100,000}{16}\int_{0.2}^{1.0}\left(\frac{B}{d}\right)\left(\frac{r}{R}\right)^3 d\left(\frac{r}{R}\right)$
AR	aspect ratio, $\frac{b^2}{S}$
B	number of blades
b	wing span, ft.
C	chord, ft.
C_D	drag coefficient, $\frac{D}{\frac{1}{2}\rho V^2 S_W}$
C_L	lift coefficient, $\frac{L}{\frac{1}{2}\rho V^2 S_W}$
C_P	power coefficient, $\frac{P}{\rho n^3 d^5}$
C_T	thrust coefficient, $\frac{T}{\rho n^2 d^4}$
d	diameter, ft.
D	drag, lb.
dC_L/d_α	slope of lift curve per radian
E_s	energy supplied, ft.-lb./sec.

e	Oswald's wing efficiency factor
F	blade element in plane force, lb.
F_D	shroud drag factor
F_G	engine exhaust residual thrust, lb.
F_M	figure of merit, $.707 \frac{T}{P}\sqrt{\frac{T}{\rho \pi R^2}}$
f	equivalent flat plate area, $ft.^2$
H_F	heating value of fuel, BTU/lb.
HP_I	installed horsepower
IC_{L_i}	integrated design lift coefficient, $4\int_{.02}^{1.0} C_{L_i}\left(\frac{r}{R}\right)^3 d\left(\frac{r}{R}\right)$
J	advance ratio, $\frac{V \times 60}{Nd}$
J_E	mechanical equivalent of heat, 778 ft.-lb./BTU
K	constant as defined in the text
$K(x)$	Theodorsen circulation function
k	interference factor
k_D	drag factor, drag at cruise speed to drag at $(L/D)_{max}$
k_V	speed factor, cruise speed to speed corresponding to $(L/D)_{max}$ speed

L	lift, lb.
η	engine length, ft.
M	Mach number
N	propeller speed, revolutions per minute
n	propeller speed, revolutions per second
n_c	crash load factor
P	power, ft.-lb./sec.
P_i	ideal power, ft.-lb./sec.
p	pressure, lb./ft.^{2}
q	freestream dynamic pressure, $\frac{1}{2} \rho V^2$, lb./ft.^{2}
R	radius, ft.
r	radius of a blade element, ft.
SHP	shaft horsepower
S_W	wing area, ft.^{2}
T	thrust, lb.
TAF	total activity factor
t	temperature, °R
t_s	shroud wall thickness, ft.
t_{max}	maximum thickness, ft.
U_w	useful work, ft.-lb./sec.
V	velocity, ft./sec.

V_T	tip speed, ft./sec.
v_i	induced velocity - taken to be at propeller plane when used without subscript, ft./sec.
W_C	crew weight, lb.
$W_{c,s}$	control and starting system weight, lb.
W_d	drive system weight, lb.
W_E	empty weight, lb.
$W_{E,S}$	equipment and structural weight, lb.
W_{FS}	fuel system weight, lb.
W_G	gross weight, lb.
W_I	engine installation weight, lb.
W_ℓ	engine weight, lb.
W_P	propulsion system weight, lb.
W_{PL}	payload, lb.
W_{pr}	propeller weight, lb.
W_s	shroud weight, lb.
W_{UL}	useful load, lb.
W_W	wing weight, lb.
w_a	gas generator unsupercharged airflow lb./sec.

w_F	fuel flow rate, lb./sec.
w_o	oil weight, lb.
w_{RF}	residual fluids weight, lb.
W/b	wing span loading, lb./ft.
X,Y,Z	coordinate axis system
x	blade radial station, $\frac{r}{R}$
α	blade angle of attack, radians
Γ	blade circulation, ft.^{2}/sec.
γ	$\tan^{-1}\left(C_D/C_L\right)$ for entire blade, deg.
γ_D	strength of duct vortex, ft.^{2}/sec.
γ_p	strength of propeller vortex, ft.^{2}/sec.
Δ	increment
δ	local C_D/C_L
δ_p	duct constant
θ	blade local pitch angle, deg.
λ	inflow parameter, $\frac{V_P}{V_T}$
η_T	total propulsive efficiency, $\frac{T_T V}{P}$
η_{xmsn}	transmission efficiency
η_o	overall efficiency of propulsion system

η_c	compressor efficiency
π	constant, 3.14159
ρ	air density, slugs/cu. ft.
σ	solidity, $\frac{BC}{\pi R}$
ϕ	blade local induced angle

SUBSCRIPTS

A	aircraft
B	boattail
C	cruise
D	drag
d	ducted propeller
EW	equivalent wing
e	exit
F	fuel
f	skin friction, or frontal
i	ideal condition
J	jet
max	maximum frontal area
N	nacelle
P	power
PL	payload

p	propeller or parasite
R	ram
RW	ring wing
S	static or shroud
s	supplied
T	total or tip
te	condition at trailing edge
wet	wetted area
0	condition of freestream
1	condition ahead of propeller plane
2	condition behind propeller plane
∞	condition at far wake or at infinity

I. INTRODUCTION

In modern preliminary design of high performance aircraft, it is necessary to provide the designer with reliable means of selecting the propulsion system which would best satisfy the aircraft mission requirements. Due to recent advances in propulsion system technology, there is now a variety of propulsion systems capable of performing the same mission. Consequently, there is a need for rapid and effective analytical methods for evaluating comparative performance of various propulsion systems. This program is directed toward satisfying this need.

The main objective of this work is to perform an analytical study for comparing the performance of open and ducted propellers and turbofans and to formulate methodology for selecting the most suitable propulsion system for a given aircraft mission. Considered in this study are weight trends, installation effects, operational requirements, and complexities peculiar to each propulsive system.

In addition, methods are developed for optimizing the basic geometric parameters of each propulsion system for any flight condition from hover (static) to high forward speed. These methods also provide off-design performance for each system, thereby aiding the compromise between flight conditions while depicting the respective penalties imposed. The selection of the most suitable propulsion system for a given aircraft mission is made by a parametric trade-off analysis of the imposed performance penalties associated with each system, and that system which yields maximum overall performance is selected.

Optimization and trade-off analyses for each propulsion system can be conveniently performed by utilizing specially developed performance nomographs, samples of which are included in this report. These nomographs comprise a rapid and effective preliminary design tool for optimization and selection of the most suitable propulsion system for V/STOL aircraft.

The nomographs and other numerical results presented are based on the available performance data for the three propulsion systems considered.

Section II contains an outline of the analytical procedures for optimization and trade-off analyses. These procedures can be considerably simplified by utilizing specially developed performance nomographs which are presented in Section III. A comparative evaluation of the three propulsion systems is presented in Section IV. Finally, an application study is presented in Section V, where the most suitable propulsive system is selected utilizing a specified aircraft mission.

The theoretical analyses utilized to generate the required performance data for the three selected propulsion systems are reviewed in Appendix I. Appendix II contains comparative performance results obtained for these systems.

II. OPTIMIZATION PROCEDURES FOR PROPULSION SYSTEMS

Presented in this section are the analytical procedures for optimization and trade-off analyses of open propeller, ducted propeller, and turbofan propulsion systems. These procedures utilize the most up-to-date performance data available for each propulsion system.

Presented in Appendix I is a section comprising a brief review of the available theoretical analyses which are commonly used for performance evaluation of open and ducted propellers and turbofan propulsion systems.

A. OPEN PROPELLER

The available data which can be most readily applied to performance predictions of open propellers are presented in the form of performance maps in References 1 and 2. These data were generated utilizing the most recent refinements in the strip analysis method augmented by appropriate propeller test data. The performance maps of these references are presented as functions of the propeller blade integrated design parameters, such as blade activity factor (AF) and integrated design lift coefficient (IC_{L_i}).

The activity factor expresses the capacity of the blade to absorb power and the integrated design lift coefficient gives a measure of an averaged blade camber.

Although the performance data contained in References 1 and 2 are interchangeably used for general propeller work, the data of the former reference are herein utilized to develop the analytical procedures for optimization and trade-off analyses of open propellers. In order to better illustrate these procedures, which are outlined below, samples of the performance maps of Reference 1 are herein reproduced in Figures 1 through 3.

1. Static Condition

a. Establish the following design parameters:

(1) Design static thrust required - T_S, lb.

STATIC THRUST - 4 BLADES

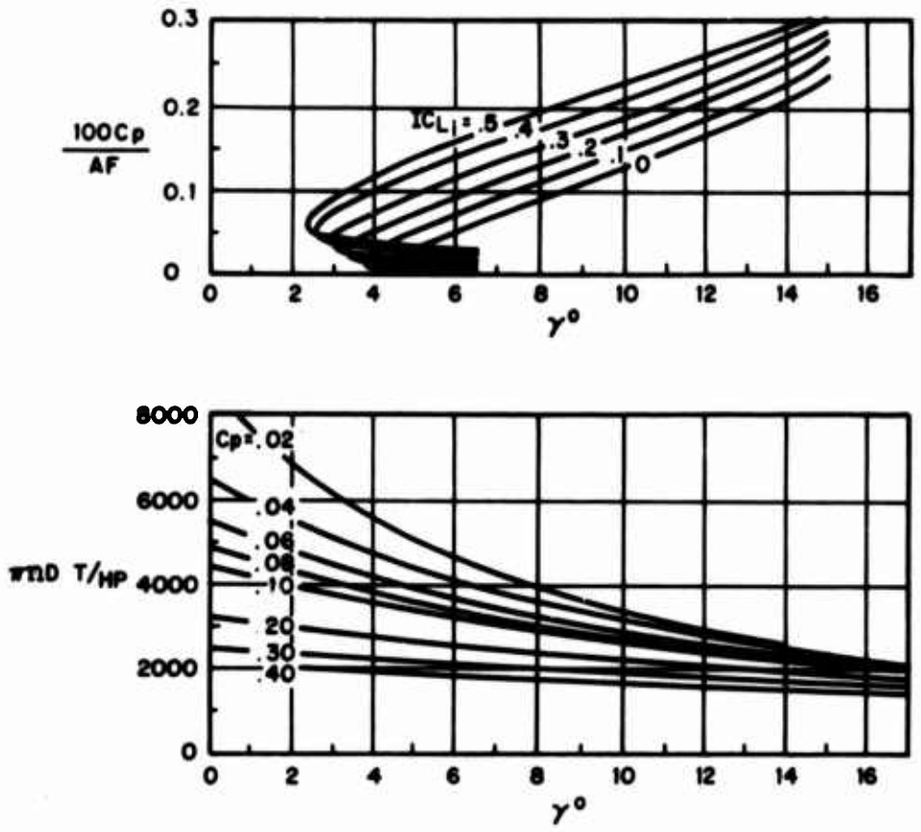

Figure 1. Static Performance Data for Open Propeller.

FLIGHT EFFICIENCY - 4 BLADES

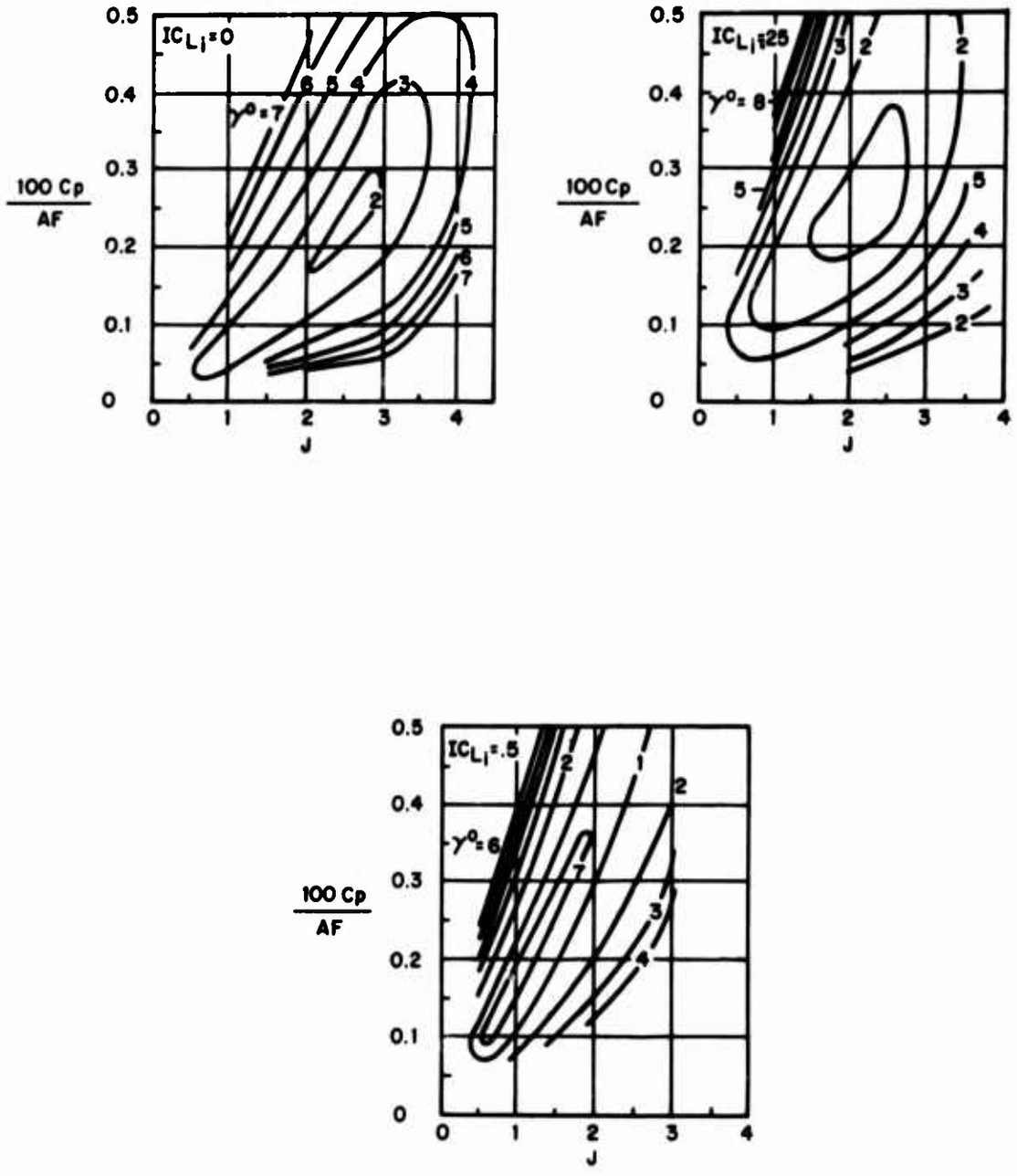

Figure 2. Cruise Performance Data for Open Propeller (100 Cp/AF Versus J for Constant IC_{L_i}).

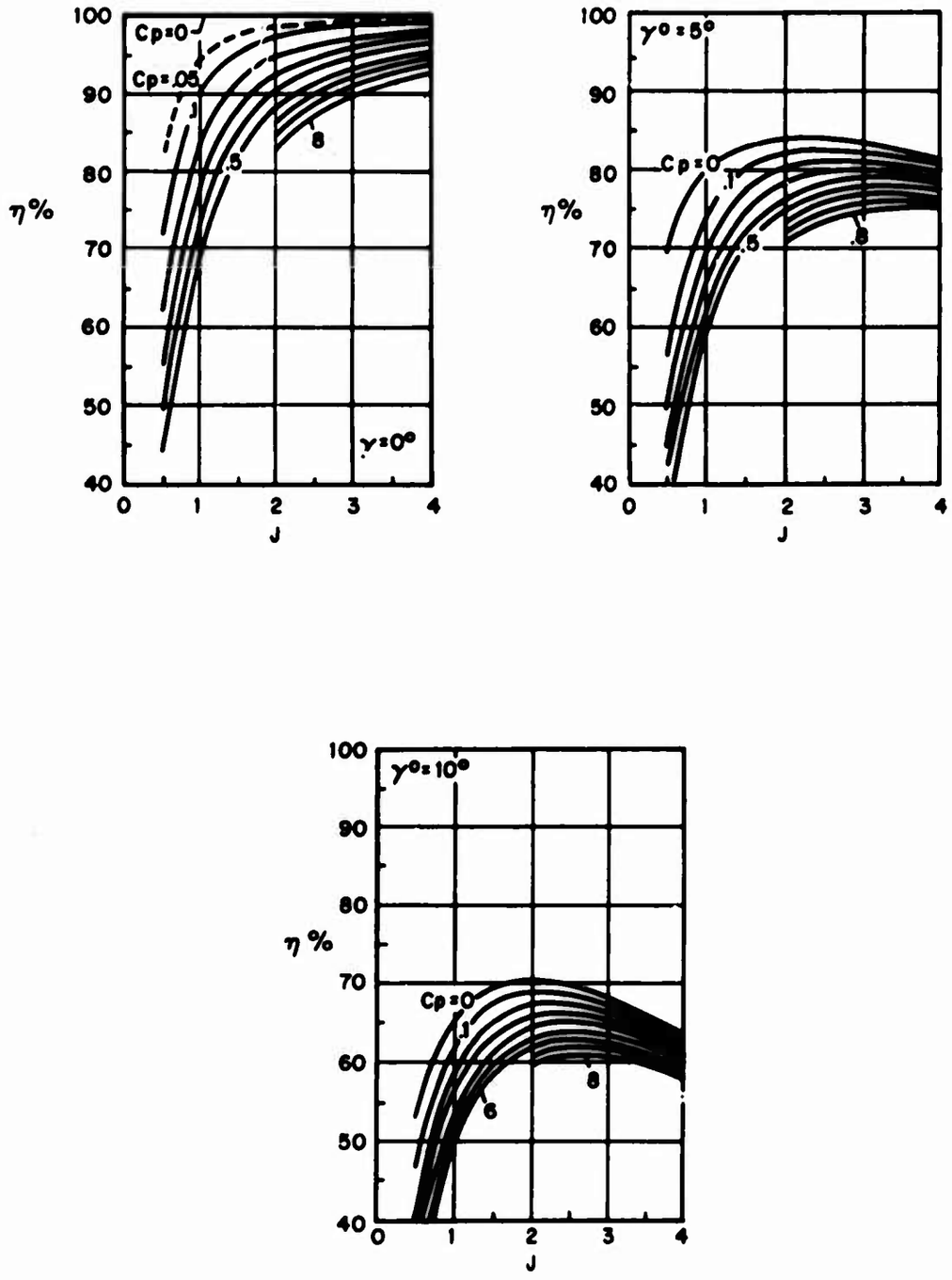

Figure 3. Cruise Performance Data for Open Propeller (η Versus J for Constant C_p).

(2) Propeller rotational speed - n, rev.p.s.

(3) Propeller diameter - d, ft.

(4) Density at any altitude - ρ, slugs/ft^3.

(5) Number of blades - B.

b. Using Figure 1(a) or the equivalent charts of Reference 1 (depending on the number of blades), select a value for integrated design C_L and determine a minimum γ and the corresponding value of 100 Cp/AF. The minimum value of γ is selected to ensure minimum average ratio of blade C_D/C_L.

c. With the minimum value of γ determined in step b, enter Figure 1(b) or the equivalent charts of Reference 1 (depending on the number of blades) and obtain a cross plot of πndT/HP versus C_P.

d. Repeat steps b and c for different values of IC_{L_i} and obtain a complete plot of πndT/HP versus C_P for the selected constant values of IC_{L_i} corresponding to the minimum γ.

e. Also, plot the relationship of 100 Cp/AF versus IC_{L_i}, using the results of step b.

f. Compute $\pi ndT/HP = K/C_P$

where $K = 550\pi T/\rho n^2 d^4$

Superimpose this relationship (i.e., K/C_P versus C_P) on the plot of πndT/HP versus C_P of step d, and obtain the points of intersection of the computed curve (K/C_{P_s}) with the chart curves (πndT/HP).

g. From the points of intersection of step f, plot the relationship C_P versus IC_{L_i}.

h. Using the values of C_P from step g, compute power (P) and then obtain the corresponding figure of merit, FM, from

$$FM = \frac{1}{\sqrt{2}} \frac{T}{P} \sqrt{\frac{T}{\rho \pi R^2}}$$

i. Plot the figure of merit versus IC_{L_i} and determine the maximum figure of merit, FM_{max}, and the corresponding value of IC_{L_i}.

j. With the value of IC_{L_i} (corresponding to the maximum figure of merit) from step i, enter the plot of C_P versus IC_{L_i} from step g and determine the corresponding value of C_P.

k. Also, using the same value of IC_{L_i} determined in step i, enter the plot of 100 C_P/AF versus IC_{L_i} from step e and determine the parameter 100 C_P/AF.

l. Knowing C_P from step i and 100 C_P/AF from step j, compute the optimum activity factor, AF, corresponding to the maximum figure of merit.

m. Tabulate optimum propeller performance parameters AF, IC_{L_i}, γ min, HP, FM.

2. <u>Cruise Condition</u>

a. Establish the following design parameters for cruise:

(1) Design cruise thrust - T_C, lb.

(2) Propeller rotational speed - n, rev.p.s.

(3) Propeller diameter - d, ft.

(4) Cruise speed - V, ft./sec.

(5) Density at any altitude - ρ , slugs/ft.^{3}

(6) Number of blades - B

b. Compute advance ratio J = V/nd using values of V, n, and d from step a. With this value of J, enter Figures 2(a), 2(b), nd 2(c) or the equivalent set of charts from Reference 1 (depending on the number of blades), and obtain a plot of 100 C_P/AF versus γ for constant values of IC_{L_i}.

c. With the same value of J as in step b, enter efficiency curves of Figures 3(a), 3(b), and 3(c) or the equivalent set of charts from Reference 1 (depending on the number of blades), and obtain a plot of $\eta = (C_T/C_P)$ J versus γ for constant values of C_P.

d. Using the plot of 100 C_P/AF versus γ from step b, determine the minimum value of γ for each IC_{L_i} and plot 100 C_P/AF versus IC_{L_i}.

e. With minimum values of γ , determined in step d, enter the plot of η versus γ from step c and obtain the relationship of η versus C_P for constant values of IC_{L_i}.

f. Using the design parameters given in step a, compute

$$\eta = K/C_P \text{ (where } K = C_T J)$$

for several values of C_P. Superimpose this relationship on the plot of η versus C_P from step e and obtain the points of intersection of the computed curve (K/C_P) with the chart curves of step e.

g. From the points of intersection of step f, determine the maximum efficiency η_{max} and the corresponding values of C_p and IC_{L_i}.

h. With the value of IC_{L_i} determined in step g, enter the plot of 100 C_p/AF versus IC_{L_i} from step d and obtain the value of 100 C_p/AF.

i. Knowing C_p from step g and 100 C_p/AF from step h, compute the optimum activity factor AF.

j. Tabulate the final results.

The above procedures yield the propeller geometry in terms of average values (i.e., activity factor, integrated design C_L), the figure of merit of an optimum static propeller, and the propulsive efficiency of an optimum cruise propeller. Since no propeller can be truly optimum in both static and forward flight, it is necessary to determine a compromise geometry. The following method incorporates a trade-off between the optimum figure of merit in static condition and the optimum efficiency in cruise condition, to determine a compromise propeller.

3. Compromise Between Static and Cruise Conditions

a. Reduce the static optimum figure of merit and the optimum cruise efficiency by an appropriate increment, e.g., 5 percent.

b. For the reduced figure of merit (FM) and the cruise efficiency (η), compute the power required, using

$$C_{P_S} = \frac{0.707 T_S}{FM\ (\rho\ n^3 d^5)} \sqrt{\frac{4T_S}{\rho\ \pi\ d^2}}$$

$$C_{P_C} = \frac{C_{T_C} J}{\eta}$$

c. Using static thrust, compute the term $(\pi ndT/HP)_S$.

d. Using Figure 1(b) and the value of $(\pi ndT/HP)_S$ from step c, plot a graph of C_{P_S} versus γ.

e. From the graph of step d and the value of C_{P_S} from step b (static case), determine the corresponding value of γ.

f. With the known value of IC_{L_i} and the value of γ from step e, enter Figure 1(a) and determine $(100\ C_P/AF)_S$.

g. Compute the static activity factor using the value of $(100\ C_P/AF)_S$ from step f and the value of C_{P_S} from step b.

h. Using the plot of η versus γ obtained in step 2.c (cruise case) and the value of cruise C_{P_C} and η from step b, determine the corresponding value for γ.

i. Using the plot of $(100\ C_P/AF)_C$ versus γ obtained in step 2.b and the value of γ obtained in step h, determine $(100\ C_P/AF)_C$.

j. Determine the cruise $(AF)_C$.

k. Reduce the efficiency in static and cruise by an appropriate increment and return to step b. Continue reducing until the activity factors in static and cruise are equal.

The results of these procedures are illustrated in Figure 4, which shows a plot of propeller activity factor as a function of percent reduction from the optimum propeller efficiency for two different propeller diameters.

The shaded areas of Figure 4 represent the regions of best compromise between static and cruise conditions. It can be seen that these regions reduce for larger propeller radii, which implies that a more effective compromise is possible with a larger diameter propeller. However, the final choice for a compromise propeller will depend on the aircraft mission and weight requirements.

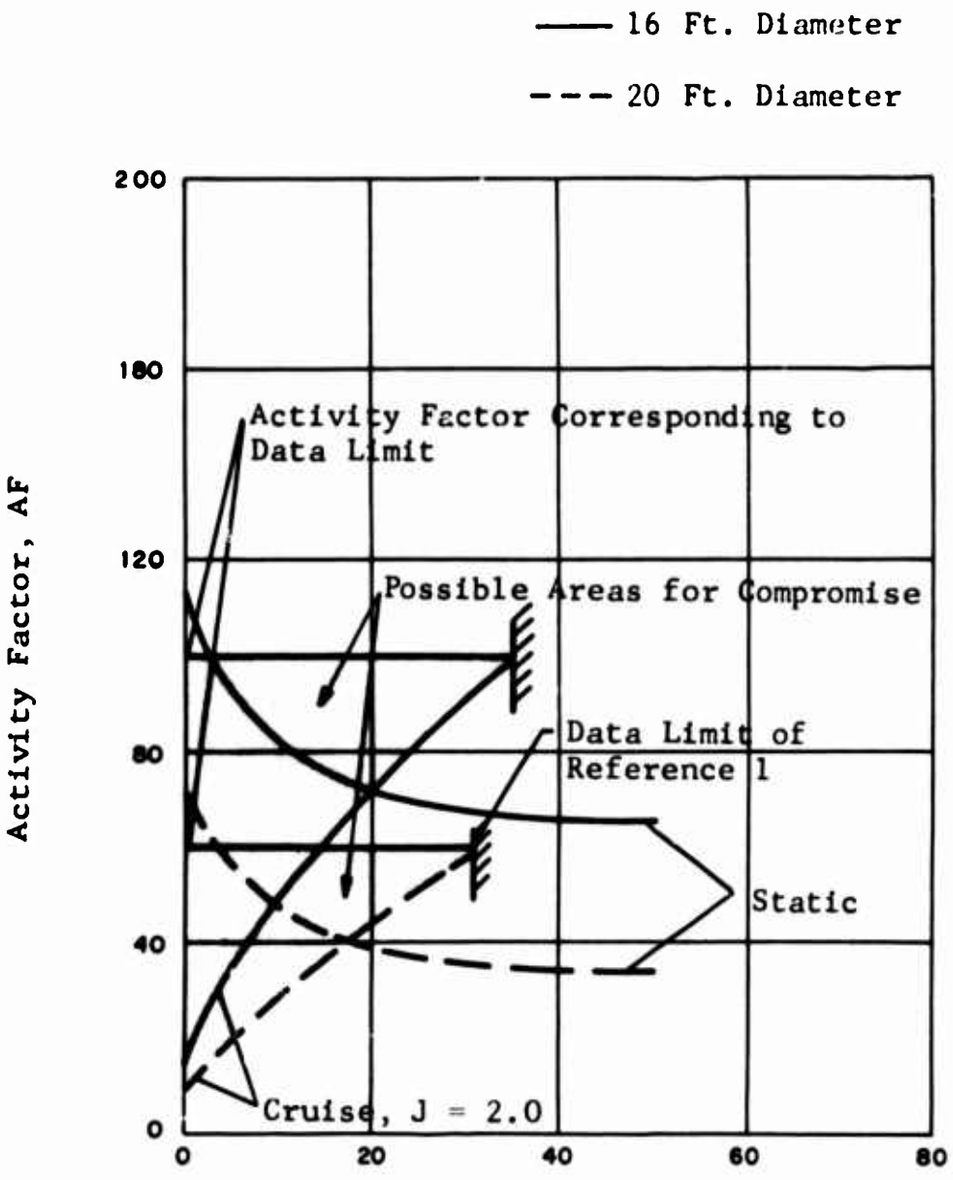

Figure 4. Variation of Propeller Activity Factor Versus Percent Reduction in Propulsive Efficiency.

B. DUCTED PROPELLER

Procedures similar to those developed for open propellers can be formulated for ducted propellers. The procedures for ducted propellers are based on the performance maps for a generalized family of shrouded propellers, as presented in Reference 3. These performance maps apply to a wide range of operating conditions, including static and high cruise speed regimes, and a wide range of duct exit area ratios. Other duct geometric parameters such as length-to-diameter ratio, blade tip clearance, and intake lip radius are considered to be typical for subsonic operations within the limitations of one-dimensional incompressible momentum theory. These limitations are that length-to-diameter ratio is greater than 1.0, that blade tip clearance is approximately zero, and that the intake lip radius is of bellmouth shape.

Reference 3 also provides compressibility correction curves as a function of propeller critical Mach number and shroud exit area ratio. These curves are herein utilized to account for compressibility effects on ducted propeller performance at high subsonic Mach numbers.

Using the data of Reference 3, the following analytical procedures can be established to determine an optimum static and an optimum cruise ducted propeller as well as a best compromise between these two flight conditions:

1. Static Condition

a. Assume the following design parameters:

(1) Propeller rotational speed - n, rev.p.s.

(2) Propeller diameter - d, ft.

(3) Total thrust - T_{T_S}, lb.

(4) Exit area ratio.

(5) Density at any altitude - ρ , slugs/ft^3.

b. Choose a value of IC_{L_i} and, using the appropriate static performance maps from Reference 3, construct a graph of C_{T_T}/C_P versus TAF for constant values of C_P.

c. On the graph of step b, construct a locus of peak C_{T_T}/C_P points corresponding to each C_P.

d. Using the values from step c, construct a graph of C_{T_T}/C_P versus C_P.

e. On the graph of step d, plot the term C_{T_T}/C_P for selected values of C_P.

(NOTE: C_{T_T} is a known parameter.)

f. The intersection of the curve of step e with the curve of step d gives the required value of C_{T_T}/C_P and C_P.

g. Using the values of C_{T_T}/C_P and C_P obtained in step f, determine the total activity factor TAF from the graph of step b.

h. Compute the figure of merit, FM, using

$$FM = 0.707 \frac{T_T}{P} \sqrt{\frac{T_T}{\rho A_p}}$$

i. Choose another integrated C_{L_i} and return to step b.

j. Choose the highest figure of merit and the corresponding values for TAF, C_P, and IC_{L_i}.

2. Cruise Condition

a. Establish the following design parameters:

1. Propeller rotational speed - n, rev.p.s.

2. Propeller diameter - d, ft.

3. Total cruise thrust - T_{T_C}, lb.

4. Exit area ratio.

5. Altitude density - ρ, slugs/ft.^{3}

b. Calculate advance ratio, J, using

$$J = V/nd$$

c. Choose an integrated C_L and, using the efficiency charts from Reference 3, construct a graph of η_T versus C_P for constant values of TAF.

d. On the graph of step c, construct a locus of peak efficiencies.

e. Using the values from step d, plot a graph of η_T versus C_P.

f. On the graph of step e, plot the relationship

$$\eta_T = K/C_P$$

$$\text{where } k = CT_TJ$$

g. The intersection of the curve of step e with the curve of step f yields the required values of η_T (total efficiency) and C_P.

h. Using the values obtained in step g, determine TAF from the graph of step c.

i. Choose another value of IC_{L_i} and return to step c.

j. Select the highest total efficiency, η_T, and the corresponding values for IC_{L_i}, TAF, and C_P.

Similar to the analysis for the free propeller, the preceding procedures determine the geometry in terms of average values (i.e., total activity factor, integrated design C_L) and the efficiency of an optimum static propeller and an optimum cruise propeller in a duct. The following procedure develops a compromise ducted propeller between static and cruise requirements.

3. Compromise Between Static and Cruise

a. Reduce the static optimum figure of merit and the optimum cruise efficiency by an appropriate increment, i.e., 5 percent.

b. For the reduced figure of merit, FM, and efficiency, η_T, compute the power required, using

$$C_{P_S} = \frac{.707\ T_{T_S}}{FM(\rho n^3 d^5)} \sqrt{\frac{T_{T_S}}{\rho A_p}}$$

$$C_{P_C} = \frac{C_{T_{T_C}} J}{\eta_T}$$

c. Compute $(C_{T_T}/C_P)_S$ using static thrust.

d. Using the values of C_{P_S} and $(C_{T_T}/C_P)_S$ obtained in steps b and c, respectively, enter the plot of $(C_{T_T}/C_P)_S$ versus TAF in step 1.b and read off the value of TAF for static case.

e. Similarly, using the values of η_T and C_{P_S} obtained in step b, enter the plot of η_T versus CP_C in step 2.c and read off the value of TAF for cruise case.

f. Reduce the efficiency in static and cruise by an appropriate increment and return to step b. Continue reducing until the total activity factors in static and cruise are equal.

C. TURBOFAN

The available turbofan performance data which are presented for concentric fans cannot be used to determine performance of fans alone. Therefore, it is not possible to formulate analytical procedures for optimization of fan parmeters as in the case of open or ducted propellers. Instead, turbofan systems can be optimized on the basis of fan-engine overall performance as is accomplished in the comparative study, Section IV of this report.

III. SIMPLIFIED PERFORMANCE METHOD

The analytical procedures for optimization and trade-off analyses of propulsion systems described in Section III can be considerably simplified by the use of specially developed performance nomographs. Sample nomographs for open and ducted propellers operating in static and cruise conditions are presented in Figures 5 through 8. The open propeller nomographs are derived from the available propeller performance data presented in References 1 and 2, whereas those for ducted propellers are based on the performance data of Reference 3. The nomographs for turbofans could not be presented in the same form as those for open or ducted propellers due to difference in parameters utilized for performance computations of combined fan-engine propulsion system. The nomographs (Figures 5 through 8) represent a rapid performance method which can be used to determine an optimum propulsive device for a given flight condition, an off-design performance for a given system, or a best compromise between static and cruise operation. The charts can also be used as a basis for studies of the trade-off between performance of various propulsion devices; as such, they represent an effective preliminary design tool for selection of the most suitable propulsion system for a given aircraft mission.

In applying these performance charts to propeller or ducted propeller design problems, the following input parameters are required: static thrust, cruise thrust, propeller diameter, propeller rotational speed, number of blades, and cruise speed. The output parameters obtainable from the nomographs are: blade activity factor or, in the case of ducted propellers, total activity factor, integrated design C_L, figure of merit, cruise efficiency, power required, and power loading (T/HP) in static and cruise conditions. The power loading of a given propulsion system is herein defined as the ratio of total thrust per horsepower (T/HP).

This section presents a brief description of the nomographs, their usage, and sample calculations. Experimental verification of the accuracy of these charts is also provided.

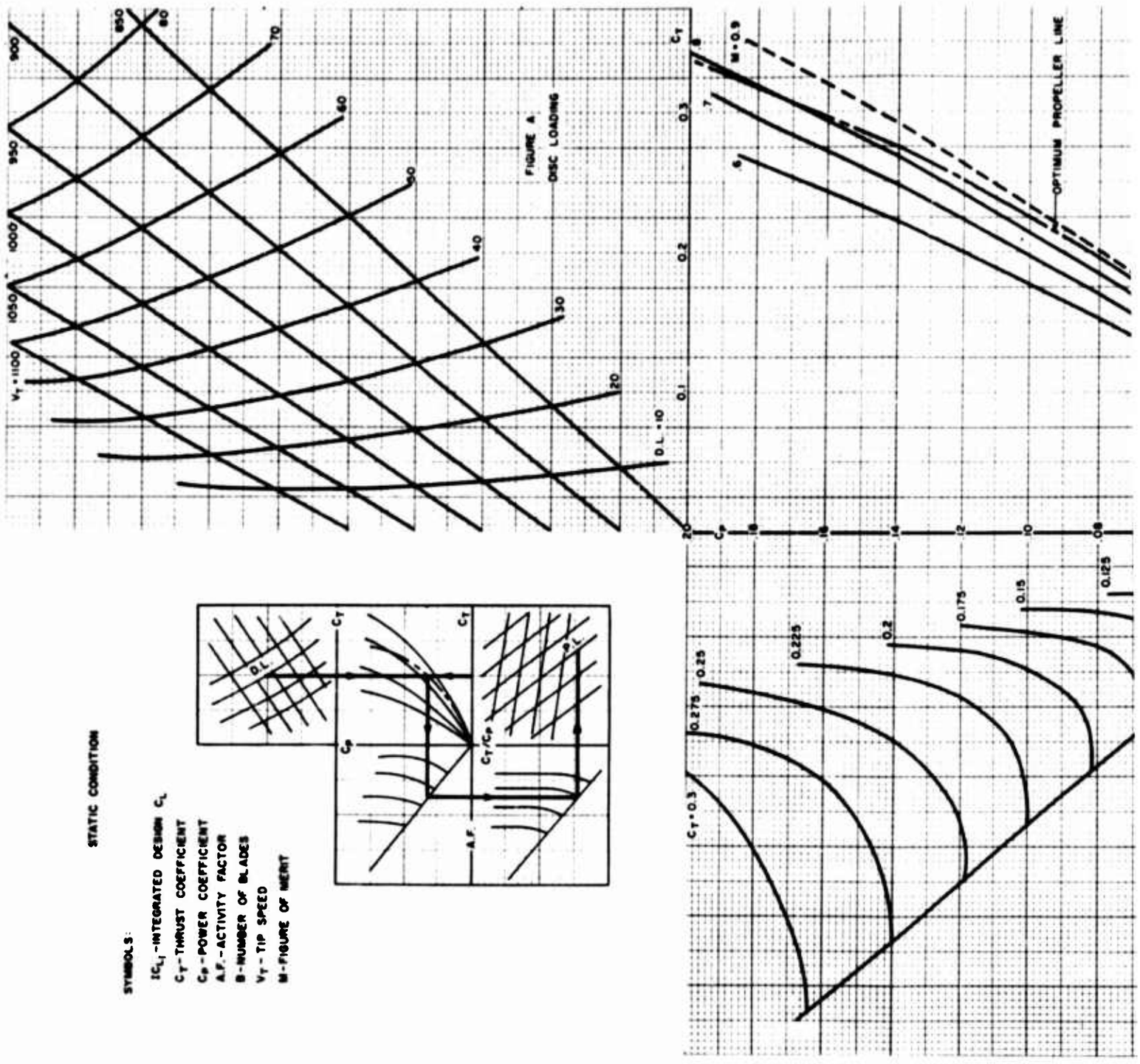

Figure 5. Nomograph for Determining Performance of Open Propellers - Static Condition.

A

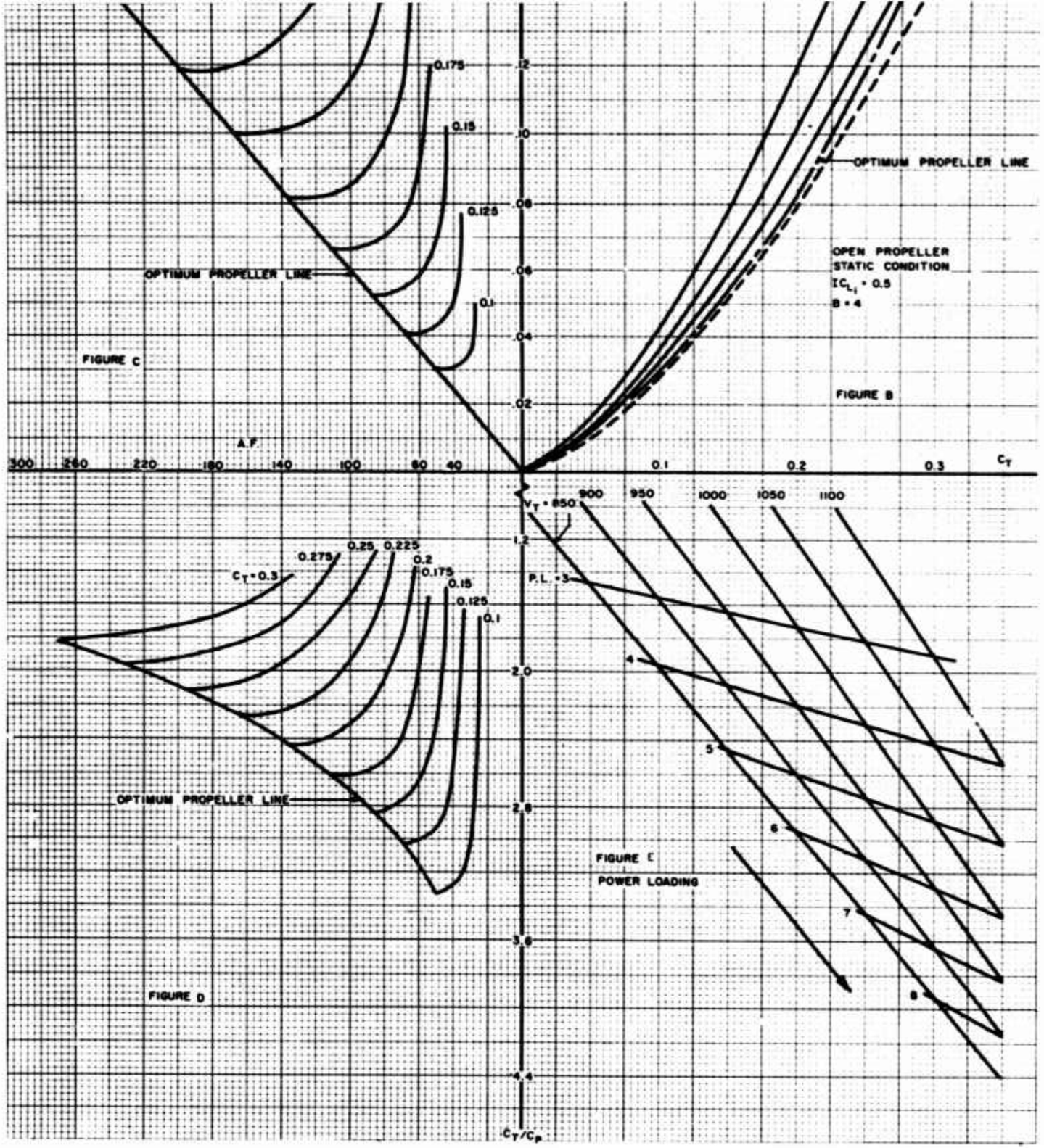
0.175
0.15
0.125
0.1
OPTIMUM PROPELLER LINE
FIGURE C
OPTIMUM PROPELLER LINE
OPEN PROPELLER
STATIC CONDITION
IC_{L_i} = 0.5
B = 4
FIGURE B
A.F
300 260 220 180 140 100 80 40
0.1 0.2 0.3 C_T
V_T = 850
900 950 1000 1050 1100
C_T = 0.3
0.275 0.25 0.225 0.2 0.175 0.15 0.125 0.1
P.L. = 3
4
5
6
7
8
OPTIMUM PROPELLER LINE
FIGURE D
FIGURE E
POWER LOADING
.2 .1 .08 .06 .04 .02
1.2 2.0 2.8 3.6 4.4
C_T/C_p

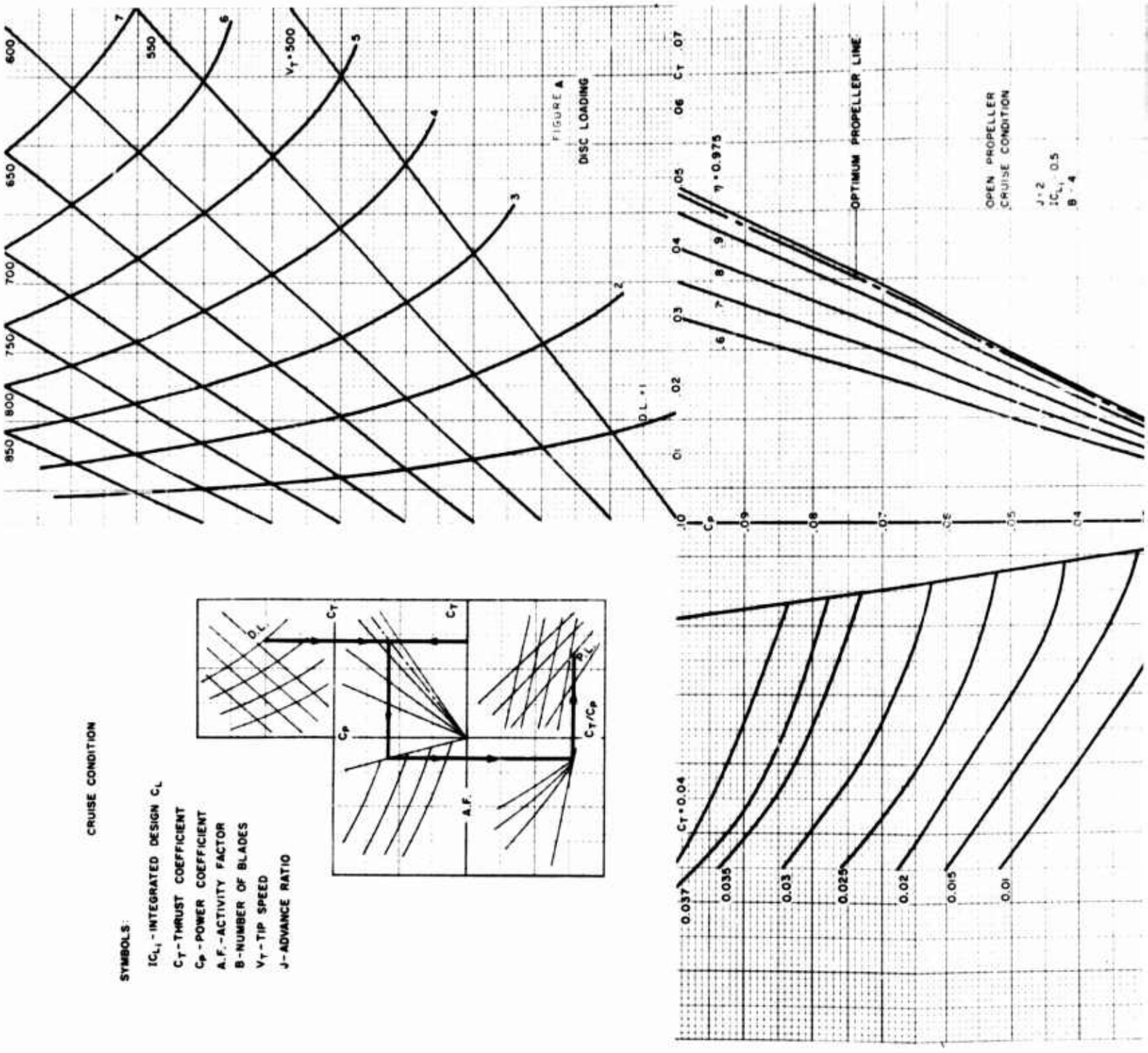

Figure 6. Nomograph for Determining Performance of Open Propellers - Cruise Condition.

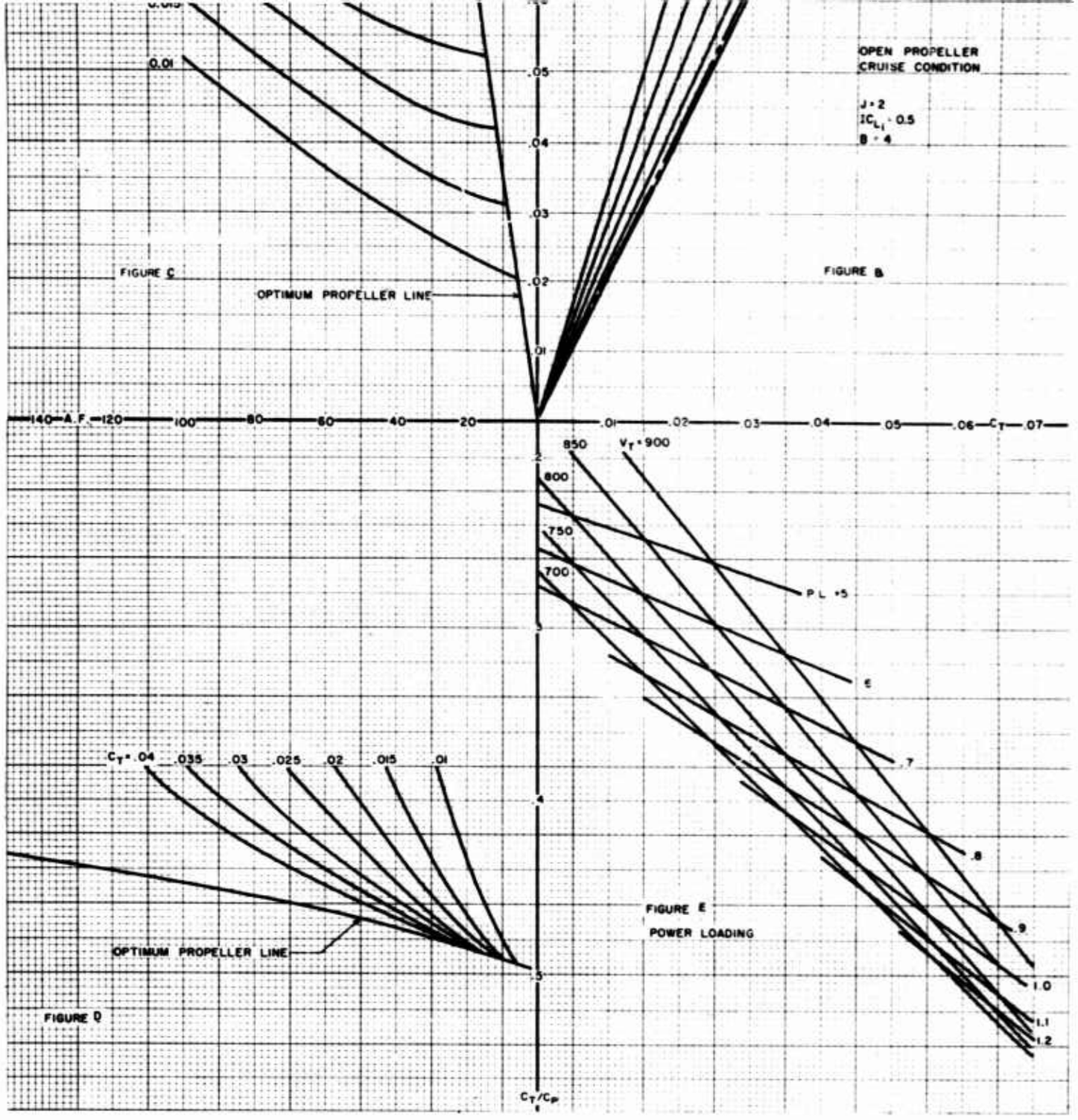
OPEN PROPELLER
CRUISE CONDITION
J = 2
IC_{L_i} = 0.5
B = 4
0.01
.05
.04
.03
.02
.01
FIGURE C
OPTIMUM PROPELLER LINE
FIGURE B
140 A.F. 120 100 80 60 40 20 .01 .02 .03 .04 .05 .06 C_T .07
V_T = 900
850
800
750
700
PL = 5
6
7
8
9
1.0
1.1
1.2
C_T = .04 .035 .03 .025 .02 .015 .01
OPTIMUM PROPELLER LINE
FIGURE D
FIGURE E
POWER LOADING
C_T/C_p

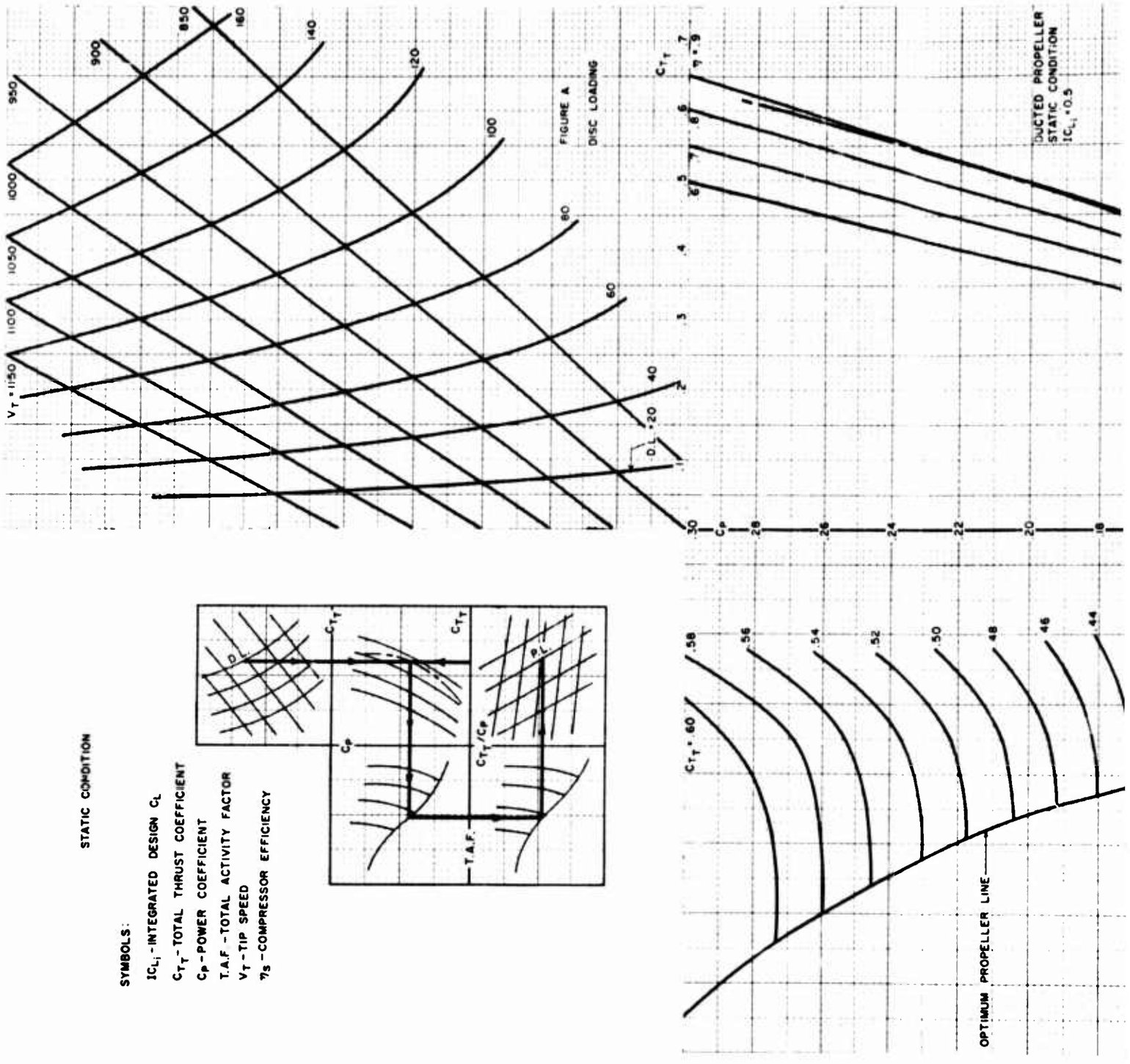

Figure 7. Nomograph for Determining Performance of Shrouded Propellers - Static Condition.

A

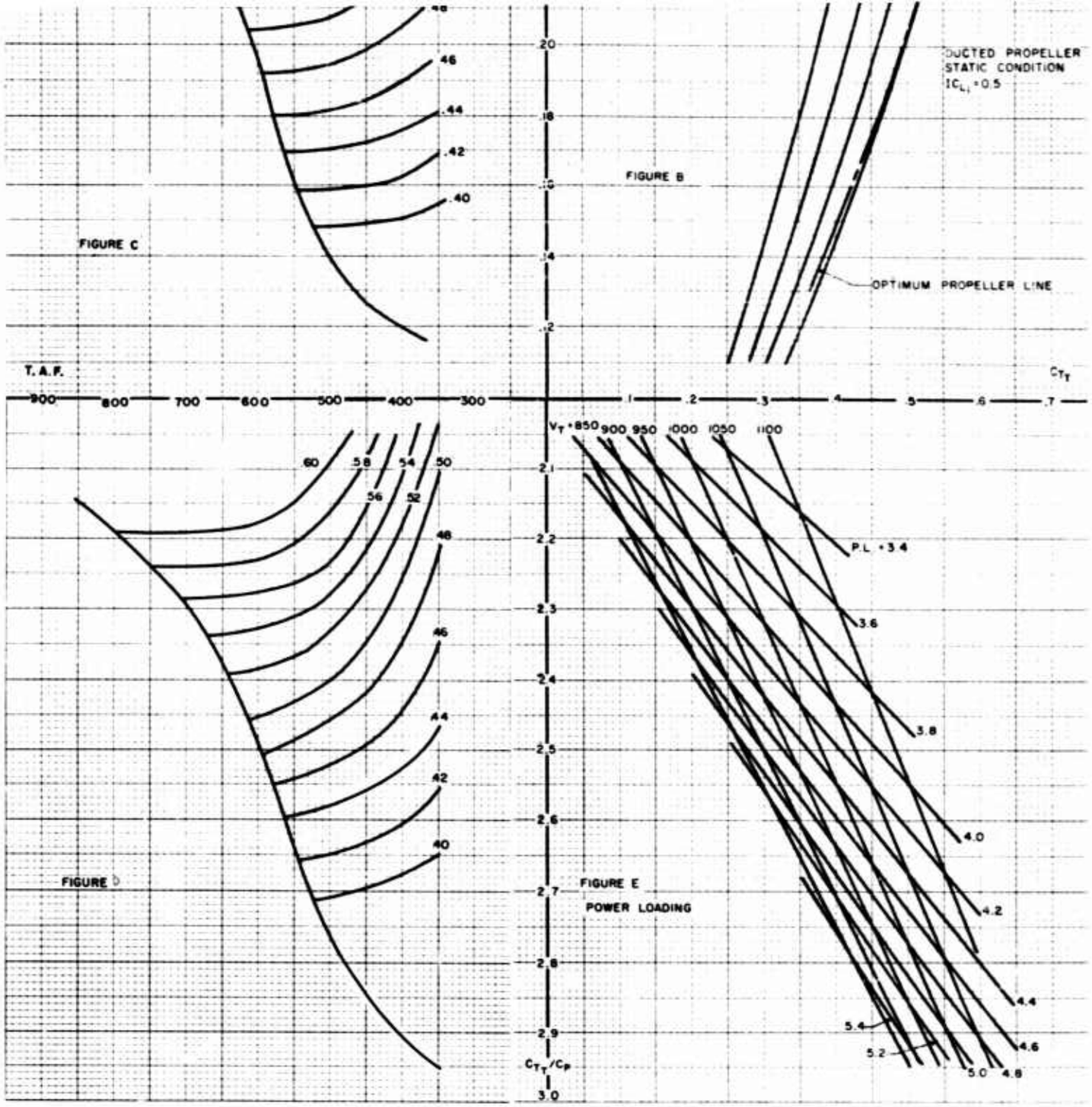
DUCTED PROPELLER
STATIC CONDITION
IC_{L_i} = 0.5
FIGURE B
OPTIMUM PROPELLER LINE
FIGURE C
T. A. F.
900 800 700 600 500 400 300
C_{T_T}
.1 .2 .3 .4 .5 .6 .7
V_T = 850 900 950 1000 1050 1100
60 58 54 50
56 52
48
46
44
42
40
P.L. = 3.4
3.6
3.8
4.0
4.2
4.4
4.6
4.8
5.0
5.2
5.4
FIGURE D
FIGURE E
POWER LOADING
C_{T_T}/C_P
2.1 2.2 2.3 2.4 2.5 2.6 2.7 2.8 2.9 3.0

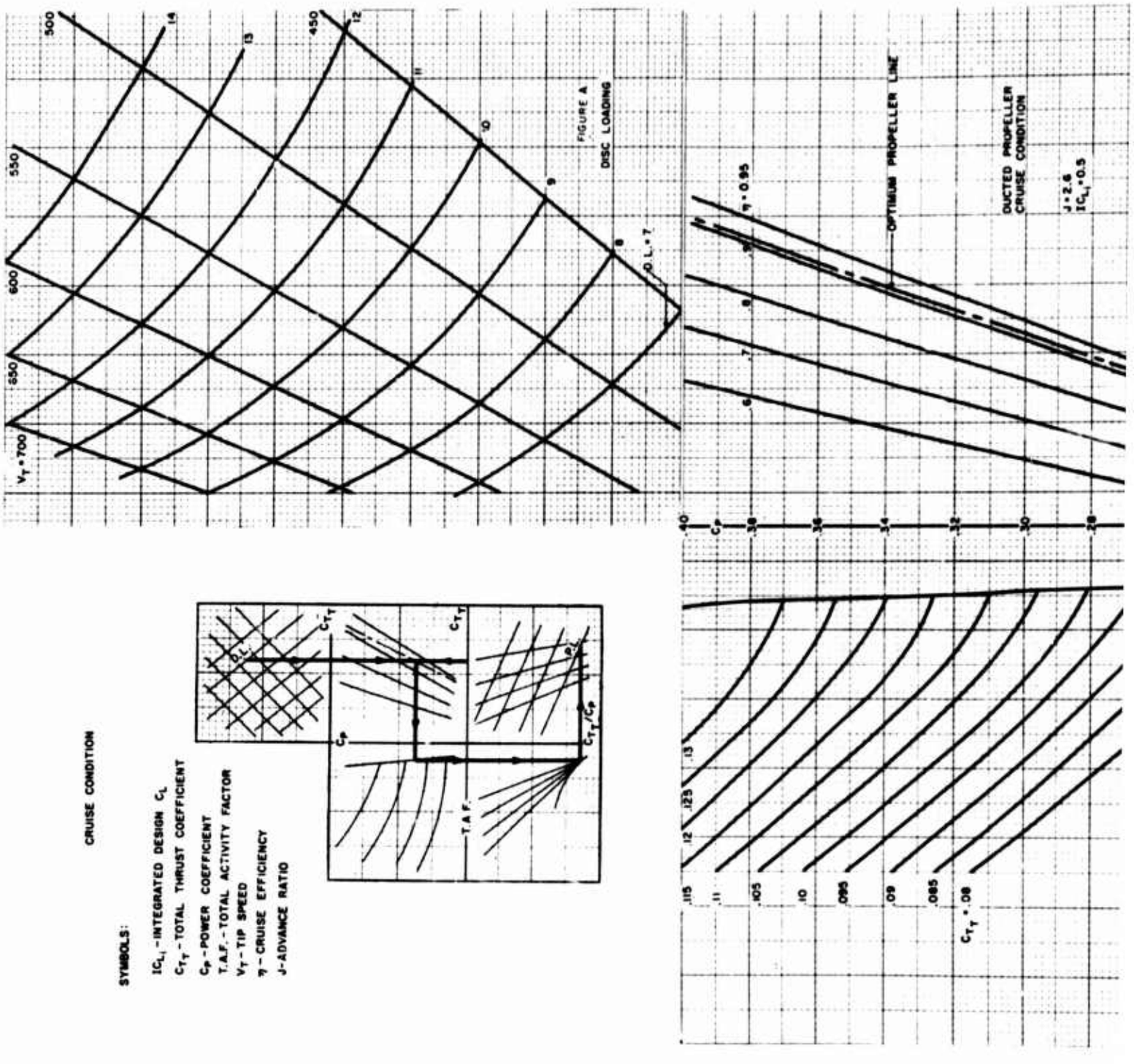

Figure 8. Nomograph for Determining Performance of Shrouded Propellers - Cruise Condition.

B

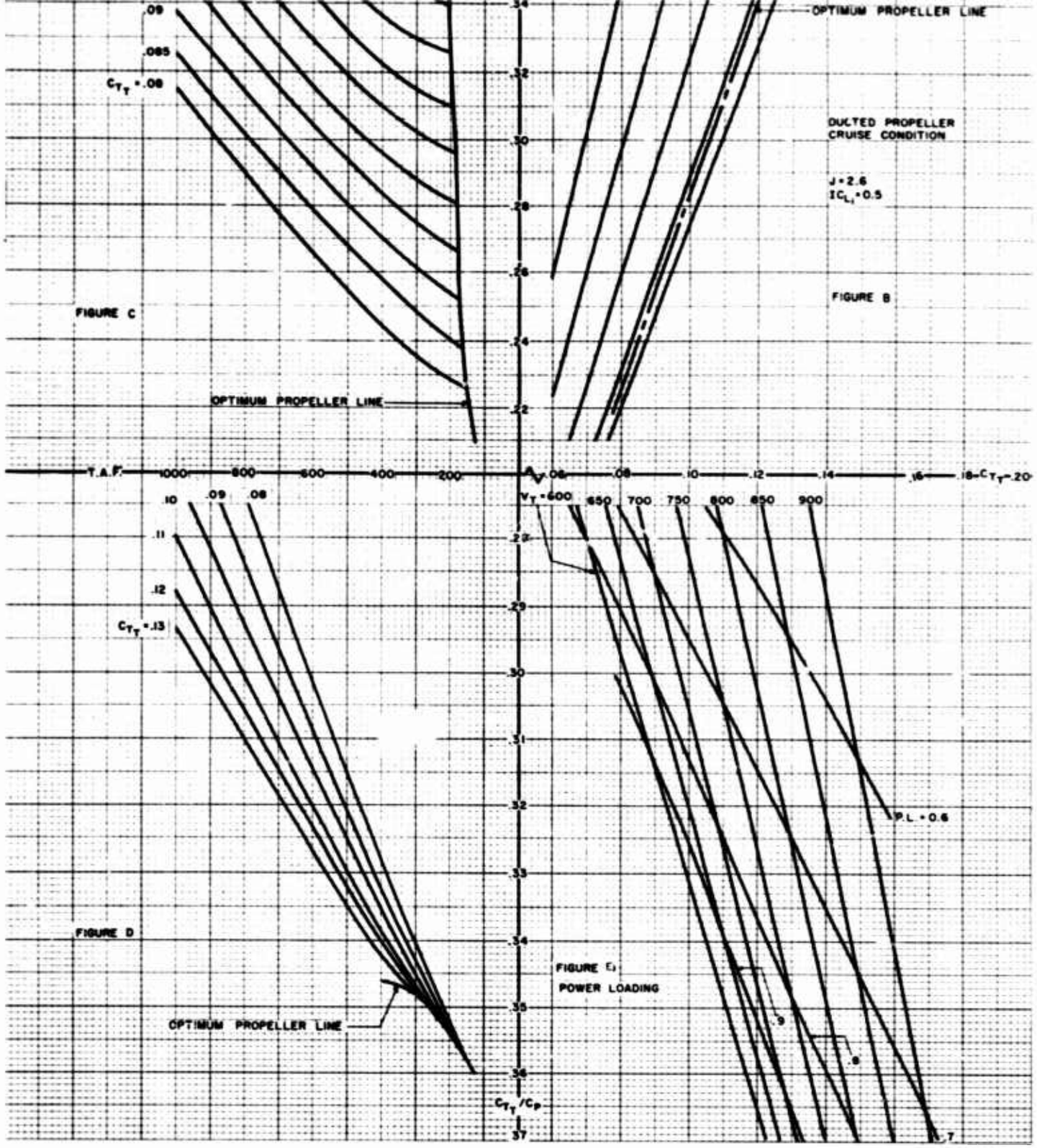
OPTIMUM PROPELLER LINE
DUCTED PROPELLER
CRUISE CONDITION
J = 2.6
IC_{L_i} = 0.5
FIGURE B
.09
.085
C_{T_T} = .08
FIGURE C
OPTIMUM PROPELLER LINE
T.A.F.
1000
800
600
400
200
V_T = 600
650
700
750
800
850
900
.10
.09
.08
.11
.12
C_{T_T} = .13
FIGURE D
OPTIMUM PROPELLER LINE
P.L. = 0.6
.9
.8
.7
FIGURE E
POWER LOADING
C_{T_T}/C_p

A. DESCRIPTION OF NOMOGRAPHS

The nomographs presented in Figures 5 and 6 apply to open propellers operating in static and cruise conditions ($J = 2.0$), respectively. These charts were derived for a near optimum blade-integrated design lift coefficient of $IC_{L_i} = 0.5$ and apply to propellers having four blades ($B = 4$). The open-propeller nomographs utilize activity factor (AF) as the primary blade design parameter.

Figures 7 and 8 present similar nomographs for ducted propellers operating in static and cruise conditions ($J = 2.6$), respectively. These charts utilize the total activity factor (TAF) as the primary blade design parameter and therefore apply to ducted propellers with any number of blades.

Each nomograph (Figures 5 through 8) consists of a set of five related charts designated as Figures A through E. The first chart (Figure A) of each nomograph presents a carpet plot of propeller or ducted propeller disc loadings versus tip speed, and the corresponding thrust coefficient.

Figure B of each nomograph shows a plot of thrust coefficient versus power coefficient for constant values of propeller figure of merit (for static conditions) and cruise efficiency (for cruise conditions). The lines of optimum figure of merit for static conditions and optimum cruise efficiency for cruise are also indicated on each plot, respectively.

Figure C of each nomograph relates propeller power coefficient to blade activity factor (or total propeller activity factor for ducted propellers) for constant values of thrust coefficient. The lines of optimum activity factor (or total activity factor) are also indicated on each plot.

Figure D represents a relationship between blade activity factor (or total activity factor for ducted propeller) and the corresponding thrust coefficient to power coefficient ratio for constant values of thrust coefficient. The corresponding optimum propeller lines are also shown on each plot.

Finally, Figure E presents a carpet plot relating thrust coefficient to power coefficient ratio versus propeller tip speed and power loading (T/HP).

B. USE OF THE NOMOGRAPHS

The basic procedure for utilizing the nomographs is explained graphically in the key of each chart. As mentioned previously, the nomographs can be used to determine an optimum static and an optimum cruise open or ducted propeller system, and to determine the best compromise system for the two operating conditions. These procedures are outlined below:

1. Optimum Propulsion System for Static or Cruise Conditions

   a. Determine the following parameters:

      (1) Total thrust in static or cruise conditions - T, lb.

      (2) Propeller diameter - d, ft.

      (3) Propeller rotational speed or tip speed - V_T, ft./sec.

      (4) Number of blades.

      (5) Density at any altitude - ρ , slugs/ft.^{3}

   b. Compute the required thrust coefficient using

$$C_T = \frac{\pi^2 T}{\rho V_T^2 d^2}$$

      Then, for a given tip speed (from step a), obtain the corresponding disc loading using Figure A of the appropriate nomographs.

Alternatively, compute disc loading using

$$DL = \frac{4T}{\pi d^2}$$

Then, for a given tip speed, (from step a), obtain the corresponding thrust coefficient using Figure A.

c. With a known value of thrust coefficient (C_T) (from step b), enter Figure B of the appropriate nomograph and read off propeller power coefficient (C_P) corresponding to an optimum figure of merit or an optimum cruise efficiency.

d. Using C_P from step c, enter Figure C of the appropriate nomograph and obtain the optimum activity factor (or total activity factor for ducted propeller) corresponding to the optimum propeller line.

e. Using the value of optimum activity factor from step d, enter Figure D of the appropriate nomograph and obtain the thrust coefficient-to-power coefficient ratio corresponding to the optimum propeller line.

f. With known values of thrust coefficient-to-power coefficient ratio (from step e) and propeller tip speed (from step a), enter Figure E of the appropriate nomograph and obtain the corresponding power loading (PL).

2. Compromise System Between Static and Cruise Operating Conditions

In order to determine a propulsion system geometry which would represent the best compromise between static and cruise operating conditions, the following procedure can be utilized:

a. Determine static and cruise thrust coefficients as shown in step b above.

b. With the known values of thrust coefficients (from step a), enter Figure B of the appropriate nomographs (one for static and one for cruise for the same propulsion system) and obtain the values of optimum figure of merit and optimum cruise efficiency.

c. Reduce the values of optimum figure of merit and optimum cruise efficiency by appropriate increments (e.g., 5 percent), and read off the corresponding static and cruise power coefficients using Figure B of the appropriate nomographs.

d. With known values of static and cruise power coefficients (from step c) and fixed values of the static and cruise thrust coefficients (from step a), enter Figure C of the appropriate nomographs and obtain the corresponding values of activity factors (or total activity factors for ducted propeller system).

e. Using the results of step d, obtain a plot of activity factor (or total activity factor for ducted propeller system) versus figure of merit and cruise efficiency. Select a common activity factor for the two operating conditions. This selection can be performed on the basis of a given mission requirement or on the basis of a fixed percent reduction from maximum efficiency either in static or cruise condition.

f. Using the common activity factor determined in step e and known values of static and cruise thrust coefficients from step a, enter Figure D of the appropriate nomographs and obtain the thrust-to-power coefficient ratio for each operating condition.

g. Using the values of thrust-to-power coefficient ratio from step f and the known values of propeller tip speed, enter appropriate nomographs, Figure E, and read off the static and cruise power loadings.

C. SAMPLE CALCULATIONS

In order to better illustrate the nomograph performance procedures, the following sample calculations are presented:

1. Optimum Static Propeller

a. Assume the following parameters:

T_S = 11,000 lb., V_T = 900, and d = 19.5 ft.

b. Compute the required thrust coefficient C_T using the following equation:

$$C_{T_S} = \frac{\pi^2 T_S}{\rho V_T^2 d^2} = .148$$

Then, using V_T = 900 ft./sec., enter Figure 5A and obtain the disc loading (DL).

$$DL = 37$$

or alternatively, compute the disc loading (DL) using the following equation:

$$DL = \frac{4\ T_S}{\pi d^2} = 36.83$$

Then, using V_T = 900 ft./sec., enter Figure 5A and obtain the required C_{T_S}.

$$C_{T_S} = .148$$

c. Using the value of C_{T_S} from step b, enter Figure 5B and read off the power coefficient, C_{P_S} corresponding to the optimum figure of merit line, thus:

$$C_{P_S} = .053$$

d. Using C_{P_S} from step c, enter Figure 5C and obtain the optimum activity factor corresponding to the optimum propeller line, thus:

$$(AF)_S = 89$$

e. Using the value of optimum activity factor AF from step c, enter Figure 5D and obtain the value of $(C_T/C_P)_S$ corresponding to the optimum propeller line, thus:

$$(C_T/C_P)_S = 2.81$$

f. With the known value of C_T/C_P from step e and V_T = 900 ft./sec. from step a, enter Figure 5E and obtain the power loading PL.

$$(PL)_S = 5.4$$

2. Optimum Cruise Propeller

a. Assume the following parameters:

T_C = 935.4 lb., V_T = 540, d = 19.5, and J = 2.00

b. Compute the required C_{T_C} using the following equation:

$$C_{T_C} = \frac{\pi^2 T_C}{\rho V_T^2 d^2} = .035$$

Then, using V_T = 540 ft./sec., enter Figure 6A and obtain the disc loading DL.

$$DL = 3.1$$

Alternatively, determine the disc loading (DL) using the following equation:

$$DL = \frac{3T_C}{\pi d^2} = 3.13$$

Then, using V_T = 540 ft./sec., enter Figure 6A and obtain the required C_{T_C}.

$$C_{T_C} = .035$$

c. With the known value of C_{T_C} from step b, enter Figure 6B and read the required power coefficient C_{P_C} corresponding to the optimum cruise efficiency line, thus:

$$C_{P_C} = .074$$

d. Using C_{P_C} from step c, enter Figure 6C and obtain the optimum activity factor (AF) corresponding to the optimum propeller line.

$$(AF)_C = 21$$

e. Using the value of optimum activity factor (AF) from step d, enter Figure 6D and read off the value of $(C_T/C_P)_C$ corresponding to the optimum propeller line.

$$(C_T/C_P)_C = .485$$

f. With $(C_T/C_P)_C$ from step e and V_T = 540 from step a, enter Figure 6E and obtain the power loading PL.

$$(PL)_C = 1.56$$

3. <u>Compromise Open Propeller</u>

a. With the values of static and cruise thrust coefficients of C_{T_S} = 0.148 and C_{T_C} = 0.035 determined in steps 1(b) and 2(b), respectively, enter Figures 5B and 6B (optimum propeller lines) and read off the corresponding values of optimum figure of merit and the optimum cruise efficiency, thus:

$$FM = 0.970 \text{ and } \eta = 0.96$$

b. Reduce the values of optimum figure of merit and optimum cruise efficiency using appropriate increments (e.g., 5 percent), and for known values of C_{T_S} and C_{T_C} obtain the corresponding power coefficients C_{P_S} and C_{T_C} using Figures 5B and 6B, respectively.

c. Using the values of C_{T_S} and C_{P_S}, and C_{T_C} and C_{P_C} from step b, enter Figures 5C and 6C, respectively, and obtain the corresponding static and cruise activity factors. Summarize the results thus obtained as shown in Table I below.

TABLE I

PRELIMINARY RESULTS FOR DETERMINING COMPROMISE OPEN PROPELLER

Static				Cruise			
C_{T_S}	FM	C_{P_S}	$(AF)_S$	C_{T_C}	η	C_{P_C}	$(AF)_C$
0.148	0.87	0.054	89	0.035	0.96	0.074	20
	0.80	0.058	60		0.90	0.078	48
	0.75	0.062	58		0.85	0.083	70
					0.80	0.087	84

d. Using the results of Table II, plot the propeller activity factors obtained for static and cruise conditions versus figure of merit and cruise efficiency, respectively, as shown in Figure 9. If the criterium for compromise is that both efficiencies for static and cruise conditions are equal, then the common propeller activity factor from Figure 9 is 72.5 and the corresponding efficiencies are 0.84 percent.

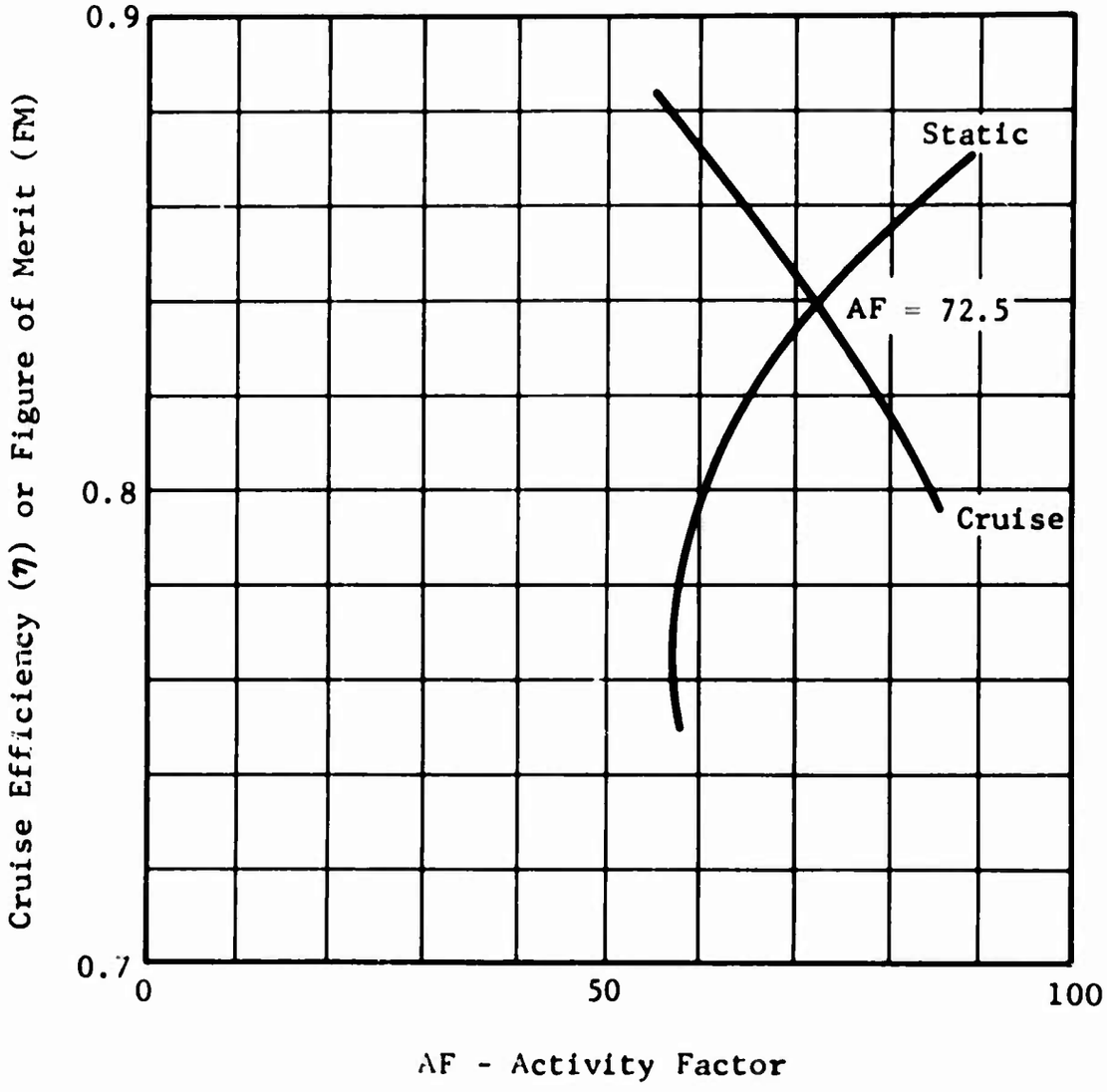

Figure 9. Variation of Propeller Activity Factor With Figure of Merit and Cruise Efficiency.

e. Using this common activity factor of AF = 72.5, and the values of C_{T_S} = 0.148 and C_{T_C} = 0.035, enter Figures 5D and 6D, respectively, and obtain the corresponding thrust power coefficients, thus:

$$(C_T/C_P)_S = 2.79$$

$$(C_T/C_P)_C = .423$$

f. With the static and cruise values of (C_T/C_p) obtained in step e and the corresponding propeller tip speeds, enter Figures 5E and 6E, respectively, and read off the power loadings, thus:

$$(PL)_S = 5.3$$

$$(PL)_C = 1.2 \text{ (extrapolated for 540 fps)}$$

The sample calculations for ducted propellers can be performed in exactly the same manner as those outlined above for open propellers. In this case, the nomographs in Figures 7 and 8 would be utilized.

D. EXPERIMENTAL VERIFICATION OF THE NOMOGRAPHS

This section contains an experimental verification of the performance results presented in the nomographs with the available test data contained in References 4 through 7.

1. Correlation of Nomograph Results With Test Data of Reference 4

Reference 4 presents the test data for open propellers operating in static conditions (J = 0). These data apply to the propeller having the following geometric parameters: IC_{L_i} = 0.5, AF = 103, d = 13 ft. 1 in., and B = 4 blades. Table II shows a comparison of the measured values of T/SHP and the corresponding results obtained from the nomograph in Figure 5.

TABLE II

CORRELATION OF THE NOMOGRAPH RESULTS (FIGURE 5) WITH THE TEST DATA OF REFERENCE 4

J	C_P	T/SHP	
		Reference 4	Nomograph Figure 5
0	0.119	3.45	3.7
0	0.057	5.2	5.3

The above table indicates a good correlation of the test data and the nomograph results.

2. Correlation of Nomograph Results With Test Data of Reference 5

Reference 5 presents the open propeller test data for static and cruise conditions. The propeller geometry was IC_{L_i} = 0.498, AF = 90, d = 14 ft., and B = 4 blades. Table III shows a comparison of the measured and the nomograph values of thrust coefficients obtained for various power settings.

TABLE III

CORRELATION OF THE NOMOGRAPH RESULTS (FIGURES 5 AND 6) WITH THE TEST DATA OF REFERENCE 5

J	C_P	C_T	
		Reference 5	Nomographs Figures 5 and 6
0	0.08	0.177	.17
	0.06	0.151	.16
	0.07	0.165	.175
2	0.04	0.01	.009
	0.06	0.01	.018
	0.08	0.031	.03

The above table indicates a good correlation of the measured and the nomograph values of thrust coefficients for both static and cruise conditions.

3. Correlation of Nomograph Results With Test Data of Reference 6

Reference 6 presents the test data for the XC-142 2FF propeller operating at advance ratio of J = 2.0. The propeller geometric parameters were IC_{L_i} = 0.5, AF = 105, d = 15.625 ft., and B = 4 blades. Table IV shows a comparison of the measured and the nomograph values of thrust coefficients obtained for various power settings.

TABLE IV

CORRELATION OF THE NOMOGRAPH RESULTS (FIGURE 6) WITH THE TEST DATA OF REFERENCE 6

(a) Static Condition

J	C_P	C_T	
		Reference 6	Nomograph Figure 5
0	.10	2.07	2.15
	.12	1.85	1.92
	.14	1.75	1.73

(b) Cruise Condition

J	C_P	C_T	
		Reference 6	Nomograph Figure 6
2.0	0.06	0.02	0.015
	0.07	0.025	0.022
	0.08	0.031	0.0275

The above table indicates good to fair correlation of the test data and the corresponding nomograph results.

4. Correlation of Nomograph Results With the Test Data of Reference 7

Reference 7 presents the data for shrouded propellers tested at static and various cruise speeds. The shrouded propeller geometry was: TAF = 960, IC_{L_i} = 0.13, d = 2 ft. 5 in., and exit area ratio = 1.0. The duct overall geometry was the same for both static and cruise tests with the exception of the duct lip radius; i.e., the lip radius for static condition was increased as compared to that at cruise. Table V shows the comparison of the measured and the nomograph performance results.

TABLE V

CORRELATION OF NOMOGRAPH RESULTS (FIGURES 7 AND 8) WITH THE TEST DATA OF REFERENCE 7

(a) Static Condition

J	C_P	C_{T_T}/C_P	
		Reference 7	Nomograph Figure 7
0	0.4	1.65	1.68
	0.3	1.9	1.9
	0.2	2.2	2.25
	0.1	2.6	2.64

TABLE V (CONTINUED)		
(b) Cruise Condition		
	C_{T_T}/C_P	
J	Reference 7	Nomograph Figure 8
1.0	0.8	0.835
1.2	0.625	0.7
1.6	0.8	0.87

The above table indicates a good correlation of the test data and the corresponding nomograph results for both static and cruise operating conditions.

IV. COMPARATIVE EVALUATION OF PROPULSION SYSTEMS

A. CRITERIA FOR COMPARISON

The comparative evaluation of open propeller, ducted propeller, and turbofan propulsion systems is herein performed on the basis of aircraft-propulsion system performance, weight, vibratory stress levels, operational requirements, and complexities peculiar to each system.

The performance computations were made assuming typical V/STOL aircraft parameters such as equivalent flat plate drag area of 8 $ft.^2$, wing span loading of 460 lb./ft., wing aspect ratio of 6.0, Oswald wing efficiency factor of 0.8, and a total design gross weight of 20,000 lb. The aircraft configuration considered is a tilt-wing type for the open propeller system and a tilt-propulsion system type for both ducted propeller and turbofan systems. Each configuration is equipped with two propulsion systems of the same type possessing concentrically located gas generators and power turbines. The propulsion systems are interconnected with shafting so as to permit single engine operation. Normally, however, the aircraft total power requirement is equally shared by the engines.

The propulsion systems were designed to a static thrust/gross weight requirement of 1.1 at 6000 ft. pressure altitude and 95°F temperature. Tables VI through VIII summarize the range of the most pertinent design parameters considered for each system.

The weight analysis was performed utilizing the most recently available weight trend data for each propulsion system. Engine installation weight was accounted for by utilizing suitable semi-empirical relationships. The aircraft equipment and structural weight was assumed to be invariant for each propulsion system considered and was computed on the basis of constant percentage of vehicle total gross weight.

The fuel weight for each propulsion system was computed for an appropriate combination of cruise speeds and ranges, assuming a total hovering time of 5 minutes at the design condition. The cruise speeds varied between the speeds

TABLE VI

OPEN PROPELLER PROPULSION SYSTEM CONFIGURATIONS

Conf. No.	Static Disc Loading Lb./Ft.^{2}	Blade Activity Factor	Remarks
1	37.2	140	All configurations are based on: 1. 4-bladed propeller 2. Blade integrated lift coefficient of IC_{L_i} = .5 3. T64-16 turboshaft engine a. Gas generator pressure ratio of 13:1 b. Maximum turbine inlet temperature of 2000°F c. Exhaust area of 450 in.^{2}
2	37.2	130	
3	37.2	120	
4	37.2	115	
5	35.2	120	
6	35.2	110	
7	35.2	100	
8	33.5	100	
9	33.5	90	
10	33.5	85	

TABLE VII

DUCTED PROPELLER PROPULSION SYSTEM CONFIGURATIONS

Conf. No.	Static Disc Loading Lb./Ft.^{2}	Total Activity Factor	Remarks
1	96.25	500	All configurations are based on: 1. 4-bladed propeller 2. Blade integrated lift coefficient of IC_{L_1} = .5 3. Shroud exit area ratio a. Cruise 1:1 b. Static 1.2:1 4. T64-16 turboshaft engine a. Gas generator pressure ratio of 13:1 b. Maximum turbine inlet temperature of 2000°F c. Exhaust area of 450 in.^{2}
2	96.25	600	
3	96.25	700	
4	88.5	400	
5	88.5	500	
6	88.5	550	
7	88.5	600	
8	75.3	400	
9	75.3	500	
10	75.3	600	

TABLE VIII

TURBOFAN PROPULSION SYSTEM CONFIGURATIONS

Conf. No.	Percent Fan Available Energy	Fan Pressure Ratio	Bypass Ratio	Remarks
1	85	1.60	5.31	All configurations are based on:
2	85	1.45	6.78	1. Direct-drive concentric front fan arrangement
3	85	1.30	9.78	2. Gas generator pressure ratio of 13:1
4	55	1.60	3.31	3. Maximum turbine inlet temperature of 2020°F
5	55	1.45	4.36	
6	55	1.30	6.43	
7	45	1.60	2.73	
8	45	1.45	3.59	
9	45	1.30	5.29	

limited by the minimum thrust required and the maximum thrust available, whereas the selected ranges considered in this study were 100, 300, and 500 nautical miles. The fuel weight was increased by approximately 15 percent to allow for 10 percent reserve fuel and 5 percent installation losses. The specific fuel consumption for each performance segment was computed based on the initial takeoff gross weight.

The vibratory stress analysis, which constitutes an important consideration in the comparative evaluation of propulsion systems, was of necessity qualitative. A quantitative analysis of vibratory stress levels requires a detailed knowledge of blade section properties and blade section airload distribution and is beyond the scope of the present program.

The comparative evaluation of open propeller, ducted propeller, and turbofan propulsion systems was performed on the basis of the following parameters:

1. Overall efficiency η_o.
2. Relative productivity, $W_{PL}V_C/W_E$.
3. Relative fuel consumption, w_F/W_{PL}.
4. Payload-to-gross weight ratio, W_{PL}/W_G.

In addition, the following operational requirements and complexities peculiar to each propulsion system were considered:

1. Installation effects.
2. Control system complexity.
3. Deicing requirements.
4. Noise.
5. Exit velocity.
6. Maintainability and reliability.

The sections below present the methods of analysis and the results obtained from the comparative evaluation study.

B. PERFORMANCE ANALYSIS

1. Total Required Thrust

The total thrust to be generated by a propulsion system can be expressed as follows:

$$T_T = D_A + D_N + F_R - F_G + D_S \tag{1}$$

where

D_A = aircraft drag, lb.

D_N = fan nacelle and/or engine nacelle drag, lb.

F_R = engine ram drag, lb.

F_G = engine exhaust residual thrust, lb.

D_S = ducted propeller shroud drag, lb.

The drag contributions of various aircraft components and the propulsion systems can be determined from the subsections below.

a. Aircraft and Propulsion System Drag (D_{A+N})

Using the equivalent flat plate area of f_A = 8 ft.^{2}, as defined in section A above, the aircraft parasite drag can be expressed as

$$D_{A_p} = 8q \tag{2}$$

Engine nacelle drag or turbofan nacelle drag can be generally expressed as follows:

$$D_N = qA_{max}\, C_{D_B} + C_{D_f} \frac{A_{wet}}{A_{max}}\, K \tag{3}$$

where the ratio of nacelle wetted surface area A_{wet} and nacelle maximum frontal area A_{max} is defined by geometry as

$$\frac{A_{wet}}{A_{max}} = 2\,\frac{\ell}{d_{max}}\left(\frac{d_J}{d_{max}} + 1\right) \qquad (4)$$

where

d_{max} = maximum frontal diameter, ft.

d_J = jet exhaust diameter, ft.

ℓ = engine length, ft.

Using References 8 and 9, the following engine nacelle parameters are obtained for the T-64-GE-16 engine:

$$\frac{\ell}{d_{max}} = 2.0,\ \frac{d_J}{d_{max}} = 0.7,\ K = 1.0,\ A_J = 450 \text{ in.}^2$$

$$A_{max} = A_J \Big/ \left(\frac{d_J}{d_{max}}\right)^2 = \frac{450}{0.49} = 918 \text{ in.}^2 = 6.37 \text{ ft.}^2$$

$$C_{D_B} = 0.05,\ C_{D_f} = 0.0025$$

Substituting the above values into equations (3) and (4) yields

$$\frac{A_{wet}}{A_{max}} = 6.8$$

$$\therefore D_N = 0.425 \times q \text{ per engine}$$

For two engines, the total nacelle drag is

$$D_N = 2 \times 0.425q = 0.85q$$

$$\text{or } f_N = D_N/q = 0.85 \text{ ft.}^2$$

The above value of f_N is herein utilized to account for engine nacelle drag for both open propeller and ducted propeller aircraft configurations.

For the turbofan configuration, the nacelle drag is based on the fan nacelle maximum frontal area, $A_{f_{max}}$, which depends on turbofan bypass ratio and pressure ratio. Since the latter parameters are considered as variables, it is convenient to express the turbofan nacelle drag in terms of $A_{f_{max}}$.

Thus, using Reference 8, the following turbofan parameters are obtained:

$$\frac{\ell}{d_{max}} = 1.15, \qquad \frac{d_J}{d_{max}} = 0.98, \qquad K = 1.1$$

$$C_{D_B} = 0.0213, \; C_{D_f} = 0.0025$$

Substituting the above values into equations (3) and (4) yields

$$\frac{A_{wet}}{A_{max}} = 2 \times 1.15 \ (0.98 + 1) = 2.3 \times 1.98 = 4.554$$

$$D_N = (q)A_{f_{max}} \ (0.0213 + 0.0025 \times 4.554) \ 1.1$$

$$= 0.036(q)A_{f_{max}}/\text{engine}$$

For two turbofan systems,

$$D_N = 0.072(q)A_{f_{max}}$$

$$\text{or} \quad f_N = D_N/q = 0.072 \ A_{f_{max}}$$

The total equivalent flat-plate area for the aircraft and the propulsion system drag can be expressed as follows:

$$f = f_A + f_N \tag{5}$$

The combined aircraft, nacelle, and wing-induced drag at any cruise speed can be conveniently determined by utilizing the established performance methods of Reference 10. From this reference, the cruise speed and the corresponding aircraft drag for maximum lift-to-drag ratio are given by

$$V_{(L/D)_{max}} = \frac{12.9}{\sqrt[4]{ef}} \sqrt{W/b} \tag{6}$$

and

$$(D_{A+N})_{(L/D)_{max}} = 1.132 \ \frac{W}{b}\sqrt{f/e} \tag{7}$$

where

W/b = wing span loading, lb./ft.

e = Oswald wing efficiency factor (0.8)

f = equivalent flat plate area (equation 5)

For any cruise speed and $V_{(L/D)_{max}}$, given by equation (6), the cruise speed factor k_V can be determined as

$$k_V = \frac{V_C}{V_{(L/D)_{max}}} \tag{8}$$

With a known k_V factor (given by equation 8), the corresponding drag factor k_D can now be determined using Figure 10 reproduced from Reference 10. The combined aircraft nacelle and wing drag for any cruise speed can then be computed from the following relationship:

$$D_{(A+N)} = (k_D) D_{(A+N)_{(L/D)_{max}}} \tag{9}$$

where $D_{(A+N)_{(L/D)_{max}}}$ is given by equation (7).

b. Engine Exhaust Thrust (F_G), Ram Drag (F_R), and Ducted Propeller Shroud Drag (D_S)

The engine exhaust residual gross thrust (F_G), engine ram drag (F_R), and ducted propeller shroud drag (D_S) (if applicable) can be determined by a simple, rapidly convergent iteration procedure. This procedure is as follows:

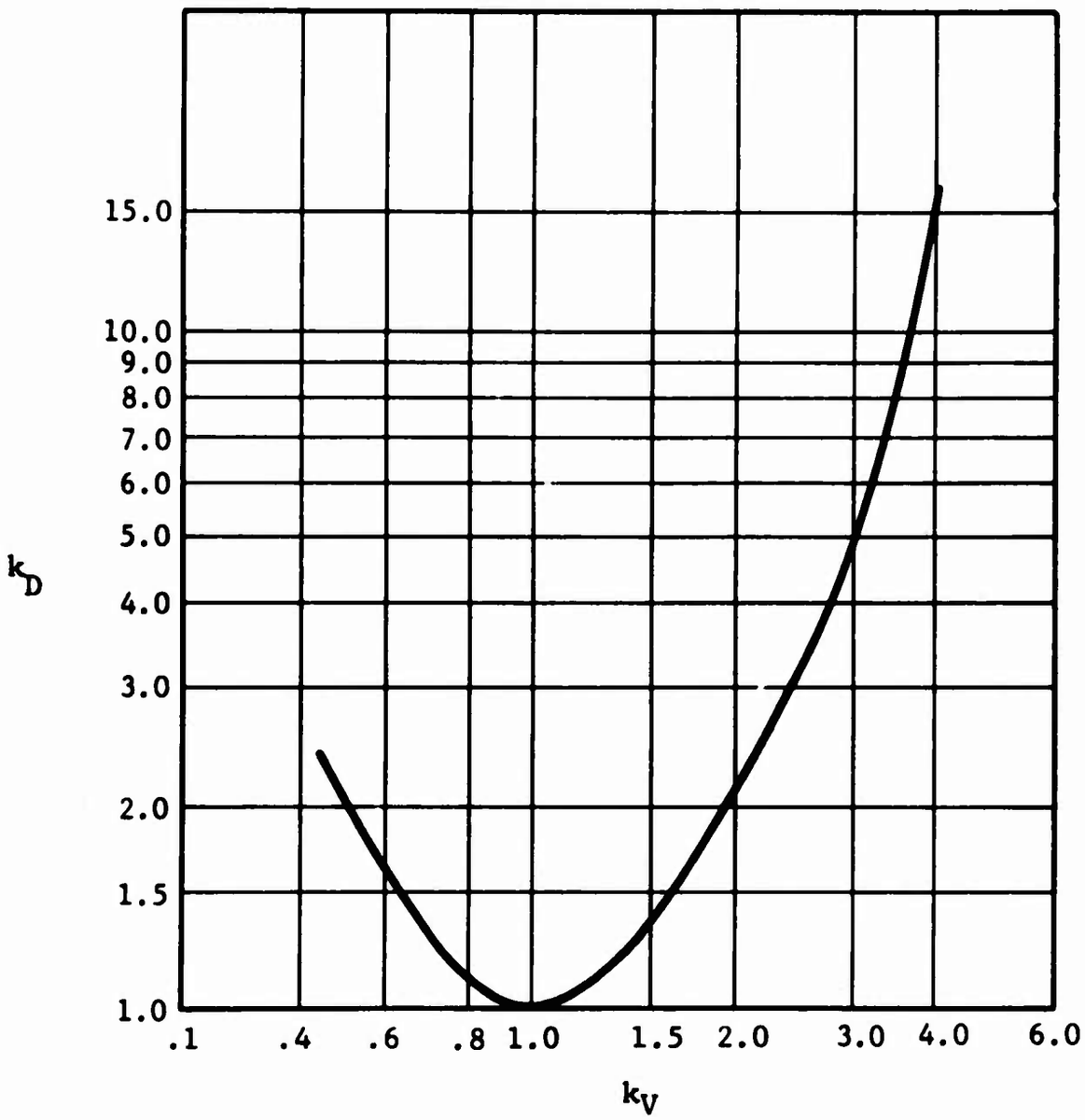

Figure 10. Generalized Performance Data
Variation of k_D With k_V.

(1) For a given cruise speed, compute combined aircraft and nacelle drag as given by equation (9) and determine

$$C_T = \frac{T_T}{\rho n^2 d^4} = \frac{D_{(A+N)}}{\rho n^2 d^4}$$

$$C_P = \frac{P}{\rho n^3 d^5} = \frac{D_{(A+N)}\ V_o}{\rho n^3 d^5}$$

$$J = \frac{V_o}{nd}$$

and

$$\eta = \frac{C_T J}{C_P}$$

(2) Also, compute engine shaft horsepower as follows

$$SHP = \frac{D_{(A+N)}\ V_o}{\eta\ \ 550}$$

(3) With a known shaft horsepower and a cruise speed, enter the engine specification charts and read off engine residual exhaust thrust F_G. Also, obtain the airflow w_A and compute engine ram drag using

$$F_R = \frac{w_A}{q} V_o$$

(4) Calculate a better approximation for total thrust from

$$T_T = D_{(A+N)} + F_R - F_G$$

(5) For open propeller and turbofan systems, repeat steps (1) through (4) until convergence in total thrust is achieved. This will yield the final value of the total thrust required for open propeller and turbofan propulsion systems.

(6) For ducted propeller propulsion systems, enter the value of total thrust from step (4) into ducted propeller charts, Figures 1.2 through 1.9 of Reference 3, and obtain shroud drag factor F_D.

(7) Compute the ducted propeller shroud drag:

$$D_S = T_T(1-F_D)$$

where T_T is obtained in step (4).

(8) Calculate the better approximation for total thrust using

$$T_T = D_{(A+N)} + F_R - F_G + D_S$$

(9) Repeat steps (1) through (4) and (6) through (8) until convergence in T_T is achieved. This will yield the final value of total thrust required for ducted propeller propulsion systems.

2. Ring Wing Equivalent

In comparative evaluation of the performance of the three propulsion systems considered, it is necessary to account for the increment of lift due to the shroud of a ducted propeller or turbofan. This can be performed by determining a ring wing equivalent.

According to Reference 11, the lift developed by a ring wing is twice the lift of an elliptic wing with a root chord equal to the chord of the ring airfoil and a span equal to the ring wing diameter. If the ring airfoil lift coefficient is based on its projected planform area, then

$$L_{RW} = 2\ L_{EW} \qquad (10)$$

or

$$\left(\frac{dC_L}{d\alpha} \alpha q S \right)_{RW} = 2\left(\frac{dC_L}{d\alpha} \alpha q S \right)_{EW} \tag{11}$$

$$\left(\frac{dC_L}{d\alpha} \right)_{RW} dC = 2\left(\frac{dC_L}{d\alpha} \right)_{EW} \frac{\pi dC}{4} \tag{12}$$

$$\left(\frac{dC_L}{d\alpha} \right)_{RW} = \frac{\pi}{2} \left(\frac{dC_L}{d\alpha} \right)_{EW} \tag{13}$$

From Reference 12, the lift curve slope for an elliptic wing is given by

$$\left(\frac{dC_L}{d\alpha} \right)_{EW} = \frac{2\pi AR}{AR + \frac{2(AR+4)}{AR+2}} \tag{14}$$

Substituting equation (14) into equation (13) and simplifying, there results

$$\left(\frac{dC_L}{d\alpha} \right)_{RW} = \frac{\pi^2}{2\left(1+\frac{4}{AR}\right)} \tag{15}$$
$$1+\frac{}{AR+2}$$

The aspect ratio for an elliptic wing is defined as

$$AR = \frac{4d}{\pi C} \tag{16}$$

Substituting equation (16) into equation (15) and simplifying, there follows

$$\left(\frac{dC_L}{d\alpha}\right)_{RW} = \frac{\pi 2}{1+(1+\pi C/d)/(1+\frac{2d}{\pi C})} \tag{17}$$

In order to maintain a constant aircraft total lift (equal to gross weight) for all three propulsion systems, an appropriate reduction in wing area must be made for ducted propeller and turbofan propulsion systems. This wing area reduction is given by

$$\Delta S_W = 2\, S_{RW}\left(\frac{dC_L}{d\alpha}\right)_{RW}\Big/\left(\frac{dC_L}{d\alpha}\right)_W \tag{18}$$

where for the conventional wing

$$\left(\frac{dC_L}{d\alpha}\right)_W = \frac{a_o}{1+\frac{a_o}{\pi AR}} \tag{19}$$

For the ducted propeller shroud geometry given by C/d = 0.5 and the turbofan nacelle geometry given by C/d = 1.15, the corresponding reductions in wing area (AR = 6.0) are given by;

For ducted propeller

$$\Delta S_W = 1.16d^2$$

For turbofan

$$\Delta S_W = 1.31d^2$$

3. Overall Propulsion System Efficiency

One of the parameters used for comparative evaluation of various propulsion systems is overall efficiency. This efficiency is defined as the ratio of useful work performed to the total supplied energy; thus,

$$\eta_o = \frac{U_W}{E_s} \tag{20}$$

The useful work performed is the product of aircraft total drag and the flight speed; thus

$$U_W = D_A V_C \tag{21}$$

This useful work can also be expressed in terms of ambient absolute temperature (t°,R) and aircraft flight Mach number (M), as follows:

$$U_W = (D_A)49\sqrt{t}\ M \tag{22}$$

The energy supplied to the propulsion system is given by

$$E_s = J_E\ H_F\ w_F/3600 \tag{23}$$

where

J_E = mechanical equivalent of heat, 778 ft.-lb./BTU

H_F = heating value of the fuel, BTU/lb.

w_F = fuel flow rate, lb./hr.

Substituting equations (22) and (23) into equation (20), there follows

$$\eta_o = \frac{226.74\ D_A \sqrt{t}\ M}{H_F\ w_F} \tag{24}$$

Assuming a sea level standard condition and a fuel heating value of H_F = 18,400 BTU/lb., equation (24) is reduced to

$$\eta_o = 0.28 \frac{D_A M}{w_F} \tag{25}$$

C. WEIGHT ANALYSIS

1. Total Aircraft Weight (W_G)

The total aircraft weight can be expressed as follows:

$$W_G = W_{UL} + W_E \tag{26}$$

where

W_{UL} = useful load, lb.

W_E = empty weight, lb.

2. Useful Load (W_{UL})

The useful load is given by

$$W_{UL} = W_{PL} + W_C + w_F + w_o + w_{RF} \tag{27}$$

where

W_{PL} = payload, lb.

W_C = crew weight, lb.

w_F = fuel weight, lb.

w_o = oil weight, lb.

W_{RF} = residual fluids weight, lb.

In the present analysis the following were considered as fixed weights:

$$W_{fixed} = W_C + w_o + w_{RF} = 550 \text{ lb.} \tag{28}$$

Using the above value of fixed weight, the useful load can be expressed as

$$W_{UL} = 550 + W_{PL} + w_F$$

3. Empty Weight (W_E)

The aircraft empty weight can be expressed as follows:

$$W_E = W_P + W_I + W_{E,S} - \Delta W_W \tag{29}$$

where

W_P = propulsion system weight, lb.

W_I = engine installation weight, lb.

$W_{E,S}$ = equipment and structural weight, lb.

ΔW_W = reduction of wing weight due to decrease of wing area to account for propulsion system shroud lift, lb.

a. Propulsion System Weight (W_P)

The open and ducted propeller propulsion system weight is given by

$$W_P = W_e + W_{Pr} + W_S + W_d + W_{C,S} + W_{FS} \tag{30}$$

where

W_e = engine weight, lb.

W_{Pr} = propeller weight, lb.

W_S = shroud weight, lb.

W_d = drive system weight, lb.

$W_{C,S}$ = control and starting system weight, lb.

W_{FS} = fuel system weight, lb.

Each of the above propulsion system weight components can be obtained utilizing the following relationships:

From Reference 9,

$$W_e = 690\ N_P \tag{31}$$

From Reference 2,

$$W_{Pr} = 271\left[\left(\frac{d}{10}\right)^{1.85}\left(\frac{B}{4}\right)^{0.7}\left(\frac{AF}{100}\right)^{0.6}\left(\frac{N_d}{20,000}\right)^{0.5}\left(\frac{SHP}{10\ d^2}\right)^{0.12}\left(M + 1.0\right)^{0.5}\right] N_P \tag{32}$$

From Reference 13,

$$W = .718\left[T_T d^2 C/t_C\right]^{0.4} N_P \tag{33}$$

From Reference 14,

$$W_d = .095Q^{0.84} N_P \quad (34)$$

$$W_{C,S} = 50 N_P \quad (35)$$

$$W_{FS} = 30 N_P + .3 w_F/6.5 \quad (36)$$

where

B = number of propeller blades

N_P = number of engines (or number of propulsion systems in this analysis)

AF = blade activity factor

Q = engine torque

M = design Mach number

t_C = shroud wall thickness

SHP = design value of shaft horsepower

The turbofan propulsion system weight can be directly obtained from Figure 11. This weight, which is a function of fan pressure ratio, bypass ratio, and the airflow, includes the weight of gas generator, controls and accessories, shaft and bearings, turbine, nacelle, and fan.

b. Engine Installation Weight (W_I)

The open and ducted propeller installation weight includes the weight of nacelles and attachments and is given by

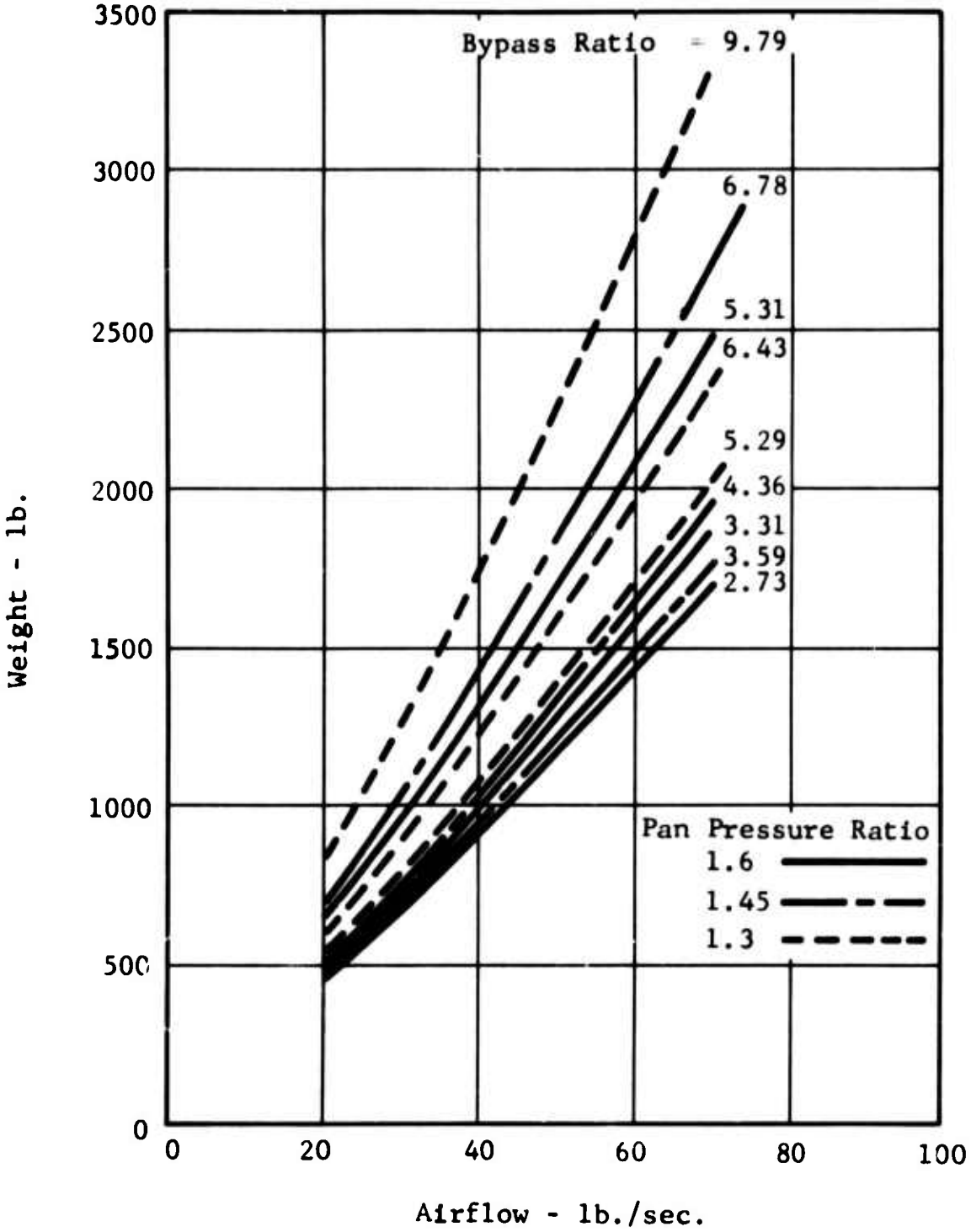

Figure 11. Direct-Drive Concentric Front Fan System Weight as a Function of Gas Generator Unsupercharged Airflow, Turbine Inlet Temperature of 2020°F.

$$W_I = 7\left(\frac{HP_I}{100}\right)^{2/3} N_P \qquad (37)$$

where

HP_I = installed horsepower

The turbofan installation weight includes the weight of pylons and attachments and according to Reference 14 can be expressed as follows:

$$W_I = \left(W_P n_c\right)^{0.41} N_P \qquad (38)$$

where

n_c = crash load factor

c. Equipment and Structural Weight ($W_{E,S}$)

This weight includes total aircraft body weight (with wings, tailplane, vertical fin, etc.), weight of cross-shafting between propulsion systems, flight control weight, alighting gear weight, instrument and navigational equipment weight, and air-conditioning and deicing weight. In the present analysis, the equipment and structural weight was assumed to be equal to 40 percent of the total aircraft gross weight for each propulsion system analyzed. Thus,

$$W_{E,S} = 0.4\ W_G \qquad (39)$$

d. Wing Weight Reduction (ΔW_W)

Although the total wing weight is included in the structural weight (equation (39)), a small reduction in wing weight ΔW_W is achievable as a result of propulsion system shroud lift. In order to maintain a constant aircraft lift (equal to total gross weight) for all propulsion systems, the basic wing area can be reduced by the amount of ΔS_W as given by equation (18). Due to this reduction in wing area, the wing weight for ducted propeller and turbofan propulsion systems can be reduced by

$$\Delta W_W = 2.96\left(\frac{W_G}{10^3}\right)^{1.974}\left\{1-\left[1 - 1.48\left(\frac{10^3 d}{W_G}\right)^2\right]^{0.658}\right\} \quad (40)$$

D. VIBRATORY STRESS ANALYSIS

The prediction of vibratory stress levels for a propulsion system requires knowledge of the mass and elastic properties of the blades, as well as the blade airload distribution. Hence, the vibratory stress levels cannot be predicted from the generalized parameters utilized in the present study, i.e., IC_{L_i}, AF, etc. Unfortunately, there exists no reliable method by which a vibratory stress trend can be predicted at the present time.

One of the most critical operating conditions which gives rise to high vibratory stress levels on open propellers is the skew flow field resulting from the propeller axis not being aligned to the airstream.

The dynamic problem which must be solved is the coupling between blade aeroelastic deflection and its effect on the blade airload distribution. Such an analysis is presented in Reference 15, which predicts both the performance and the vibratory stress levels of VTOL-type propellers in presence of the nacelles and wings. However, the validity of the analytical method presented in Reference 15 has not been

fully substantiated, although work is presently being performed to obtain the required experimental verification of this analysis.

The vibratory stress analysis of ducted propellers has two additional factors which give rise to periodic airloads. The first of these is the structural struts (stators) which support the duct. The second is the skewed flow, and possibly the flow separation, which occurs at the inlet when the duct is inclined with respect to the airstream.

The strut effect can, in principle, be treated by the method of singularities. However, none of the present analyses, i.e., References 16 and 17, incorporate this effect. Measurements of stress levels in Reference 18 indicate that the airframe and wind direction can exert a major influence on the vibratory stress levels. However, no open literature was available on this subject.

The determination of turbine blade vibrating stress levels also requires a detailed knowledge of both blade design and the frequencies and amplitudes of the exciting forces. If any of the aerodynamic disturbances have a frequency close to the natural frequency of vibration of any one of the blade modes, then the blades will vibrate at large amplitudes and may ultimately suffer fatigue failure. In Reference 19, it was found that reduction in the fan blade thickness and a consequent reduction in critical frequencies can be accomplished by the use of appropriate materials such as boron and beryllium.

In summary, vibratory stress trends could not be predicted for comparison of the three different propulsion systems since data were lacking at the present time; however, it is realized that this is an area of primary importance in V/STOL aircraft propellers, and one should be constantly aware of the presence of these vibratory stresses in hopes of incorporating propeller and propulsion system component designs to reliably operate in this environment.

E. RESULTS OF THE COMPARATIVE STUDY

The results of the comparative study of open propeller, ducted propeller, and turbofan propulsion systems presented herein

are based on the methods and procedures outlined in the previous sections. These results show a direct comparison of overall performance of the three propulsion systems and depict operational requirements and complexities peculiar to each system.

1. Performance Results

The performance comparison of the three propulsion systems is accomplished on the basis of overall propulsive efficiency (defined in Section B.3 above), relative productivity W_{PL} $(V_C)/W_E$, relative fuel consumption w_F/W_{PL}, and payload-to-gross weight ratio W_{PL}/W_G. These results are discussed below.

a. Overall Efficiency (η_o)

Figure 12 shows a comparison of overall efficiency η_o for open propeller, ducted propeller, and turbofan propulsion systems as a function of sea level cruise Mach number. This efficiency parameter represents the ratio of useful work done on the aircraft to the available heat energy supplied by the fuel; as such, it also represents a product of propulsive and thermal efficiency for each system.

Examining Figure 12, it can be noted that the overall efficiency increases with an increase in cruise Mach number for each propulsion system considered. It can be further seen that for a fixed cruise Mach number, the open propeller has a higher overall efficiency as compared to ducted propeller and turbofan propulsion systems. However, for both open and ducted propeller systems, the upper range of this efficiency (i.e., at M 0.58) is power limited, whereas the turbofan efficiency increases up to a Mach number of about 0.9.

b. Relative Productivity $[(W_{PL})(V_C)/(W_E)]$

Figure 13 shows the plots of the relative productivity of the three propulsion systems versus sea level cruise Mach number for constant values of range of 100, 300,

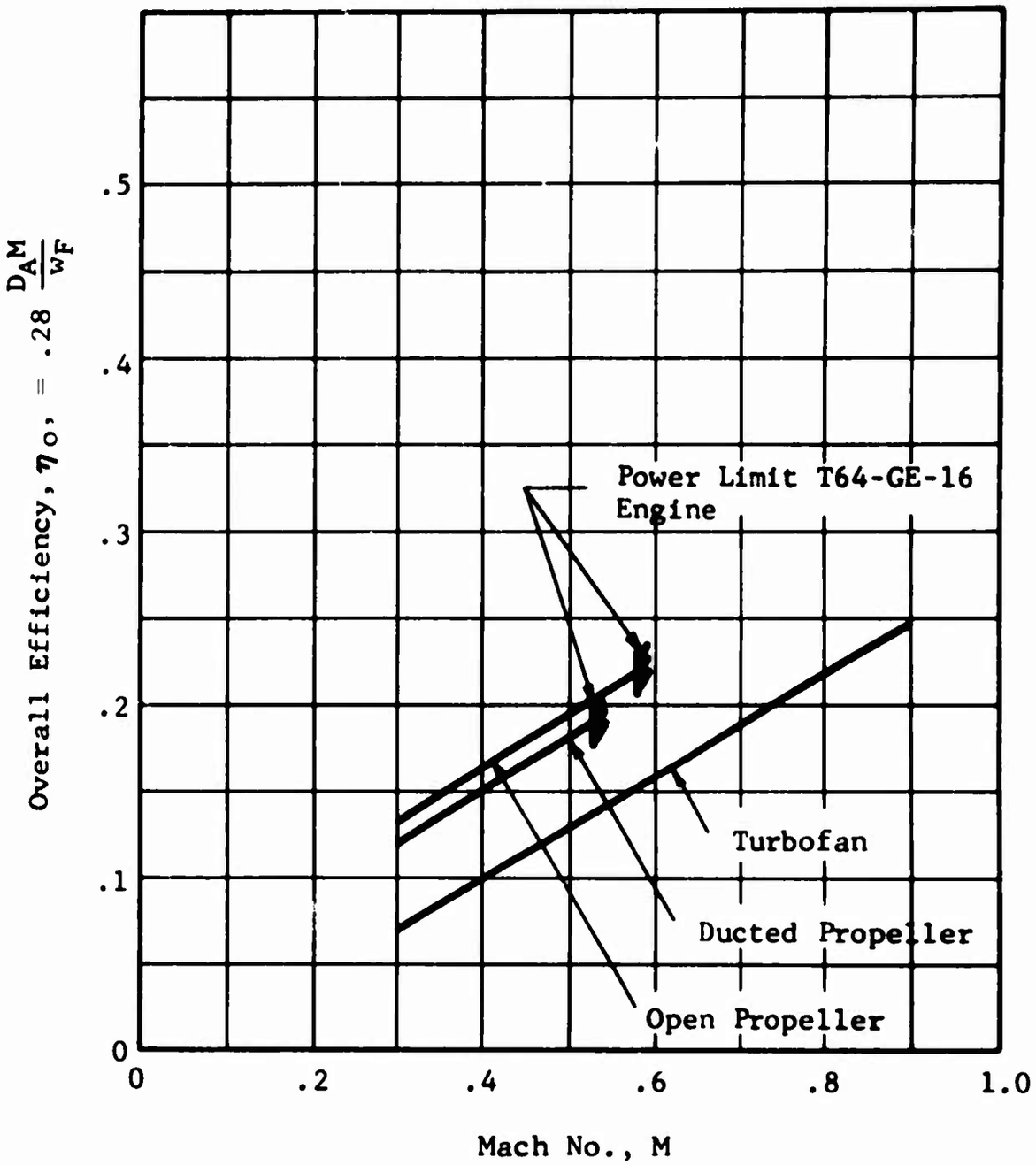

Figure 12. Overall Efficiency Versus Design Cruise Speed.

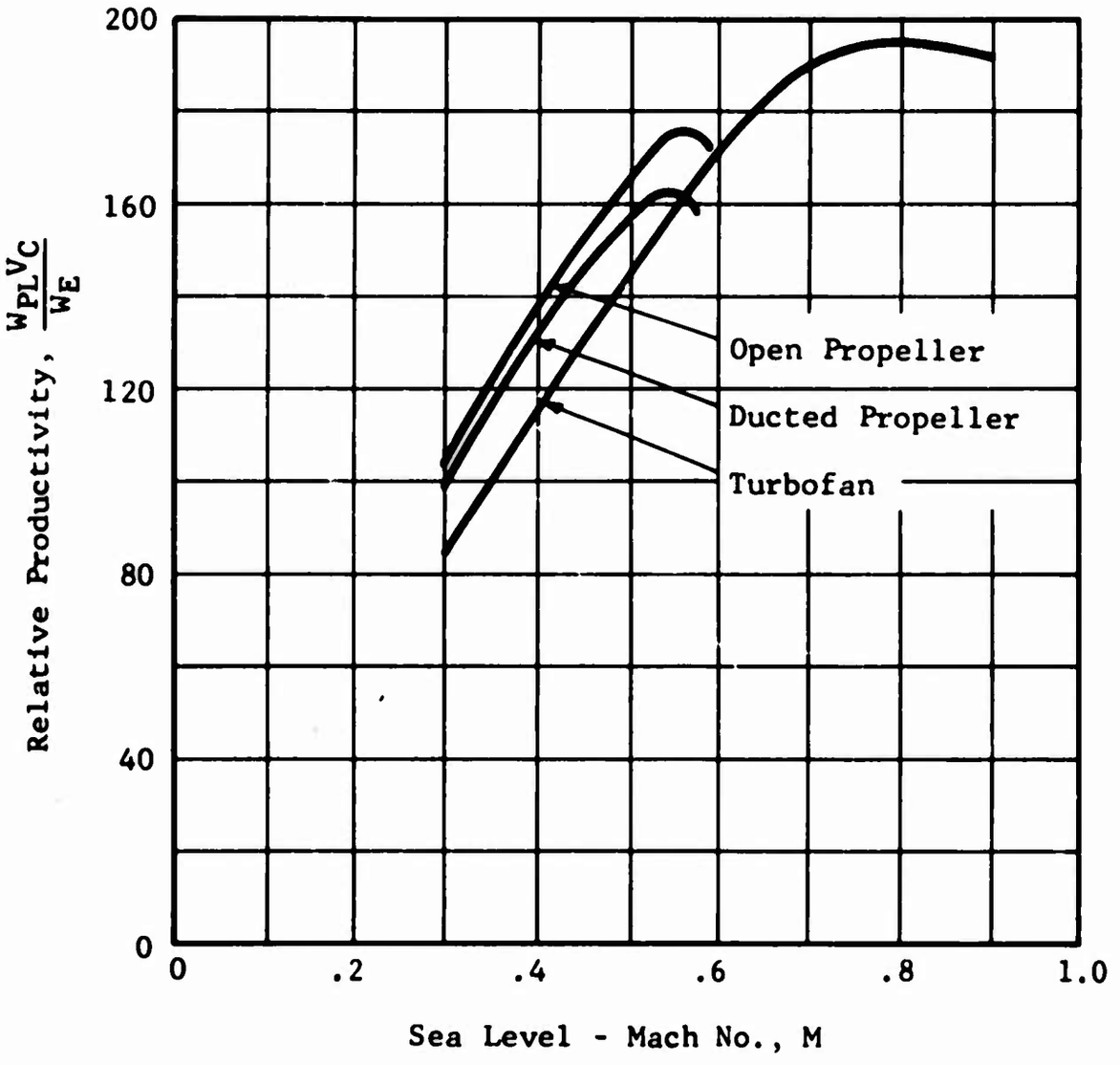

(a) R = 100 Nautical Miles

Figure 13. Relative Productivity Versus Cruise Speed.

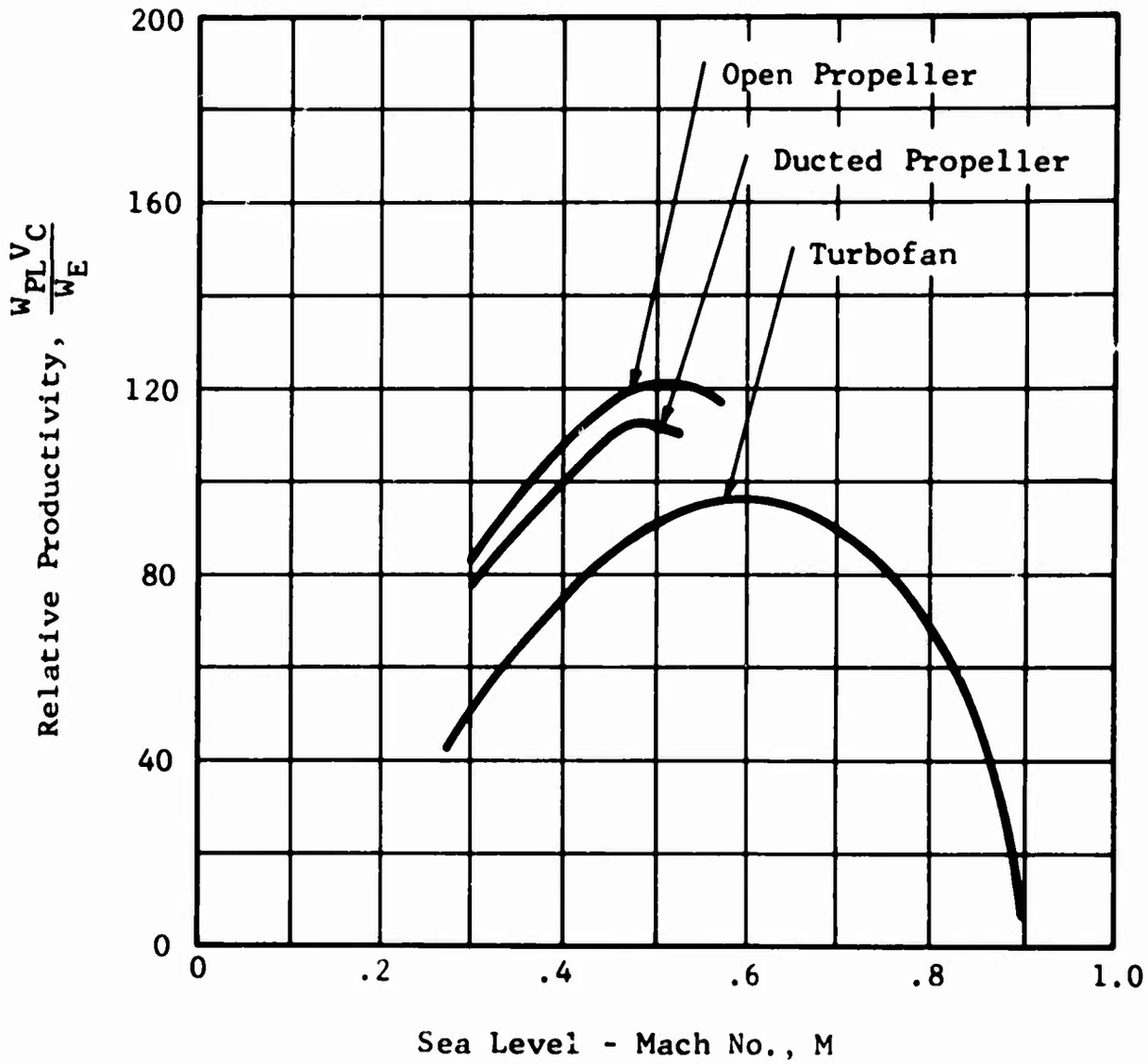

(b) R = 300 Nautical Miles

Figure 13. (Continued).

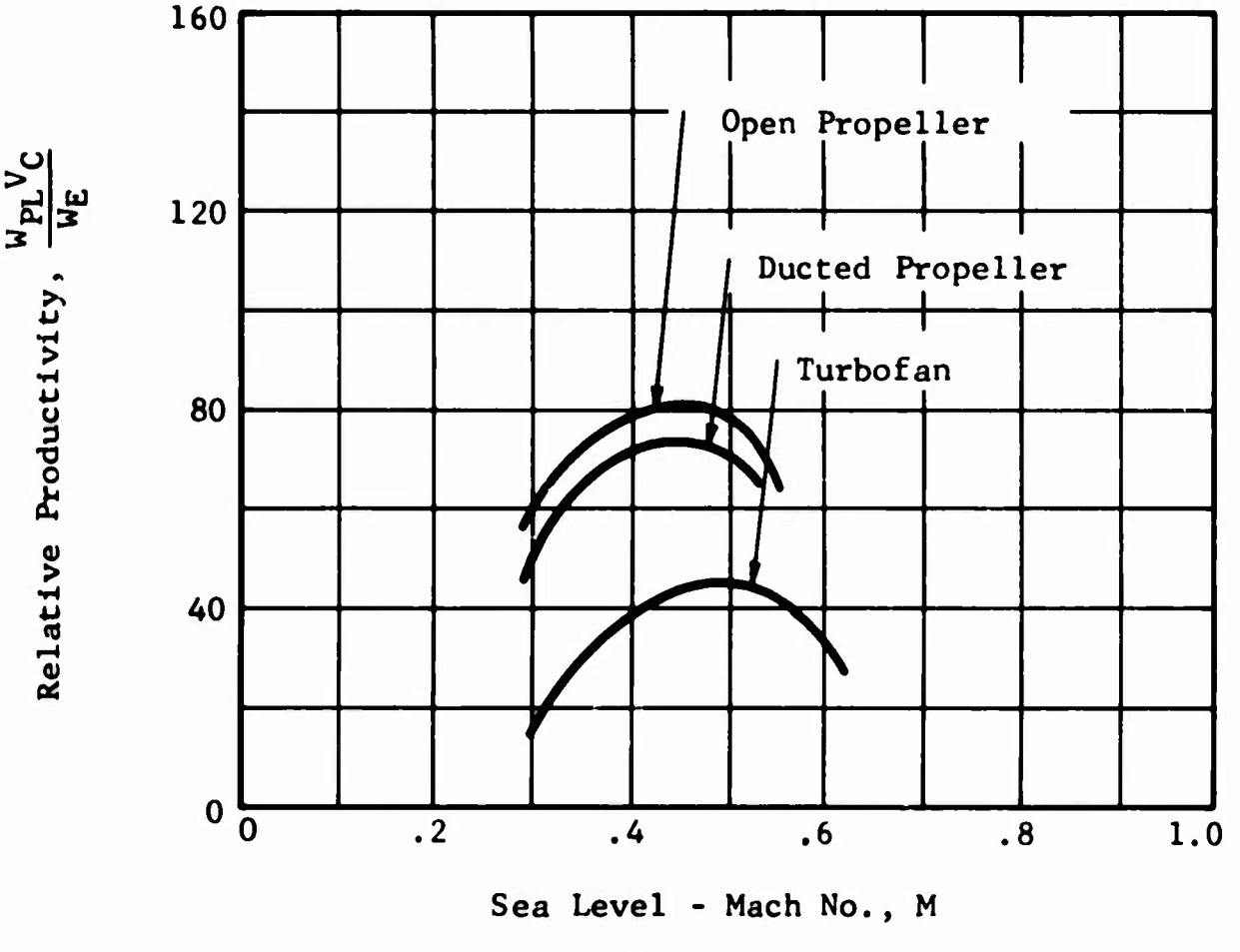

(c) R = 500 Nautical Miles

Figure 13. (Concluded).

and 500 nautical miles, respectively. The data were obtained on the basis of maximum payload-to-gross-weight ratio for each system and for each Mach number considered.

Figure 13a shows that, for a short range of 100 nautical miles, the turbofan achieves a higher maximum relative productivity and at a higher cruise Mach number than either the open or the ducted propeller system. For increased ranges, as can be seen from Figures 13b and 13c, the relative productivity of all three propulsion systems deteriorates; however, the rate of decrease for the turbofan is appreciably higher than that for either the open or the ducted propeller. This result is more clearly indicated by Figure 14, which shows a cross plot of maximum productivity for each propulsion system versus range. The variation of the corresponding Mach number at maximum productivity versus range is depicted in Figure 15.

From the results of Figures 13 and 14, it can be concluded that for ranges greater than 220 nautical miles, open propeller yields higher maximum productivity than ducted propeller or turbofan. Furthermore, the maximum productivity for open propeller is achievable at higher cruise Mach numbers as compared to ducted propeller but lower cruise Mach number as compared to turbofan.

c. Relative Fuel Consumption (w_F/W_{PL})

Figure 16 presents the plots of relative fuel consumption for the three propulsion systems versus sea level cruise Mach number for constant values of ranges of 100, 200, and 300 nautical miles, respectively. These plots show that the open propeller system exhibits the least relative fuel consumption as compared to the ducted propeller or the turbofan system for all cruise speeds and ranges of comparison.

Figure 17 shows a plot of the minimum relative fuel consumption versus range for the three systems. This

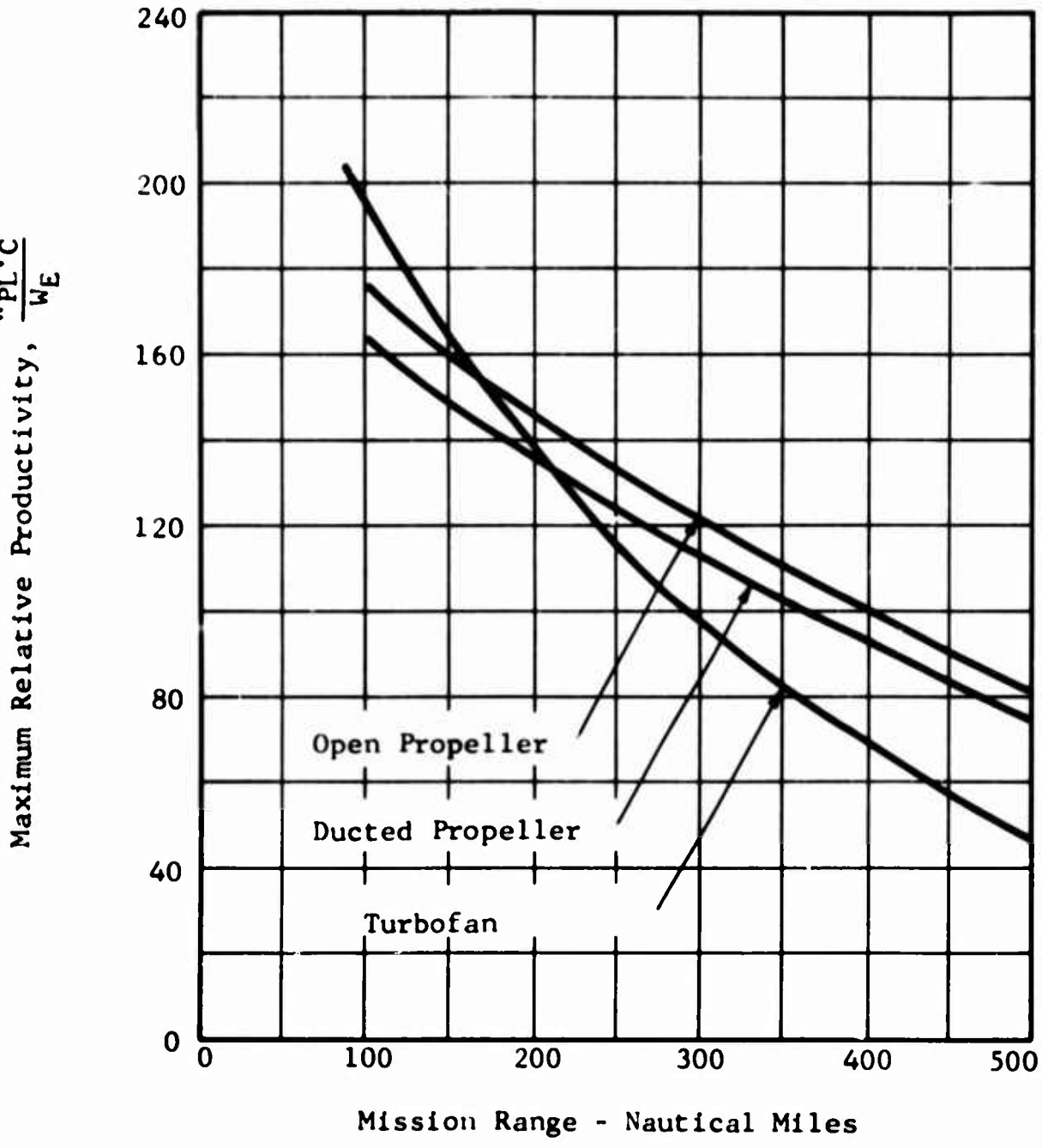

Figure 14. Maximum Relative Productivity Versus Mission Range.

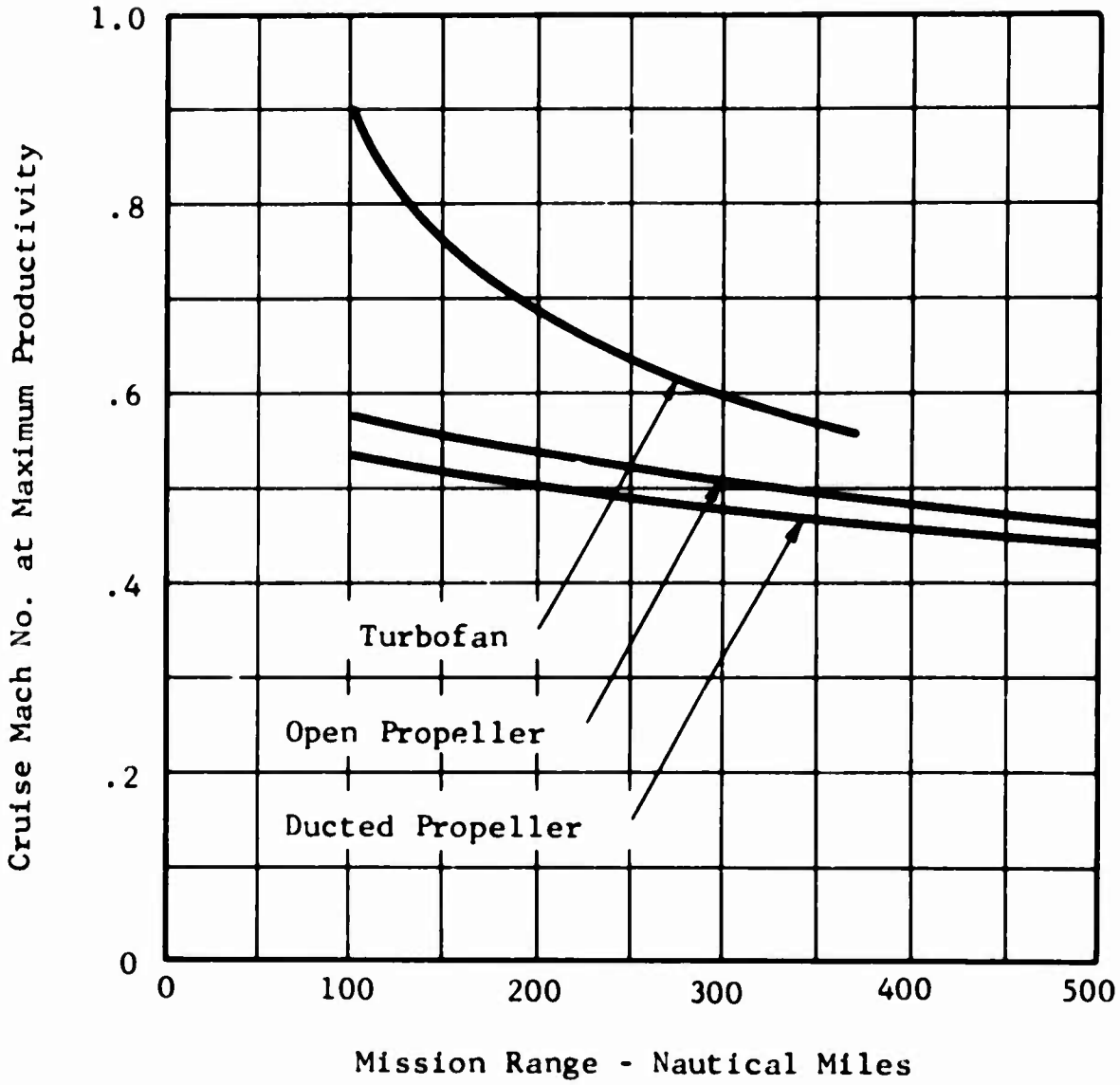

Figure 15. Cruise Mach Number at Maximum Productivity Versus Range.

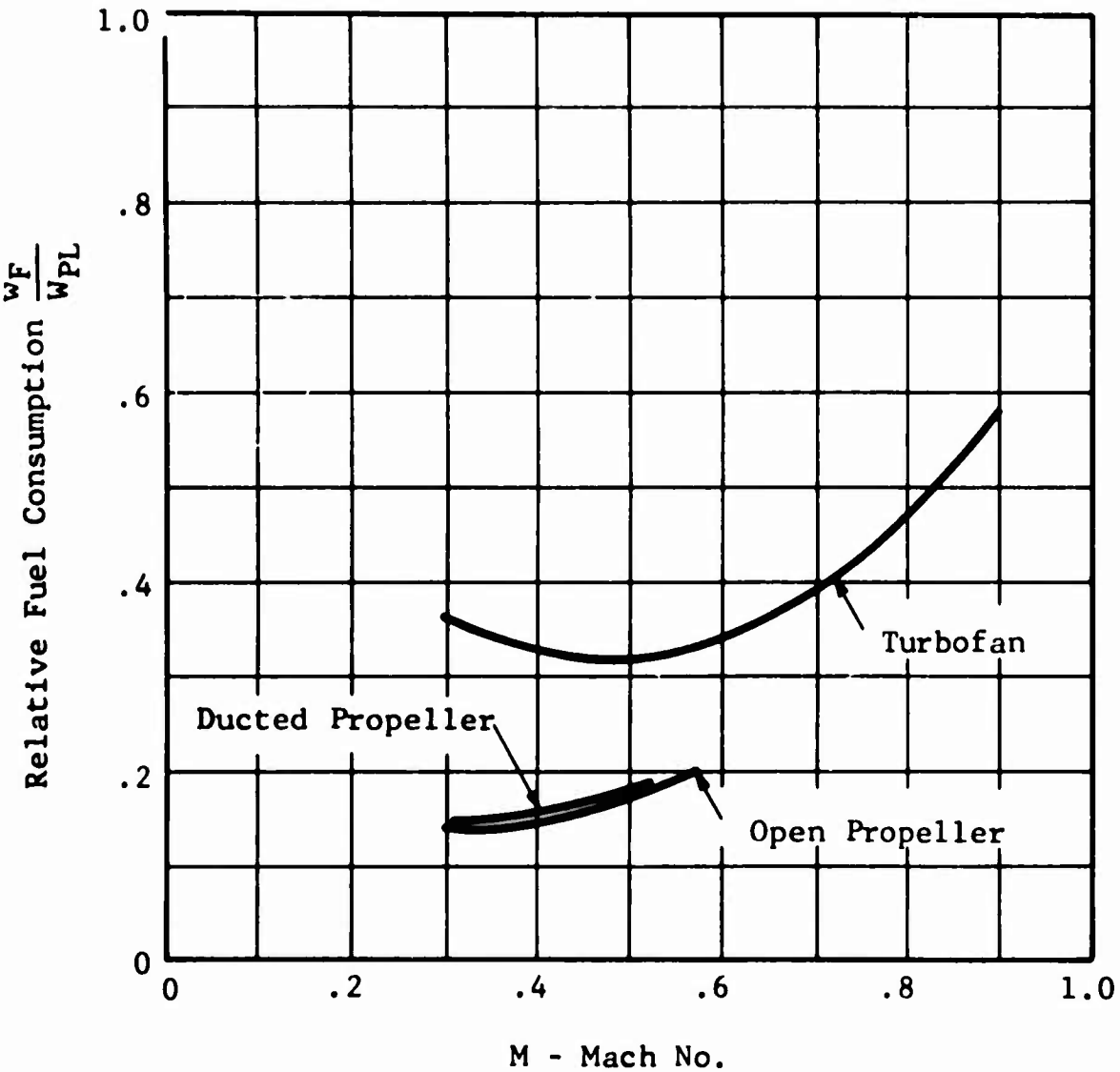

(a) R = 100 Nautical Miles

Figure 16. Relative Fuel Consumption Versus Cruise Speed.

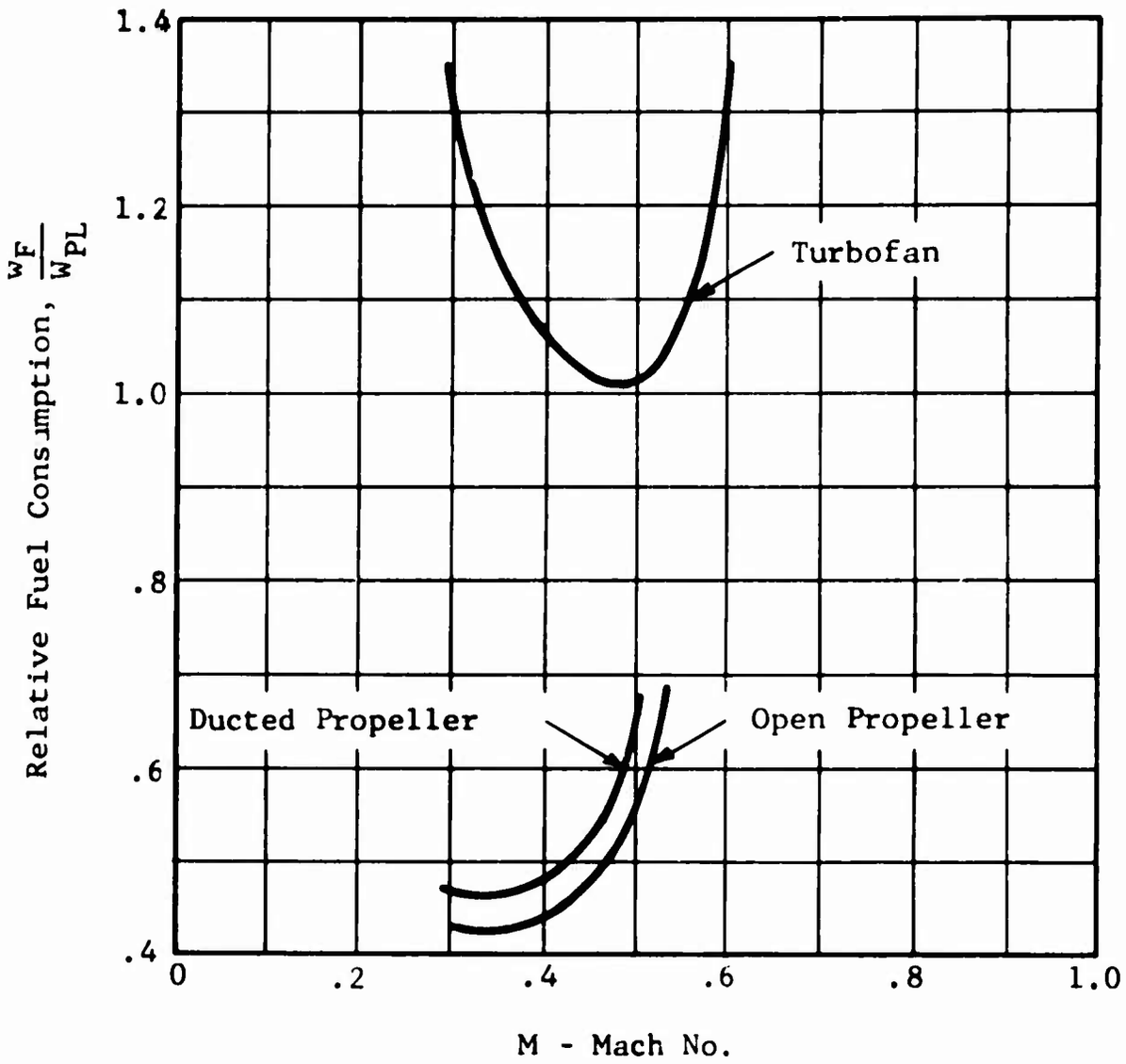

(b) R = 300 Nautical Miles

Figure 16. (Continued).

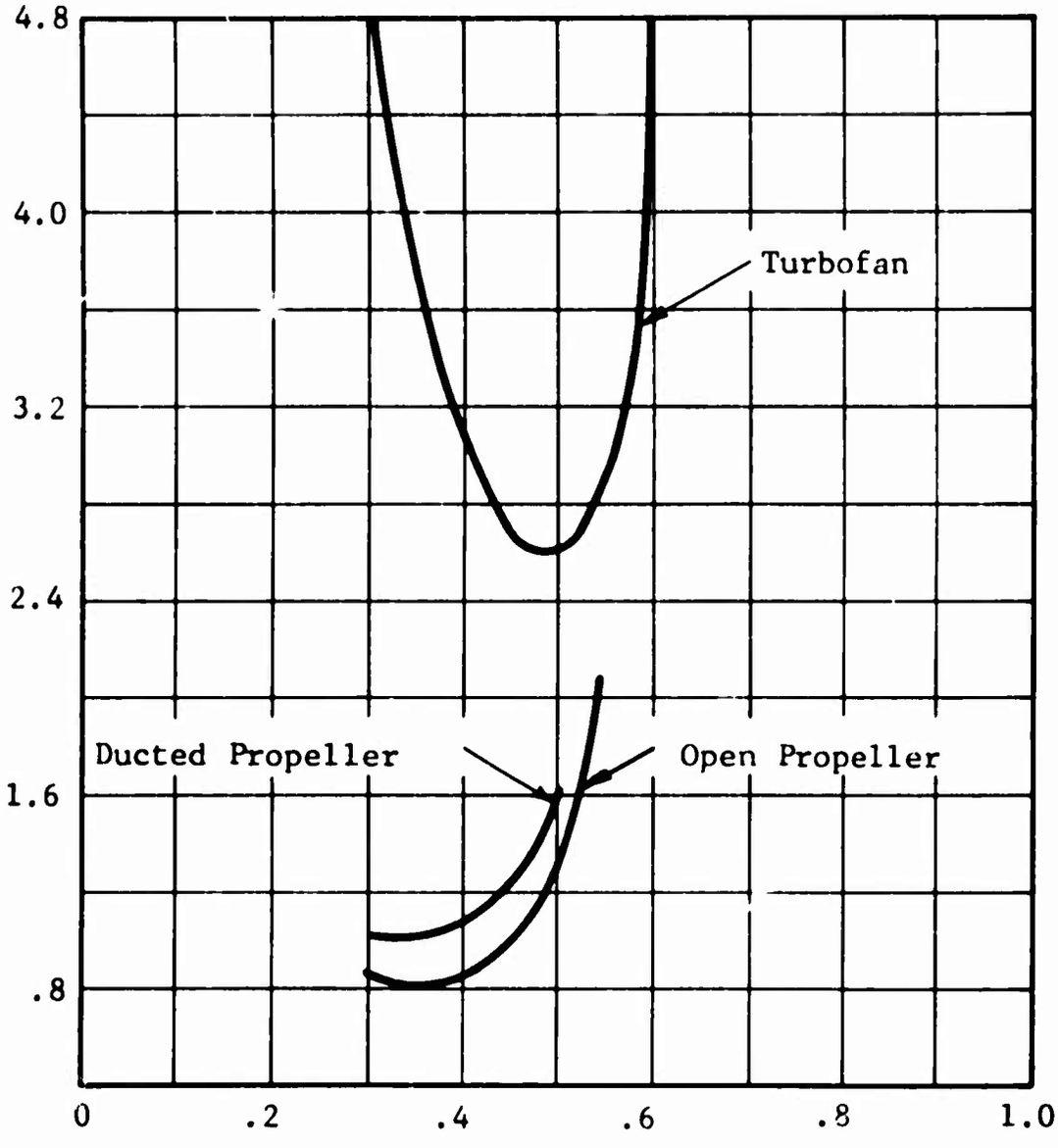

(c) R = 500 Nautical Miles

Figure 16. (Continued)

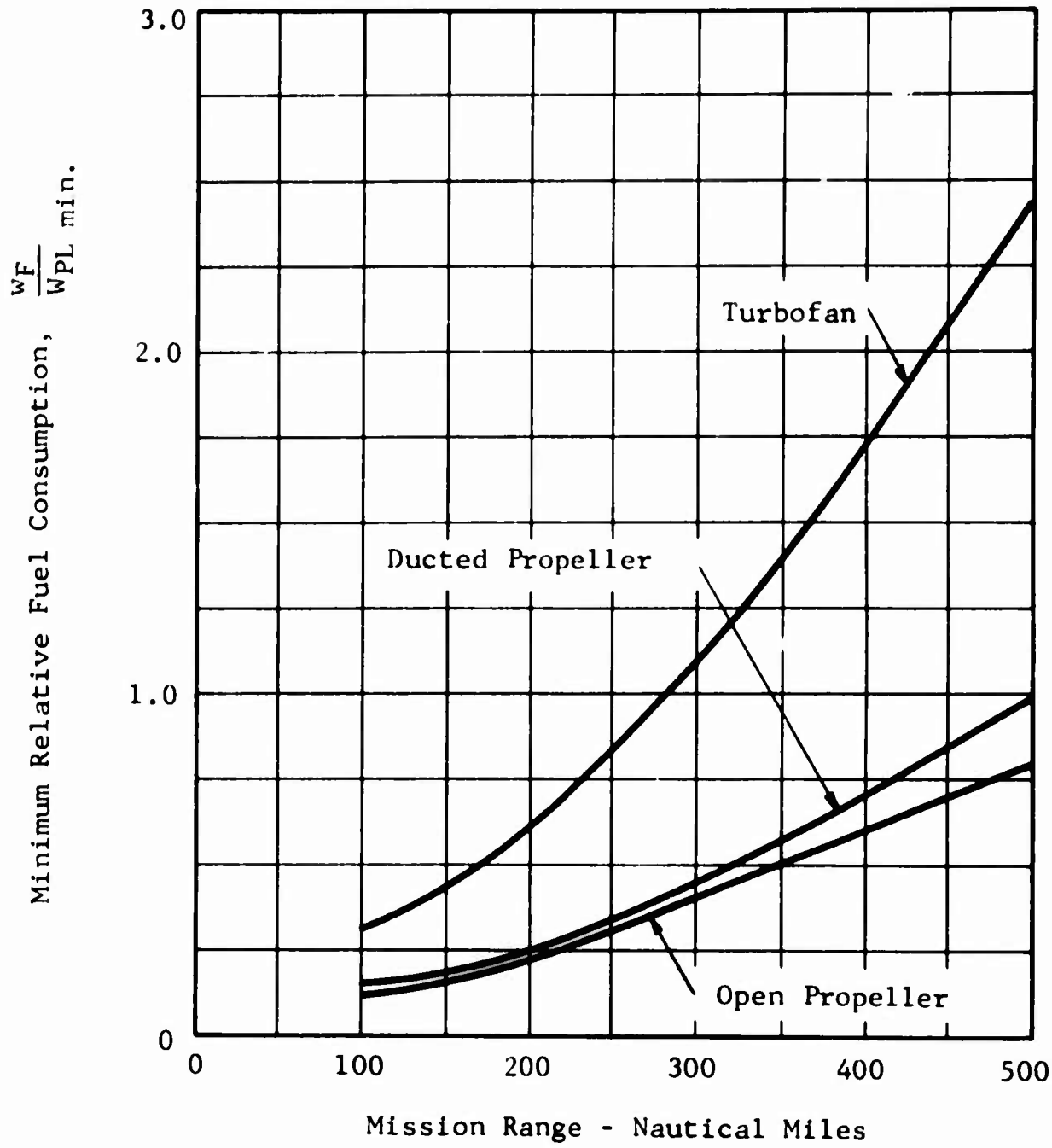

Figure 17. Minimum Relative Fuel Consumption Versus Range.

figure indicates that the minimum relative fuel consumption increases with range for each system and that the turbofan requires from two to three times more fuel than the open propeller for the values of ranges and speeds considered. Furthermore, for all three propulsion systems, the speed for the minimum relative fuel consumption is practically independent of range. This speed corresponds to M = 0.35 (231 KT) for open and ducted propeller systems and M = 0.5 (330 KT) for the turbofan system.

d. Payload to Gross Weight Ratio (W_{PL}/W_G)

Figures 18 through 20 present payload to gross weight ratio for the three propulsion systems as a function of their characteristic configuration parameters. These characteristic parameters are propeller diameter for open and ducted propeller propulsion systems and bypass ratio and the percent of the maximum available gas generator energy supplied to the fan for the turbofan propulsion system. The energy not absorbed by the fan is retained in the turbine exhaust for production of jet thrust. Since the performance of open and ducted propeller systems was based on the T64-GE-16 power plant, the energy distribution for these propulsion systems was fixed at approximately 97 percent to the propeller and 3 percent to the exhaust.

The results of Figures 18 through 20 are presented for a variety of cruise speeds and a constant range of 300 nautical miles for each system. The numerical data for ranges of 100 and 500 nautical miles are presented in tabular form in Appendix II.

Figure 18 shows the variation of payload to gross weight ratio for an open propeller propulsion system as a function of propeller diameter for constant values of cruise speeds. This figure indicates that for a constant cruise speed, the payload to gross weight ratio generally increases with increase of propeller diameter. However, the rate of increase at large propeller diameters is quite small. Furthermore, the payload to gross weight decreases with increase in

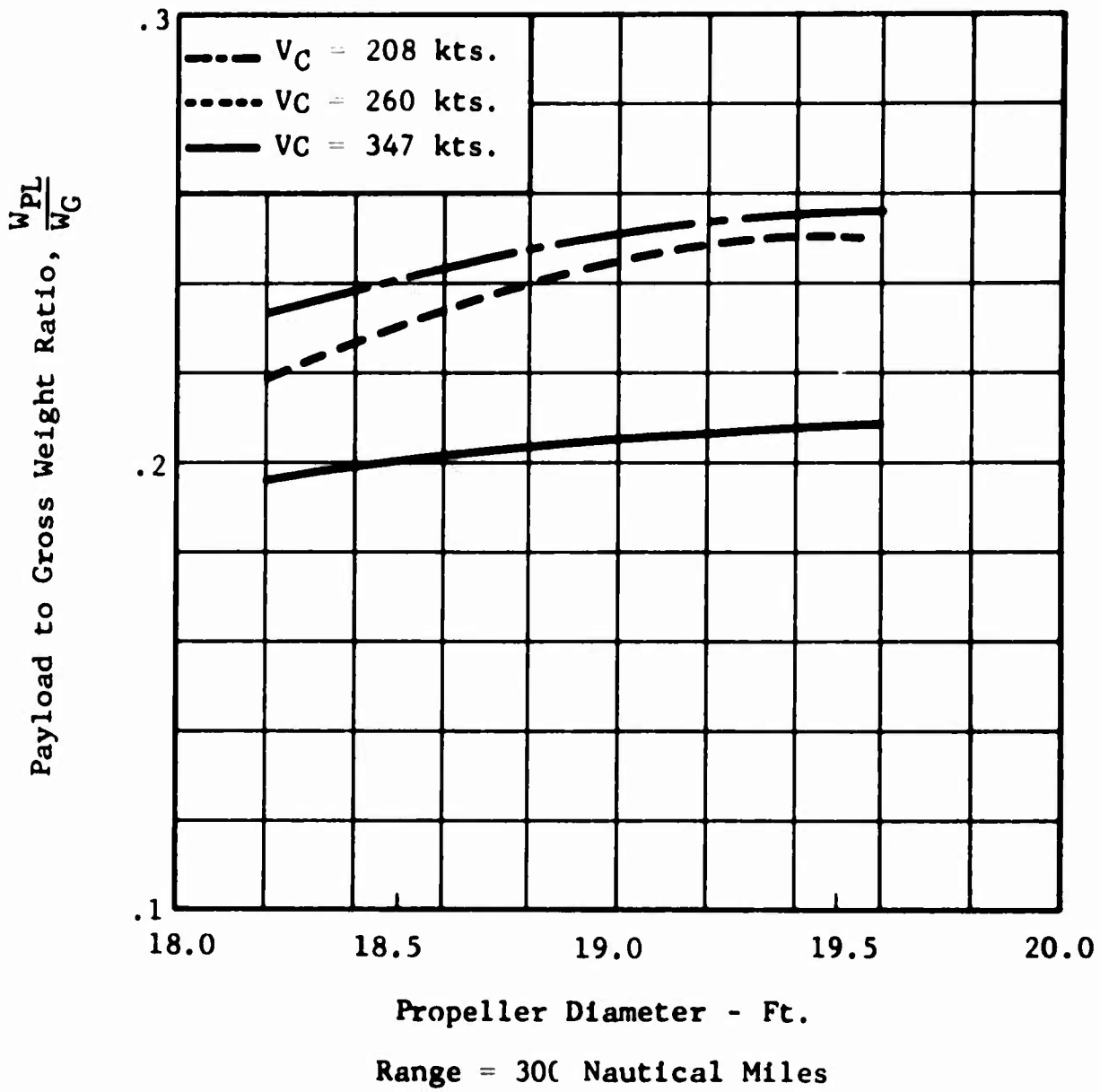

Figure 18. Payload to Gross Weight Ratio Versus Propeller Diameter - Open Propeller Propulsion System.

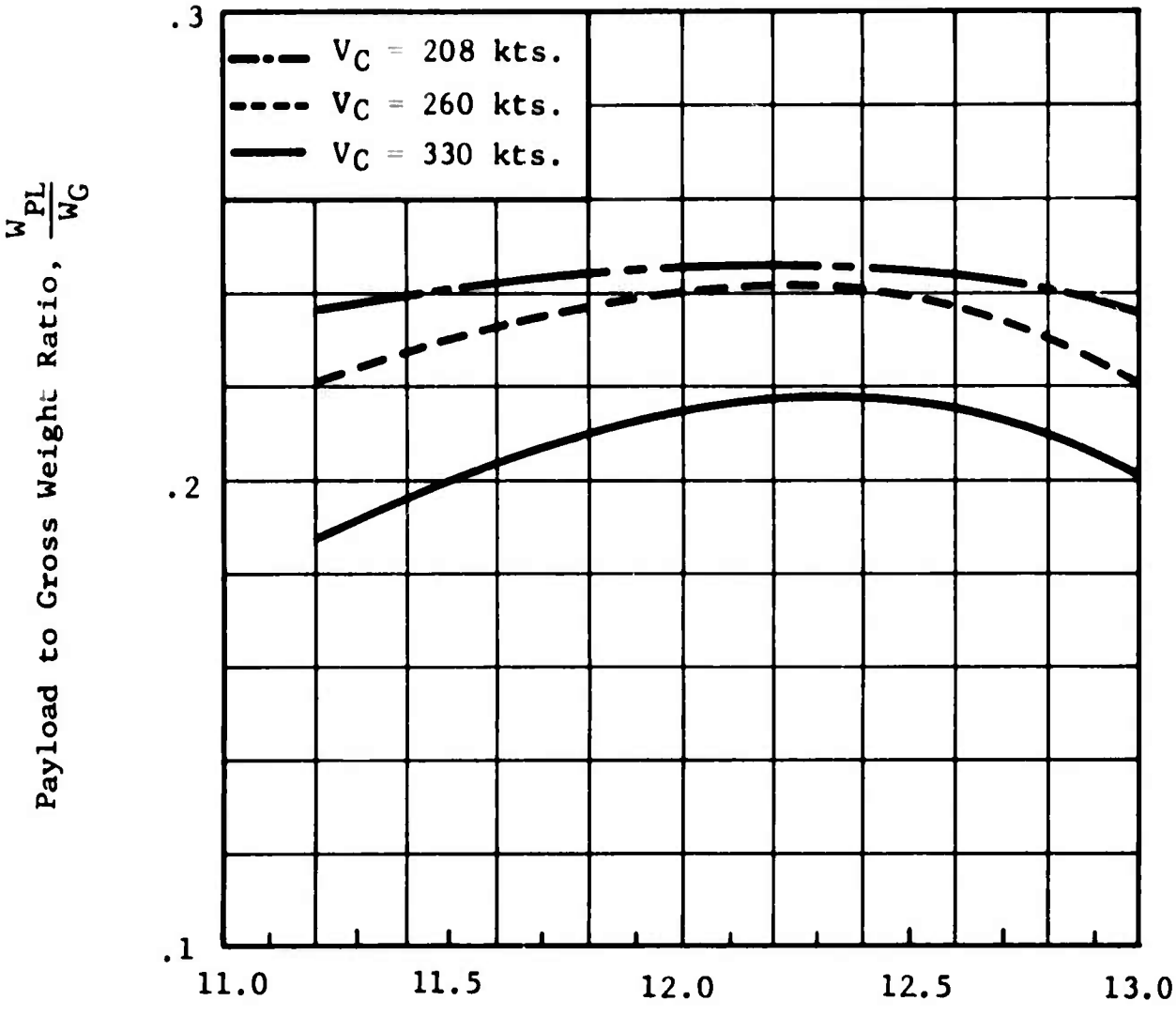

Figure 19. Payload to Gross Weight Ratio Versus Propeller Diameter - Ducted Propeller Propulsion System.

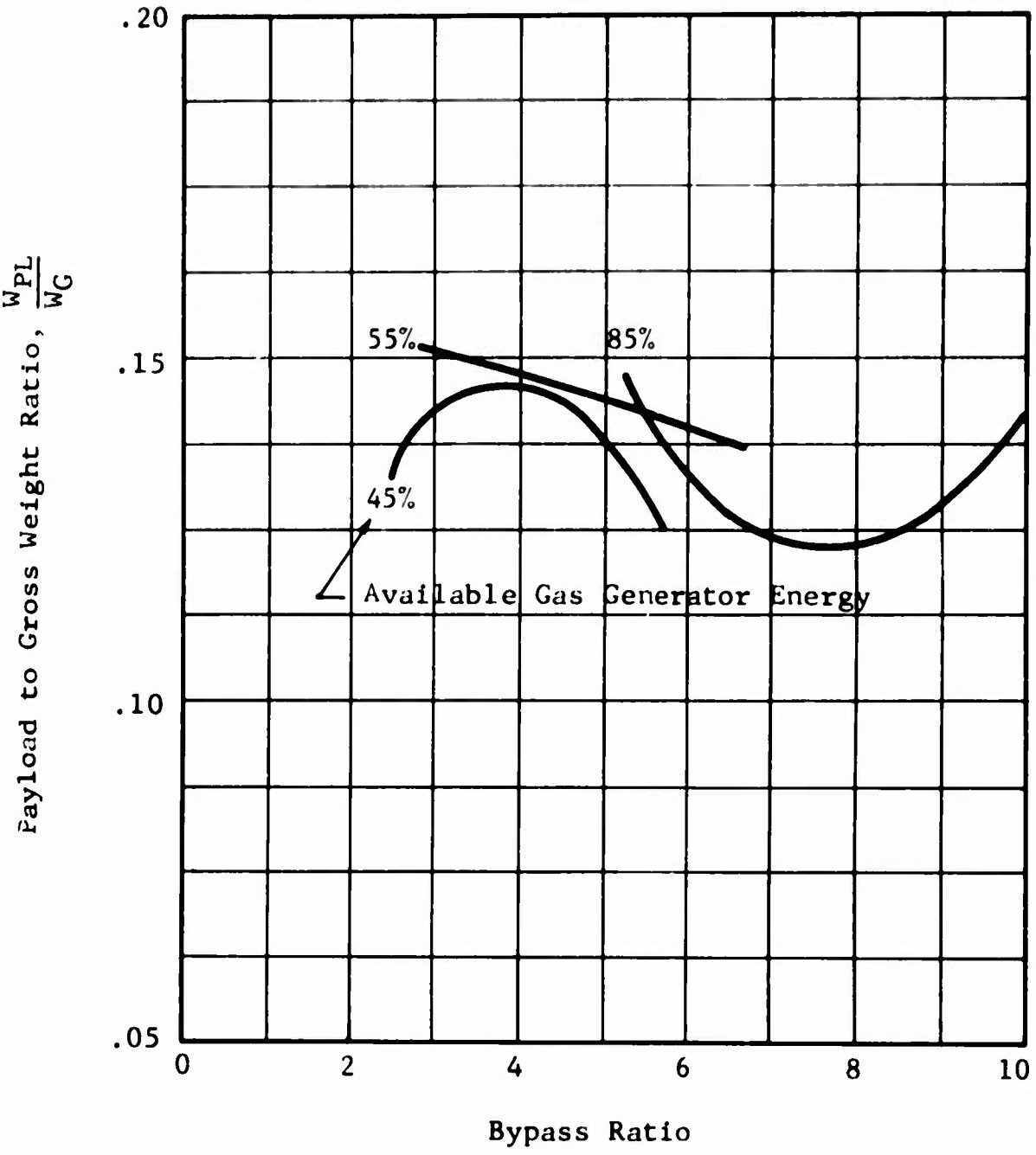

Range = 300 Nautical Miles

(a) M = 0.3

Figure 20. Payload to Gross Weight Ratio Versus Turbofan Bypass Ratio for Various Distributions of the Available Gas Generator Energy Supplied to the Fan.

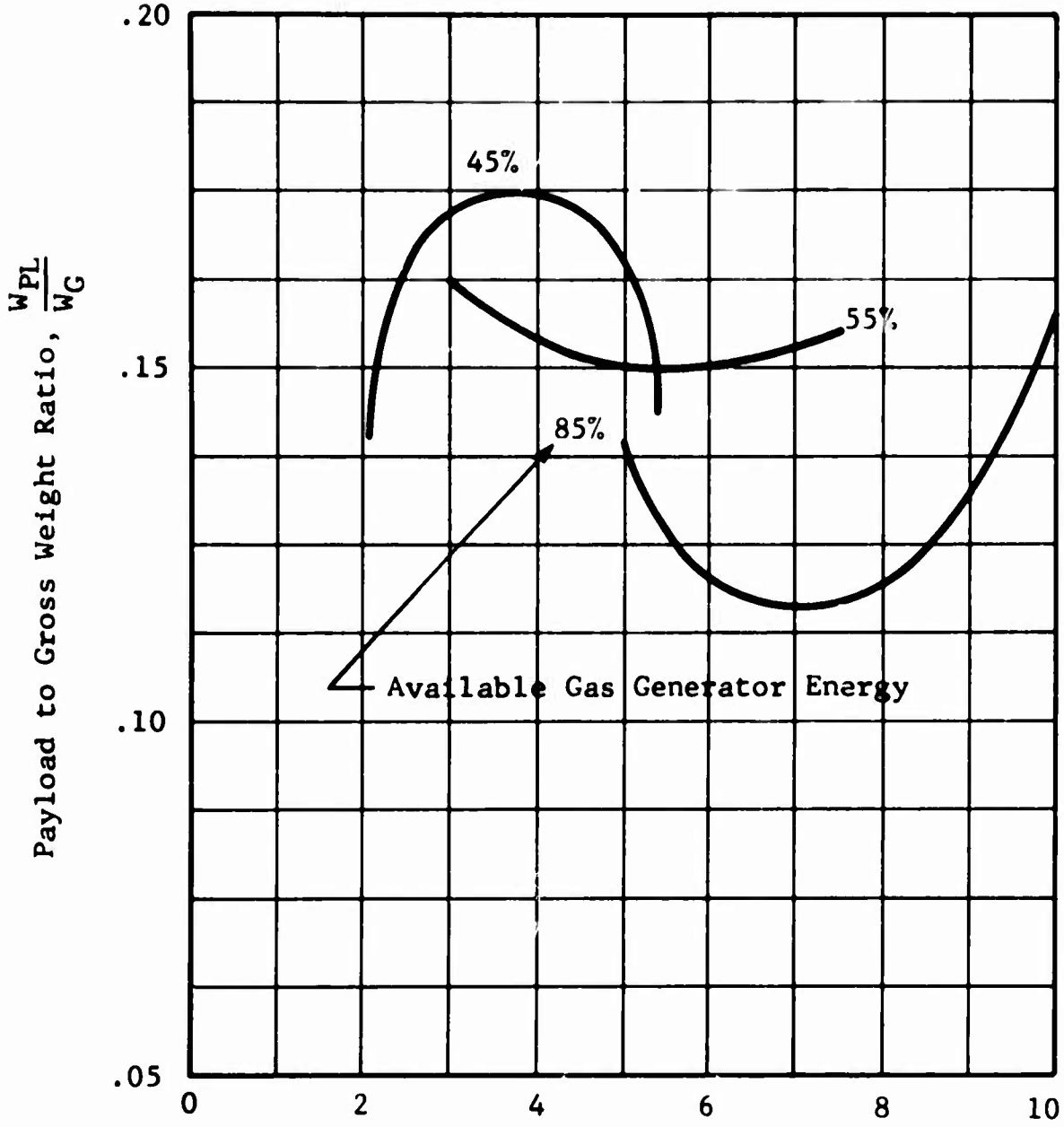

(b) M = .45

Figure 20. (Continued).

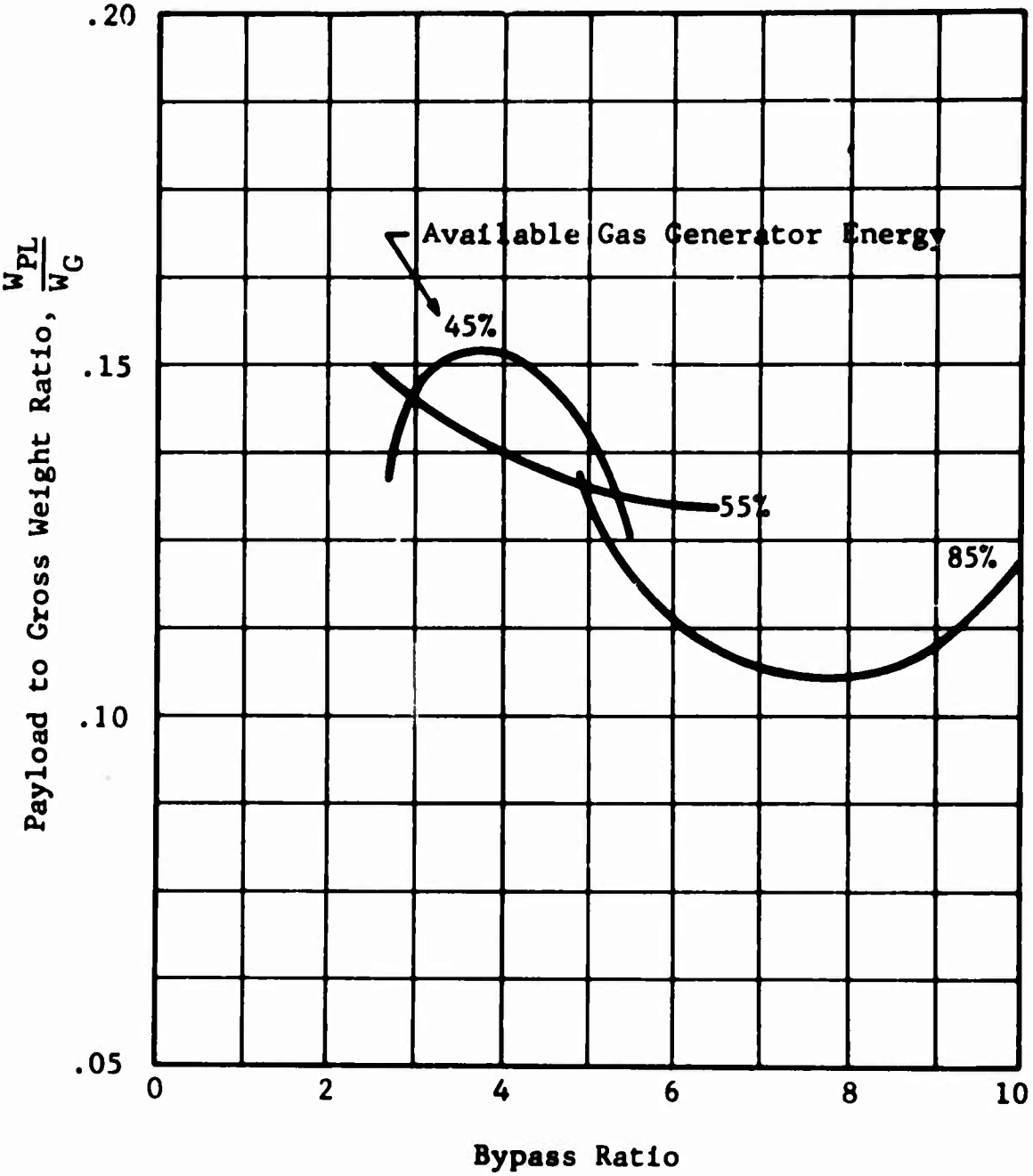

(c) M = 0.6

Figure 20. (Continued).

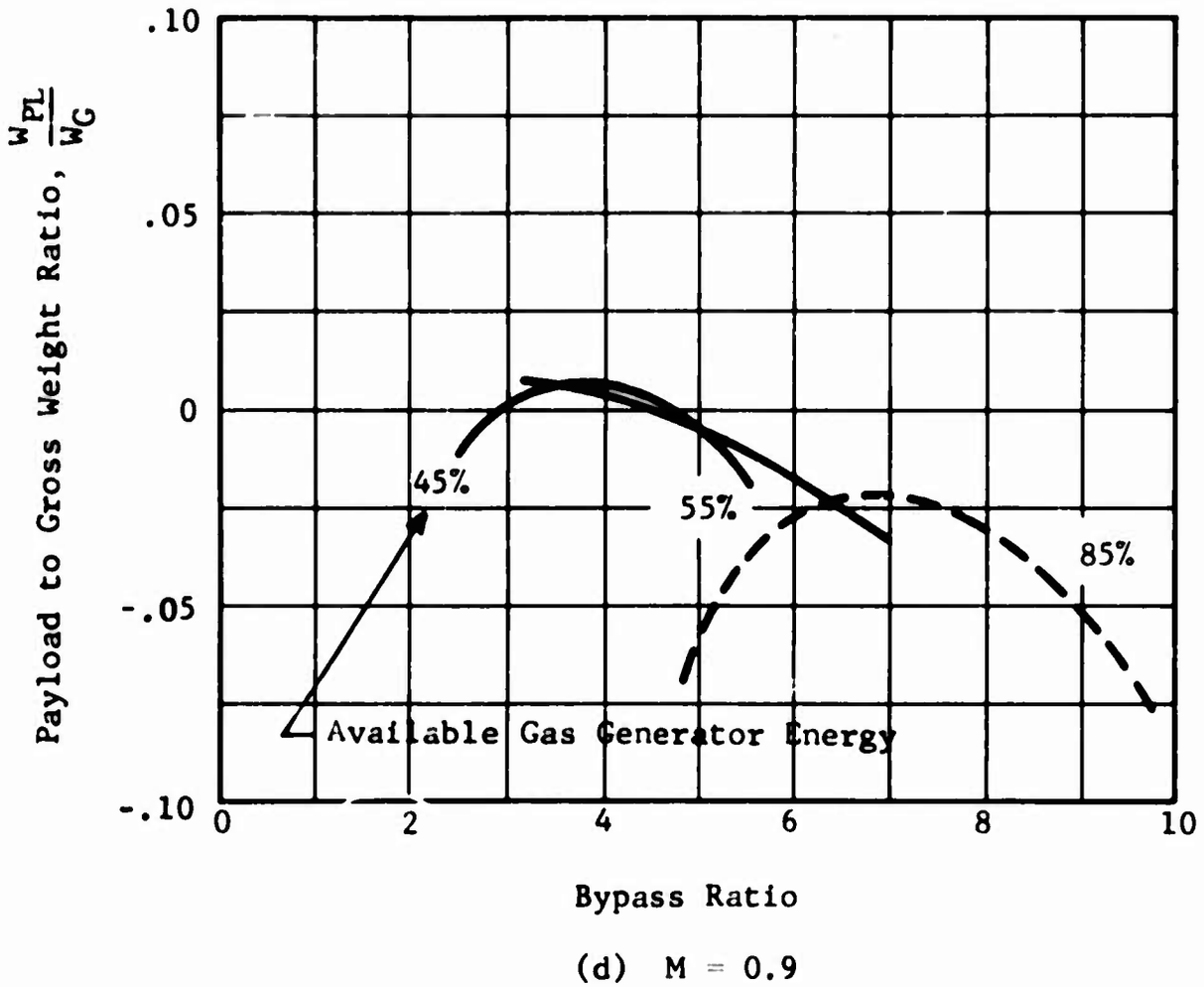

(d) M = 0.9

Figure 20. (Concluded).

cruise speed. If the results of this figure are extrapolated, it appears that a maximum payload to gross weight ratio is achievable at a forward speed of about 200 knots with propeller diameter at about 19.7 feet.

Similar trends as discussed above are indicated in Figure 19 for the ducted propeller propulsion system. In this case, the maximum value of payload to gross weight ratio is obtained with an optimum ducted propeller diameter of about 12.2 feet.

Figure 20 shows the variation of payload to gross weight ratio as a function of bypass ratio for the turbofan propulsion system. These plots are presented for constant cruise Mach numbers ranging from M = 0.3 to M = 0.9 and constant values of maximum percent of gas generator available energy delivered to the fan. Examining these plots, it can be noted that for a constant Mach number, an optimum value of payload to gross weight ratio is obtained at a bypass ratio of about 3.59 and 45 percent of the maximum available gas generator energy supplied to the fan. This corresponds to fan pressure ratio of about 1.45. It can be further noted (Figure 20b) that for this optimum configuration (i.e., at bypass of 3.59 and 45 percent energy supplied to the fan), the maximum value of payload to gross weight ratio is about 0.175, achievable at cruise Mach number of M = 0.45. As cruise Mach number increases from M = 45 to M = 0.9, the payload to gross weight ratio rapidly decreases and even becomes negative at a cruise Mach number of M = 0.9. The negative values of payload to gross weight ratios at M = 0.9 are indicative of the fact that at this cruise speed and a takeoff gross weight of 20,000 lb., the turbofan system is not capable of achieving the range of 300 nautical miles.

For other distributions of the maximum available gas generator energy supplied to the fan (i.e., 55 and 85 percent), it appears that, in general, optimum values of payload to gross weight ratio are achievable with either low bypass ratios corresponding to high fan pressure ratios, or high bypass ratios corresponding to low fan pressure ratios.

In general, the turbofan propulsion system can be optimized at any bypass ratio by establishing an appropriate distribution of the maximum available gas generator energy supplied to the fan.

2. Operational Requirements

In addition to performance evaluation, the propulsion system can be compared on the basis of the operational requirements and complexities associated with each system. Some of these requirements are discussed below.

a. Installation Effects

The installation effects are discussed in this section in terms of factors which influence performance and configuration during integration of aircraft and propulsion systems.

Concentric propulsion systems which are defined by an axial arrangement of propeller, ducted propeller, or ducted fan with gas generator, power turbine, and turbine exhaust nozzle present the lesser packaging and installation problems, as compared to non-concentric systems, thereby minimizing aircraft weight and protuberances which in turn reduce drag. Additional benefits are obtained because of propeller or fan supercharging of the basic gas generator airflow and tilting of the entire propulsion system as dictated by directly coupled components. The effects of open or ducted propeller supercharging have been included in the analysis by assuming the pressure recovery factor at the gas generator compressor inlet to be 1.0. The generalized turbofan performance data employed, Reference 8, incorporate the effects of fan supercharging, and no further corrections are warranted. Since the directly coupled components of the concentric propulsion system tilt as a unit during conversions to and from conventional and VTOL flight, the kinetic energy in the turbine nozzle exhaust is effectively utilized for both propulsion and lift. This factor is particularly important for those turbofan configurations which retain a significant portion of gas

generator available energy in the turbine nozzle exhaust.

The increment in lift from fan nacelle or duct shroud circulation is included in the analysis as a reduction in wing weight due to decreased wing area requirements. Typical wing weight reductions for the ducted propeller and turbofan propulsion systems were on the order of 2½ percent and ½ percent of gross weight, respectively.

All propulsion system configurations considered were provided with shafting so that, in the event of an engine failure, asymmetric thrust would be minimized or eliminated. Turbofan propulsion system configurations with a large portion of energy retained in the turbine nozzle exhaust will require provisions in addition to simple intershafting. Perhaps an adequate solution may be obtained with geared intershafting. This would permit the fan of the inoperative turbofan engine to operate at a higher rotational speed than that of the operative engine and thereby equalize the thrust from the fan and turbine nozzle of the operative turbofan. Admittedly, there is a definite need for further research in this problem area.

Desirability of minimum aircraft pitching moment during conversions dictated wing-mounted propulsion systems and, in addition, a wing-tip pod mounting of the turbofan propulsion system. Fuselage clearance defined the wing spanwise position of the open propeller propulsion system. Further studies are required in order to optimize the ducted propeller propulsion system spanwise wing location. The open propeller propulsion system necessitated a tilt-wing aircraft configuration in order to minimize adverse propulsion system slipstream interactions. Consideration of landing gear length for adequate ground clearance suggested a high wing location in conjunction with fuselage-mounted main landing gear.

b. Control System Complexity

The following discussion pertains to propulsion system controls and aircraft attitude controls. The latter group is included since it is affected by the particular characteristics of the propulsion system selected.

(1) Propulsion System Controls

For the open propeller propulsion system, there are two main controls operated by the pilot: the power turbine speed control and the propeller pitch control.

The power turbine output speed is controlled by a governor which activates the gas generator fuel flow rate in order to maintain the selected speed.

The propeller pitch mechanism controls the propulsion system thrust. A change in propeller pitch produces a change in power turbine speed due to the variation in torque. The power turbine speed governor then senses a discrepancy between the value selected by the pilot and that of the actual power turbine. The governor changes the gas generator fuel flow rate and thus the rpm, in order to maintain the constant value of selected speed (N_2) at the new thrust level.

The ducted propeller propulsion system is controlled in the same manner as the open propeller except for the shroud exit area. The shroud exit area can be varied by a pilot-operated two-position switch control.

Control of the turbofan propulsion system is less complex in that there is no fan pitch change mechanism. The pilot's power turbine speed control is the primary thrust control. A change in selected value of the pilot's speed control is sensed by the speed governor, which causes an appropriate adjustment of the gas generator

fuel flow rate in order to establish the desired power turbine output speed. A change in output speed reflects a change in turbofan thrust.

(2) Aircraft Controls

Lateral maneuvers are accomplished by differential thrust in the static condition and aileron deflection in forward flight for all propulsion systems.

In hover, directional motion is provided by application of differential aileron deflection for the open propeller and ducted propeller propulsion systems. Turbofan propulsion system directional control may be achieved by either of two methods: a variable pitch auxiliary fan or a pitch nozzle thrust. The first method would require auxiliary fan shafting coupled directly with the intershafting between the main propulsion systems. The second method would necessitate compressor bleed air to be delivered to reaction nozzles. Either control device would be located at the fuselage afterbody. Directional control in level forward flight is achieved through conventional rudder deflection.

Longitudinal control during static conditions is accomplished by means of a combination of monocyclic propeller pitch and flap deflection for both open and ducted propeller propulsion systems. For the turbofan propulsion system, this control is achieved by a reaction nozzle or a variable pitch auxiliary fan located in the fuselage afterbody. In level forward flight, longitudinal control is achieved through conventional elevator deflection. When two or more control systems are feasible, detailed trade-off studies should be conducted in order to determine the optimum control system for a particular application.

c. Deicing Requirements

Deicing requirements for the three propulsion systems can be accounted for as additional increments in weight of the systems. For propeller deicing, this weight increment is on the order of 1½ percent of the propeller weight. For ducted propellers, the additional weight required by the electrical heating wires imbedded in the duct inlet and struts is generally negligible. This is also true for the deicing of the bellmouth entry of ducted fans. The ducted fan inlet struts are deiced by compressor bleed which is integrated into the engine design and hence does not represent an increase in weight. However, for this propulsion system there is an increase in weight due to the power cable from the engine generator to the duct inlet and the associated control wiring. For remote engine locations, such as on the X-22A, this may amount to 2 to 3 percent of the duct weight. Since this increase in weight is expected to be within the accuracy of the weight trends (±5%), it is considered to be of secondary importance.

d. Noise

The classical Gutin propeller noise theory is still a reliable means for defining far-field propeller noise at zero airspeed. Reference 2 has presented a nomograph procedure for noise estimation restricted to static propellers. Calculations employing this nomograph procedure based on the open propeller propulsion system considered in the comparative study indicated noise levels of 102 decibel at a distance of 200 feet.

For a propeller operating at a given forward speed, a method for calculating the sound pressure field has been presented in References 20 and 21. The complexity of this method necessitates the use of a high speed digital computer and is beyond the scope of this report.

For ducted propellers the following noise information was obtained from the test data of Reference 22:

(1) The maximum total sound pressure for a two-bladed shrouded propeller will vary from one-half to twice the pressure of an unshrouded propeller.

(2) Minimum noise occurs when the flow on the shroud surface is unseparated, while separated flow will cause maximum noise.

(3) An appreciable reduction of maximum total sound pressure may be achieved by an increase in the number of blades.

Turbofan noise levels in hover and cruise modes are presented graphically in Reference 14 as a function of bypass ratio. These levels are based on inlet and exhaust noise. The former has been determined experimentally while the latter is based on Lighthill's jet parameters, which have been verified by the experimental data. Inlet noise levels at zero airspeed varied from 110 decibels at a bypass ratio of 3.0 to 99 decibels at a bypass ratio of 12.0. Exhaust noise varied from 112 to 102 decibels, while total noise level varied from 116 to 105 decibels. For the cruise flight regime, total noise level remained fairly constant at 122 decibels for all bypass ratios.

e. Exit Velocity

A number of theoretical methods are available for predicting slipstream velocities in the wake of an open propeller or a ducted propeller (see Appendix I). For the purpose of this discussion, a simple momentum approach is considered to be adequate to determine the exit velocities of open and ducted propeller propulsion systems considered.

Performing the required numerical computation, it can be shown that the open propeller propulsion system having a disc loading range of 33.5 to 37.2 lb./ft.^{2}

induces lowest wake velocities of approximately 168 to 177 ft./sec., respectively, as compared to ducted propeller or turbofan propulsion systems.

The ducted propeller exit velocities varied from approximately 178 to 201 ft./sec. for a disc loading range between 75.3 to 96.3 lb./sq. ft., respectively.

The exit velocity for the turbofan propulsion system can be directly obtained from the results of Figure 21. This figure shows that the turbofan exit velocity is a function of bypass ratio and the gas generator energy distribution delivered to the fan. Specifically, the turbofan exit velocity decreases with increase of bypass ratio for constant percent of the gas generator energy distribution to the fan.

Furthermore, for a constant bypass ratio, the exit velocity increases with increase of gas generator energy supplied to the fan.

At a bypass ratio of 2.73 and 45 percent of the gas generator energy distribution delivered to the fan, Figure 21 yields the exit velocity of 1143 ft./sec. for the turbofan propulsion system considered.

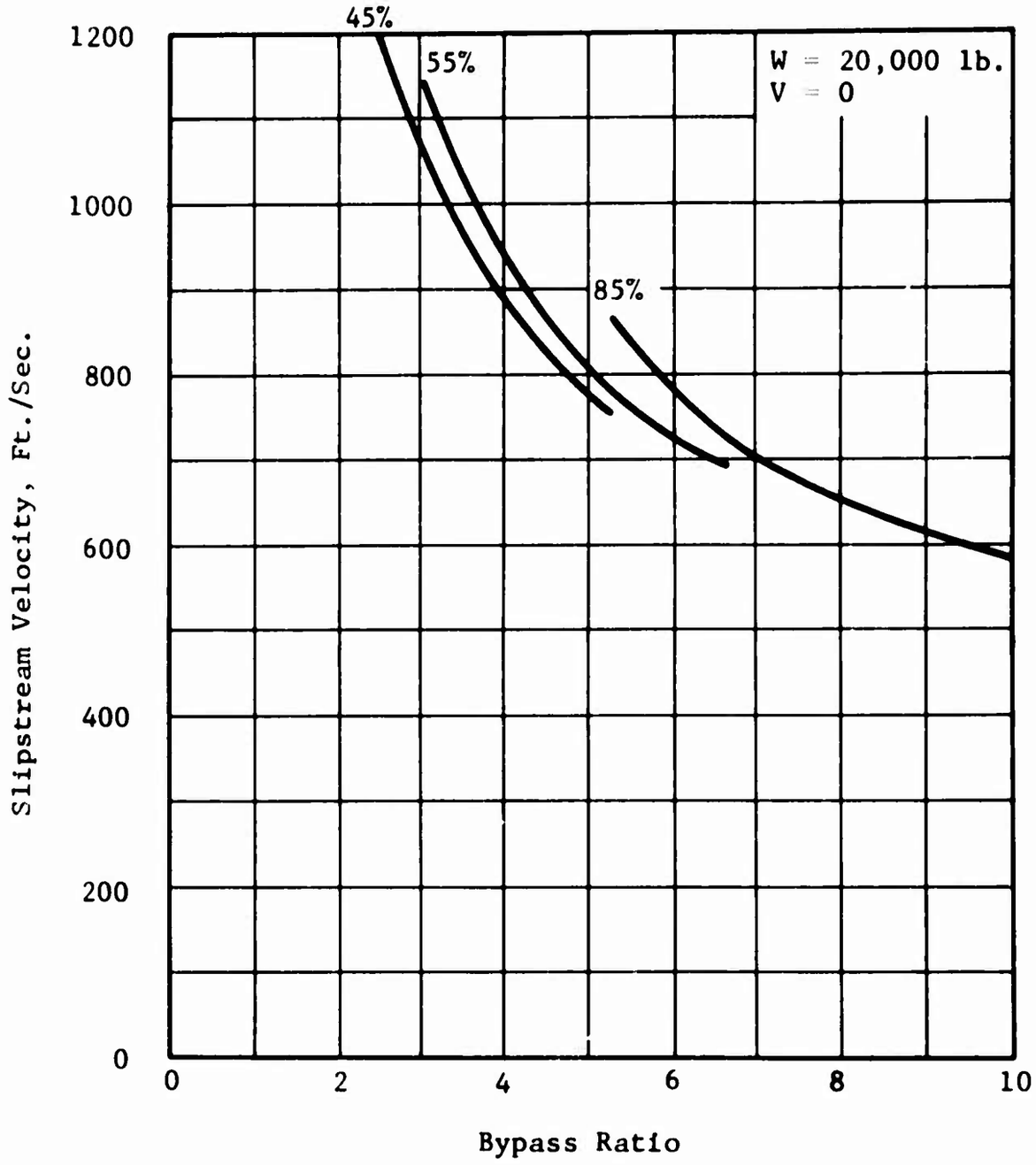

Figure 21. Turbofan Propulsion System Slipstream Velocity Versus Bypass Ratio for Various Distributions of Gas Generator Available Energy Delivered to the Fan.

V. APPLICATION STUDY

An application study was conducted for the open propeller, ducted propeller, and turbofan propulsion systems based on a selected mission profile. The results are compared in terms of relative productivity, fuel consumption, weight, static thrust margin, maximum speed, and general configuration characteristics. A method is developed for selection of the optimum propulsion system for the specified mission.

A. CRITERIA FOR SYSTEMS EVALUATION

1. Methodology

The vehicle gross weight was assumed to be 20,000 lb initially for each propulsion system. The same aircraft configuration and parameters employed in the comparative evaluation were retained for the application study. Each propulsion system configuration was selected based on the optimum performance obtained in the comparative study. A propeller static disc loading of 37.2 and 88.5 p.s.f., respectively, was selected for the open and ducted propeller propulsion systems in conjunction with the T64-GE-16 turboshaft engine. A bypass ratio of 3.6 and 45-percent design maximum distribution of available gas generator energy defined the turbofan propulsion system. The vehicle gross weight for each propulsion system was established through iterative calculations based on a payload of 2500 lb. and selected mission profile. Performance and group weights were calculated based on methods which were described within the comparative study section of this report. The assumptions used in establishing mission fuel requirements were the same as those employed in the comparative evaluation except for reserve fuel allowance, which was reduced to 5 percent of initial fuel. A layout sketch of the final geometry of each integrated vehicle-propulsion system was then constructed.

2. Mission Analysis

The application study of the three propulsion systems was based on a specific mission profile which incorporated the following segments:

a. Hover 5 minutes at 6000 ft., 95°F atmosphere.

b. Loiter 20 minutes at standard sea level atmosphere.

c. Combat 20 minutes at standard sea level atmosphere.

d. Cruise 100 nautical miles at standard sea level atmosphere.

The above mission profile did not include values of cruise, combat, and loiter speeds. In order not to adversely affect any of the propulsion systems, a basis of comparison was developed which established the cruise and combat speeds for each propulsion system as a percentage of that speed which resulted in maximum relative productivity. Also, it was evident that the optimum system could be chosen immediately based on the results of the comparative study, if the mission loiter, cruise, and combat speeds were the same for each propulsion system.

The speed for maximum relative productivity established as a function of range in the comparative study is herein defined as the optimum cruise speed. The optimum cruise speed during combat endurance and the equivalent combat range were calculated in the following manner. Values of equivalent combat range were calculated based on the product of the specified combat endurance time and assumed values of combat cruise speed. Then combat cruise speed was plotted as a function of equivalent range on the graph expressing optimum cruise speed as a function of range (see Figure 15). The optimum combat-endurance speed and the equivalent combat range were established at the point where the two curves intersected.

The mission cruise speed was selected as 80 percent of the optimum speed at the particular mission range of 100 nautical miles, while the combat cruise speed was chosen as 100 percent of the optimum speed at the specified mission endurance of 20 minutes. Loiter speeds were selected at Mach number of $M = .2$, $M = .25$, and $M = .3$, respectively, for the open propeller, ducted propeller, and turbofan propulsion systems.

The mission cruise speed was made lower than the optimum speed in order to trade off productivity for lower vehicle weight. Loiter speeds were based on estimates of speed for minimum fuel consumption for the open and ducted propeller propulsion systems, whereas the turbofan speed was selected as the lowest speed for which the turbofan performance data were available.

B. RESULTS OF THE APPLICATION STUDY

Comparative vehicle mission performance for the open propeller, ducted propeller, and turbofan propulsion systems is presented in bar chart illustrations of relative productivity (Figure 27) and vehicle weight and weight distributions (Figure 23). A tabular numerical comparison of vehicle weight and weight distribution is also included (Table IX). Finally, sketches of configuration layout for the integrated aircraft propulsion system vehicles are presented in Figures 24 through 26.

1. Performance and Weights

Figures 22 and 23 indicate that the turbofan propulsion system provides the best relative productivity of $W_{PL}\ V_B/W_E = 64$, while requiring 100 percent more fuel and 20 percent higher empty weight than the open propeller and ducted propeller propulsion systems. The relative productivity of the open propeller propulsion system is 2 percent lower than that of the turbofan propulsion system, compared to a 12-percent reduction for that of the ducted propeller propulsion system.

The available static thrust margin at the design gross weight and 6000 ft. - 95°F atmosphere is 22, 27, and 10 percent for the open propeller, ducted propeller, and turbofan propulsion systems, respectively.

Maximum sea level Mach number is M = .93 for the turbofan, M = .58 for the open propeller, and M = .53 for the ducted propeller, based on power or thrust limitations.

2. Configuration Layout Sketches

Configuration layout sketches shown in Figures 24 through 26 provide qualitative installation comparison and give further

TABLE IX

WEIGHT COMPARISON OF INTEGRATED PROPULSION SYSTEMS, lb.

Description	Propulsion System		
	Turbofan	Ducted Propeller	Open Propeller
Design Gross Weight	20048	15819	15596
Empty Weight	12488	10567	10321
Propulsion System Weight	4528	4246	3792
Engine Installation Weight	155	162	162
Equipment & Structural Weight	7959	6159	6367
Useful Load	7561	5252	5275
Crew	400	400	400
Oil & Residual Fluids	150	150	150
Fuel	4511	2202	2225
Payload	2500	2500	2500
Propulsion System Group Weights	4528	4247	3793
Engine Weight		1412	1412
Propeller Weight		676	1310
Shroud Weight		1353	-
Drive System Weight		544	808
Controls & Starting System		100	100
Fuel System Weight	268		

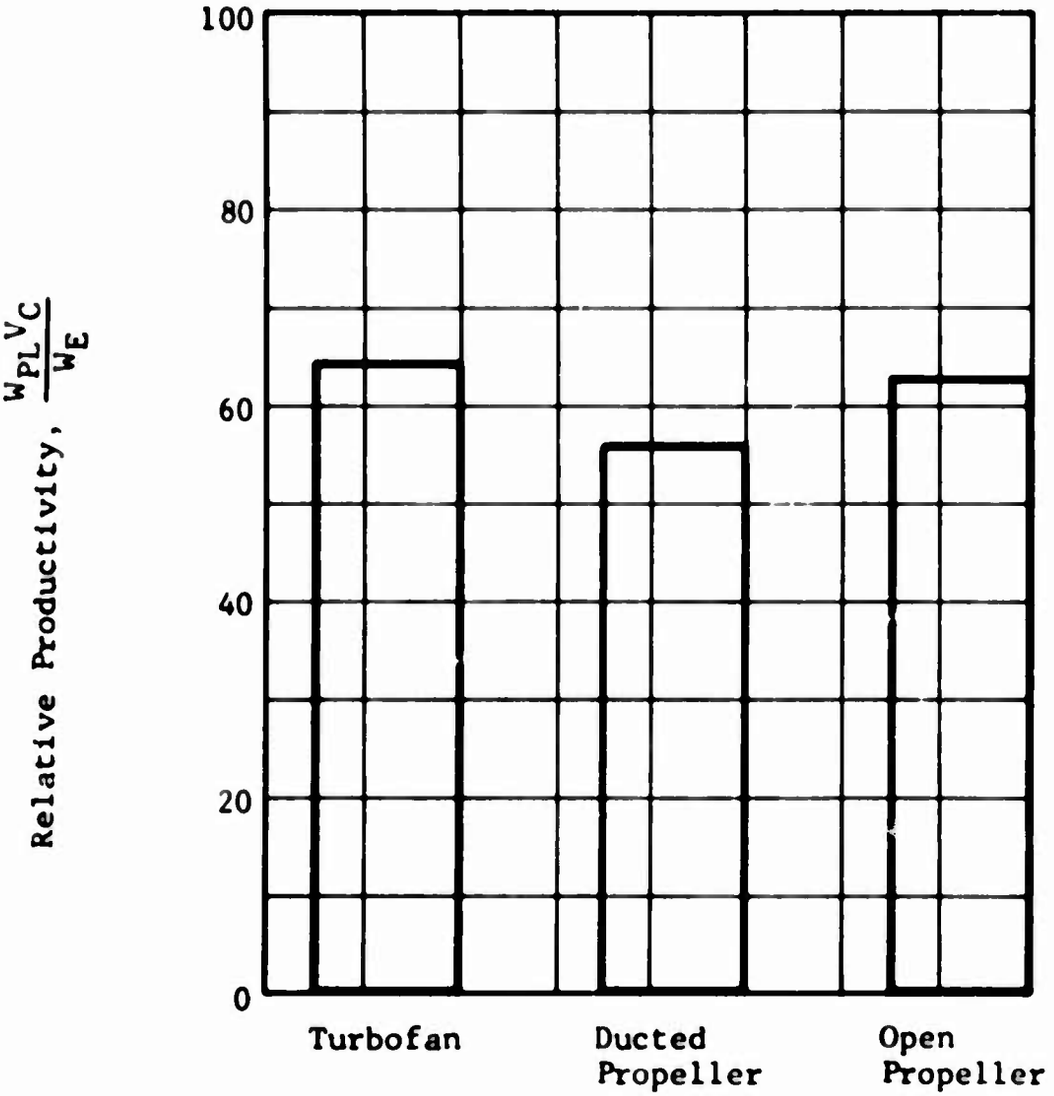

Figure 22. Relative Productivity of Three Propulsion Systems.

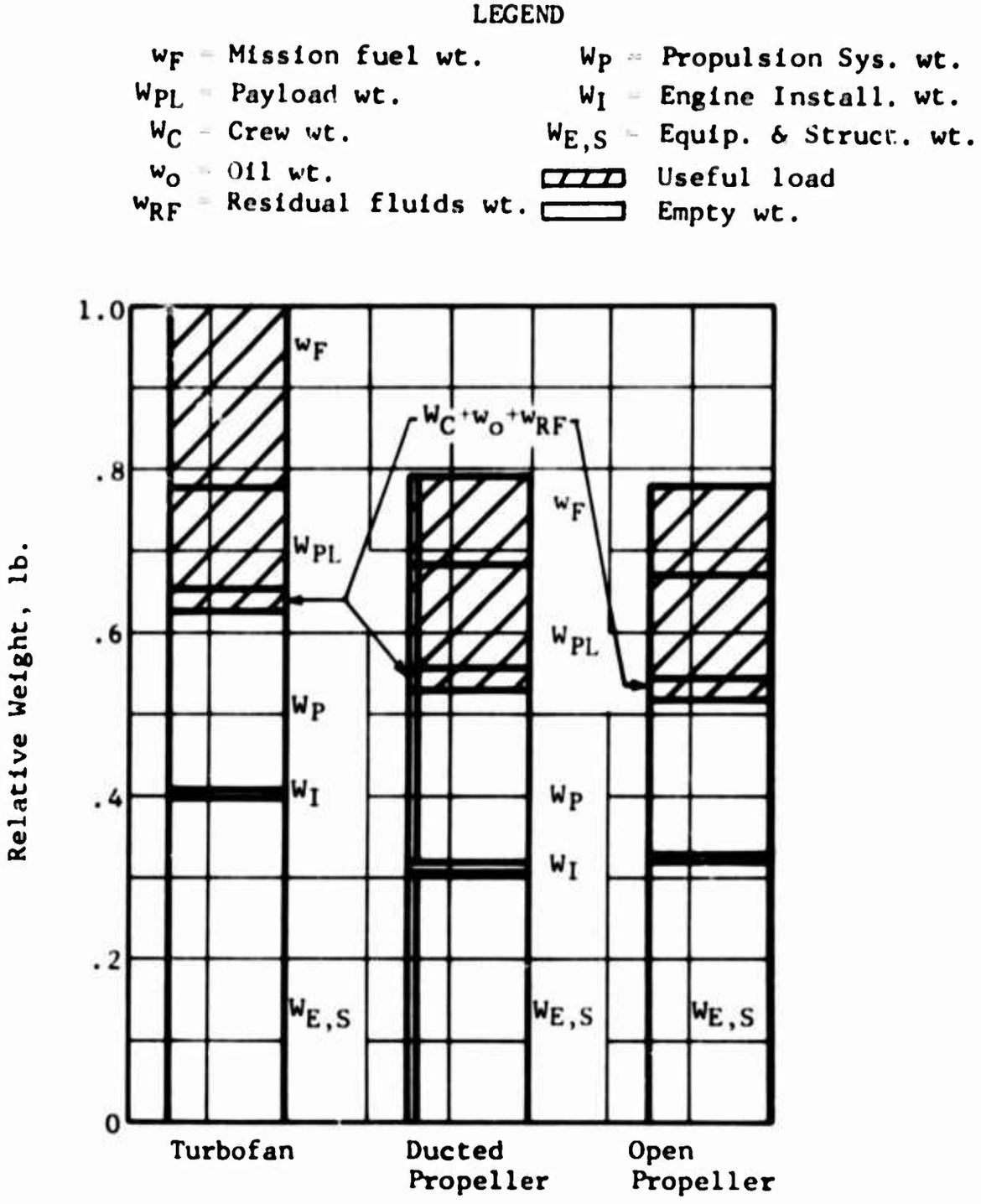

Figure 23. Relative Weight of Three Propulsion Systems.

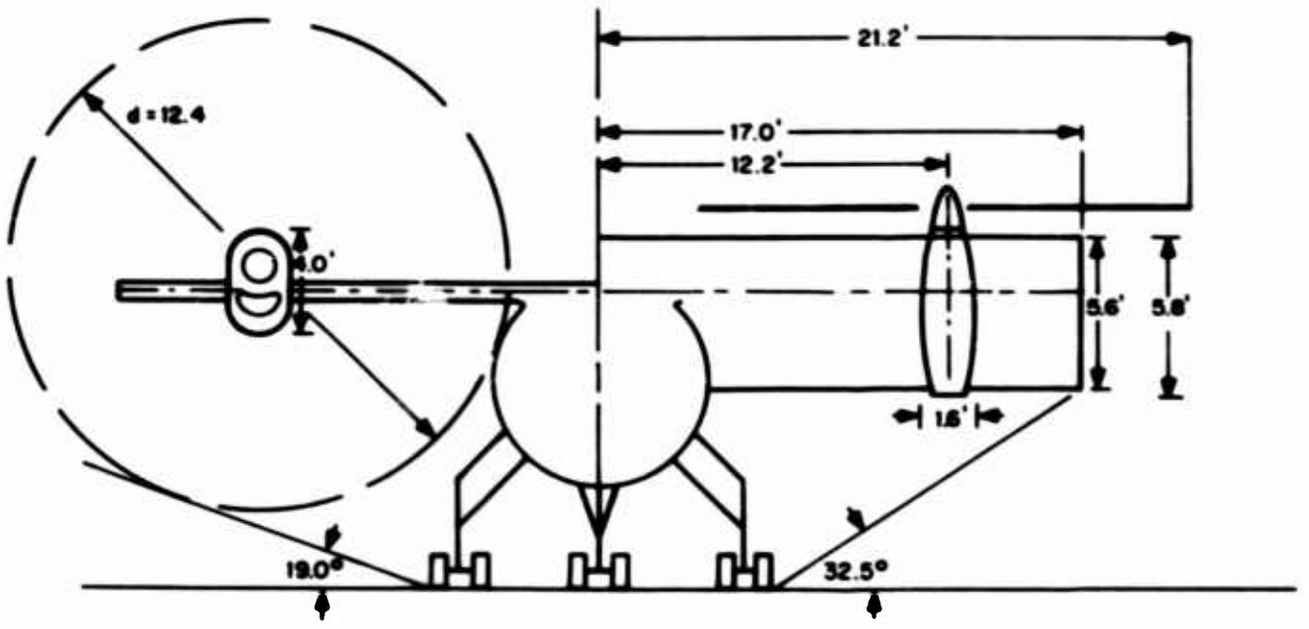

W_G = 15,596 lb.

Figure 24. Open Propeller Propulsion System Aircraft Integration Configuration.

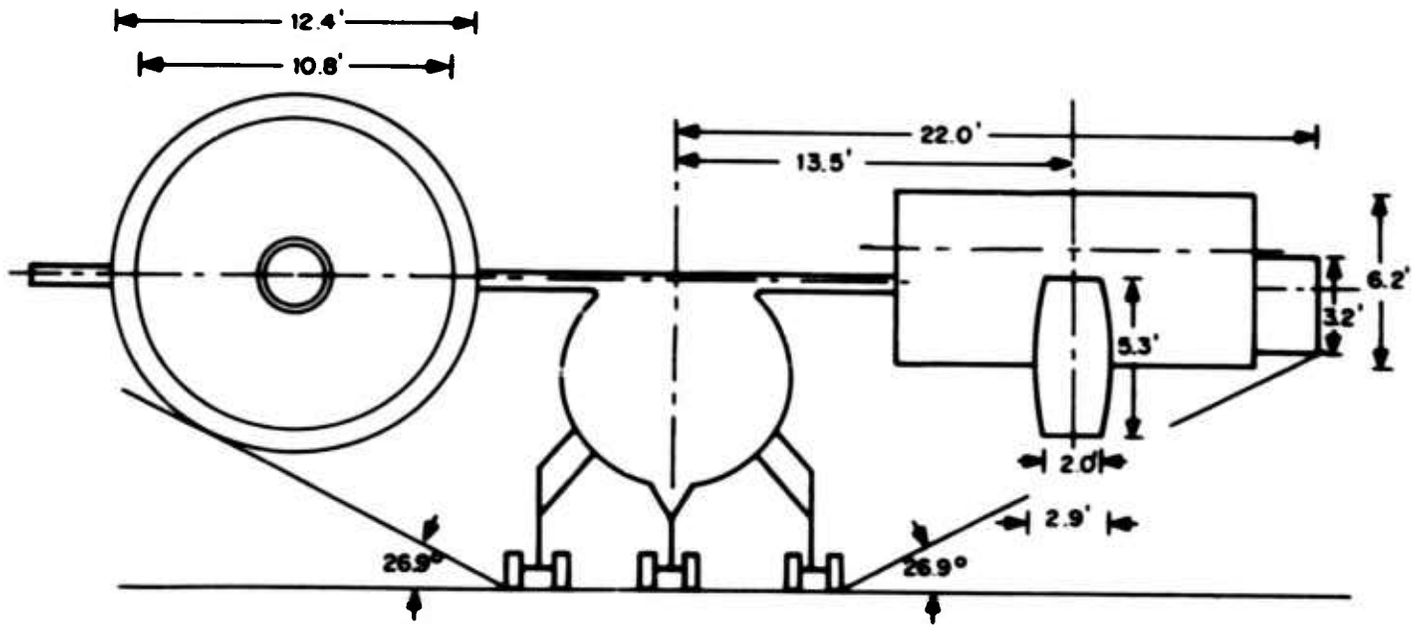

W_G = 15,819 lb.

Figure 25. Ducted Propeller Propulsion System Aircraft Integration Configuration.

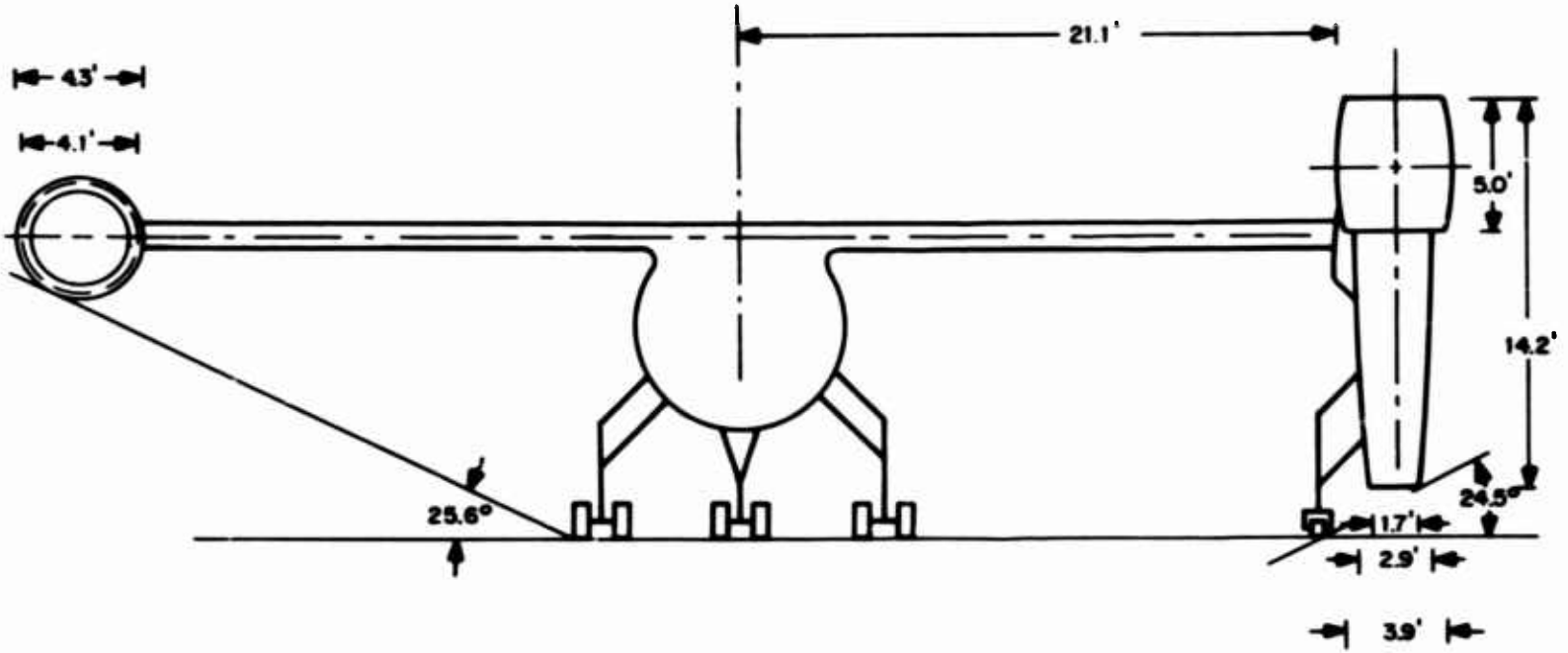

W_G = 20,048 lb.

Figure 26. Turbofan Propulsion System Aircraft Integration Configuration.

insight on possible operational problem areas. These problem areas are as follows:

a. Limited propulsion system ground clearance.

b. Ground erosion, cratering, etc.

c. Foreign object damage (FOD).

Although the tilt-wing open-propeller propulsion system configuration exhibits sufficient ground clearance, a practical limitation on propeller diameter is encountered. Additional ground clearance may be obtained by limiting the wing tilt angle during STOL phases of operation. Problems relating to ground cratering and foreign object damage are minimum for the open propeller propulsion system since it possesses the lowest slipstream velocities. Chances of ground fire are remote because of the low energy and mass flow of the residual trubine nozzle exhaust gas.

The smaller diameter of the ducted propeller propulsion system, in addition to an inboard location with respect to the wing tip, provides more than adequate ground clearance. Possibilities of ground cratering and foreign object damage are greater than the open propeller and less than the turbofan propulsion systems. Chances of ground fire should be even lower than that of the open propeller because of the higher energy flow from the ducted propeller mixing with the low energy and mass of residual turbine nozzle gas flow.

A wing tip mounting of the tilting turbofan propulsion system results in limited ground clearance during VTOL operation. However, the probability of ground contact can be eliminated by mounting auxiliary shock absorbing bumper gears on the turbofan gas generator nacelles. The turbofan engine cycle selected for the application study based on maximum performance retains a large percentage of available gas generator energy in the turbine nozzle exhaust. Consequently, the possibilities of ground fire or cratering and foreign object damage are great and will prevent operation from unprepared runways. Configuration changes to alleviate these problems are:

a. Turbofan cycles and configurations with a large portion of the available gas generator energy delivered to the fan.

b. Multiple counterrotating spool designs, gear-driven concentric front fan configurations, or other concepts that will reduce gas generator length.

c. Gear-driven remote fan configurations.

C. EVALUATION OF PROPULSION SYSTEMS

Having determined values for independent performance parameters, such as relative productivity, fuel consumption, maximum speed, and static thrust margin, there remains to integrate the relative value of each of these parameters and to establish a basis for finding the optimum propulsion system.

In applying the decision-making procedures of Reference 23, the numerical outcome or value of each of the four performance parameters was graded on the basis of ten for each propulsion system. That is, for the static thrust margin parameter, the outcome for the open propeller, ducted propeller, and turbofan propulsion systems was graded as 9.6, 10, and 8.7, respectively, based on a simple proportion of the maximum outcome 1.27 to a grade of 10. The resulting matrix is shown in Table X.

TABLE X

PERFORMANCE PAYOFF MATRIX - EQUAL RELATIVE UTILITY

Propulsion System	Relative Productivity	Fuel Consumption	Max. Speed	Static Thr. Margin
Open Propeller	9.8	10	6.2	9.6
Ducted Propeller	8.8	10	5.7	10
Turbofan	10	5	10	8.7

A conclusion cannot be drawn from the above matrix, since each of the performance parameters is presented with equal weighting or equal relative utility.

A relative utility must be established among the various parameters based on specific mission objectives and influence of operational environment. In lieu of a definitive application, values of relative utility (Schedule 1) have been assigned, based on best estimates for the application study as .5 for relative productivity, .1 for fuel consumption, .2 for maximum speed, and .2 for static thrust margin. After multiplying the elements of the original matrix by their respective utility values, the resulting payoff matrix is given in Table XI.

TABLE XI

PERFORMANCE PAYOFF MATRIX - RELATIVE UTILITY SCHEDULE 1

Propulsion System	Relative Productivity	Fuel Consumption	Max. Speed	Static Thrust Margin	Expected Payoff
Open Propeller	4.9	1.0	1.24	1.92	9.06
Ducted Propeller	4.4	1.0	1.14	2.00	8.54
Turbofan	5	0.5	2.00	1.74	9.24

The expected payoff which is to be maximized was calculated for each system as the sum of the corresponding row elements of the payoff matrix. Hence, the turbofan propulsion system is optimum.

It is interesting to note that when the relative utility values for maximum speed and static thrust margin are changed to .15 and .25, respectively (Schedule 2), the open propeller propulsion system, as indicated in Table XII, becomes the optimum configuration.

TABLE XII

PERFORMANCE PAYOFF MATRIX - RELATIVE UTILITY SCHEDULE 2

Propulsion System	Relative Productivity	Fuel Consumption	Max. Speed	Static Thrust Margin	Expected Payoff
Open Propeller	4.9	1.0	0.93	2.40	9.23
Ducted Propeller	4.4	1.0	0.86	2.50	8.76
Turbofan	5.0	0.5	1.50	2.18	9.18

Indications are that the ducted propeller system would require an extremely large static thrust margin relative utility value and very low relative utility values for maximum speed and relative productivity in order to become competitive.

Although beyond the scope of this report, numerical values for parameters which define operational characteristics and their relative utility should be included for evaluation in the payoff matrix. It is felt that these items would favor the open propeller propulsion system.

VI. CONCLUSIONS AND RECOMMENDATIONS

1. Methods have been developed for optimization and trade-off analyses of relative performance merits of open and ducted propeller and turbofan propulsion systems.

2. The comparative study of the three propulsion systems indicates that for ranges greater than 220 nautical miles, the open propeller yields higher maximum productivity than the ducted propeller or turbofan systems. Furthermore, this productivity is achievable at higher cruise speeds as compared to ducted propeller, but appreciably lower speeds as compared to turbofan.

3. The comparative study presented in this report indicates that the relative fuel consumption for open propeller propulsion system is lowest as compared to that for ducted propeller or for turbofan systems.

4. Based on the relative utility values used in the application study, open propeller was selected as the most suitable propulsion system for the specified aircraft mission.

5. The performance nomographs developed under this program represent a rapid preliminary design tool for selection of the most suitable propulsion system for a given aircraft mission.

6. It is recommended that performance nomographs be developed for all three propulsion systems and be extended to include a wider range of the pertinent performance parameters.

7. It is also recommended that further studies be conducted to obtain vibratory stress data which could be used to establish vibratory stress level trends to be applied to future designs of the propulsion systems.

VII. REFERENCES

1. Borst, H.V., A SHORT METHOD TO PROPELLER PERFORMANCE, Curtiss-Wright Corporation, Caldwell, New Jersey, July 1959.

2. GENERALIZED METHOD OF PROPELLER PERFORMANCE ESTIMATION, Hamilton Standard Division of United Aircraft Report PD 6101A, June 1963.

3. GENERALIZED METHOD OF SHROUDED PROPELLER PERFORMANCE ESTIMATION, Hamilton Standard Division of United Aircraft Corporation, Windsor Locks, Connecticut, Report No. PDB 6220.

4. Webb, Dana, Weller, Jack, PROPELLER PERFORMANCE AT ZERO FORWARD SPEED, Wright Air Development Center, Propeller Laboratory, July 1952, TR-52-152.

5. INTEGRATED GEAR CASE PROPELLER SYSTEM, CANADAIR CL-84 AIRCRAFT, Report No. 2987 Model Specification, Curtiss-Wright Corporation, Caldwell, New Jersey.

6. MODEL SPECIFICATION PROPELLER, AIRCRAFT MODEL 5008C PROPELLER SYSTEM FOR MODEL XC-142A VTOL CARGO ASSAULT AIRCRAFT, Supplement to Revision, 9 October 1963.

7. Grose, Ronald, WIND TUNNEL TESTS OF SHROUDED PROPELLERS AT MACH NUMBERS FROM 0 TO 0.60, United Aircraft Corporation, Research Department Wright-Patterson Air Force Base, Ohio, December 1958.

8. Asmus, F.J., PARAMETRIC AND PRELIMINARY DESIGN STUDIES OF HIGH SPEED AND LOW SPEED CRUISE FAN PROPULSION SYSTEMS, General Electric Company, Flight Propulson, Cincinnati, Ohio, March 1966.

9. MODEL SPECIFICATION E1123 ENGINE AIRCRAFT, TURBOSHAFT YT64-GE-16 and T64-GE-16, General Electric Company, Lynn, Massachusetts, 22 September 1966

10. Perkins, C.D., Hage, R.E., AIRPLANE PERFORMANCE STABILITY AND CONTROL, John Wiley and Sons, Inc., New York, 1949.

11. Weissinger, von Johannes, EINIGE ERGEBNISSE AUS DER THEORIE DES RINGFLUGELS IN INKOMPRESSIBLER STROMUNG, reprinted from ADVANCES IN AERONAUTICAL SCIENCES, Volume 2, Pergamon Press, New York, 1959.

12. McCormick, Barnes W., Jr., AERODYNAMICS OF V/STOL FLIGHT, Academic Press, New York, 1967.

13. DUCTED FAN WING-DUCT WEIGHT STUDY AND COMPARISON WITH A TILT WING VTOL, Report No. DS-217, Doak Aircraft Company, Inc., Torrance, California, September 1960.

14. Prager, P.C., FEASIBILITY STUDY OF CRUISE FAN PROPULSION SYSTEMS AND ASSOCIATED POWER TRANSFER SYSTEMS FOR COMPOUND/COMPOSITE AIRCRAFT, Vertol Division, Boeing Company, Morton, Pa., USAAVLABS Technical Report 67-28, U.S. Army Aviation Materiel Laboratories, Fort Eustis, Virginia, September 1967.

15. Trenka, A. R., DEVELOPMENT OF A METHOD FOR PREDICTING THE PERFORMANCE AND STRESSES OF VTOL-TYPE PROPELLERS, Cornell Aeronautical Laboratory, Inc., Buffalo, New York, USAAVLABS Technical Report 66-26, U. S. Army Aviation Materiel Laboratories, Fort Eustis, Virginia, June 1966.

16. Ordway, D.E., Sluyter, M.M., Summerup, B.O.V., THREE DIMENSIONAL THEORY OF DUCTED PROPELLERS, Therm Advanced Research, Ithaca, New York, TAR-TRG02, August 1950.

17. Greenberg, M.D., Ordway, D.E., THE DUCTED PROPELLER IN STATIC AND LOW SPEED FLIGHT, Therm Advanced Research, Ithaca, New York, TAR-TR6407, October 1964.

18. Prince, C.H., VIBRATING STRESS MEASUREMENTS ON A SHROUDED PROPELLER IN THE KELLETT AIRCRAFT CORPORATION DOWNWASH TEST FACILITY, Hamilton Standard, Report No. HSER3731, Willow Grove, Pennsylvania, October 1965.

19. Przedpelski, Zygmunt J., LIFT FAN TECHNOLOGY STUDIES, NASA CR-761, National Aeronautics and Space Administration, Washington, D.C., April 1967.

20. Garrick, I.E., and Watkins, C.E., A THEORETICAL STUDY OF FORWARD SPEED ON THE FREE-SPACE SOUND PRESSURE FIELD AROUND PROPELLERS, National Advisory Committee for Aeronautics Technical Note 3018, October 1953.

21. Watkins and Durling, A METHOD FOR THE CALCULATION OF FREE-SPACE SOUND PRESSURES NEAR A PROPELLER IN FLIGHT INCLUDING CONSIDERATIONS OF CHORDWISE BLADE LOADING, National Advisory Committee for Aeronautics Technical Note 3809, 1956.

22. Hubbard, H.H., SOUND MEASUREMENTS FOR FIVE SHROUDED PROPELLERS AT STATIC CONDITIONS, Langley Aeronautical Laboratory, Langley Air Force Base, Virginia, National Advisory Committee for Aeronautics Technical Note 2024, April 1950.

23. Miller, David W., and Starr, Martin K., EXECUTIVE DECISIONS AND OPERATIONS RESEARCH, Prentice-Hall, 1960.

24. Durand, W. F., AERODYNAMIC THEORY, Volume IV, New York, Dover Publications.

25. Goldstein, S., ON THE VORTEX THEORY OF SCREW PROPELLERS, Proc. Royal Society (London), Section A, Volume 123, No. 792, April 1929.

26. Lock, C. N. H., APPLICATION OF GOLDSTEIN'S THEORY TO THE DESIGN OF AIRSCREWS, Br. A.R.C.R. and M. 1377, 1930.

27. Theodorsen, T., DETERMINATION OF THE CIRCULATION FUNCTION AND THE MASS COEFFICIENT FOR DUAL ROTATING PROPELLERS, NACA Report No. 775, National Advisory Committee for Aeronautics, 1944.

28. Erickson, J. C., Ladden, R. M., Borst, H. V., Ordway, D. E., A THEORY FOR VTOL PROPELLER OPERATION IN A STATIC CONDITION, Curtiss-Wright Corporation and Therm Advanced Research, Inc., USAAVLABS Technical Report 65-69, U. S. Army Aviation Materiel Laboratories,

Fort Eustis, Virginia, October 1965.

29. Davenport, F. J., ANALYSIS OF PROPELLER AND ROTOR PERFORMANCE IN STATIC AND AXIAL FLIGHT BY AN EXPLICIT VORTEX INFLUENCE TECHNIQUE, Boeing Vertol, Morton, Pa. R-372, February 1965.

30. Kuchmann and Weber, AERODYNAMICS OF PROPULSION, McGraw-Hill Book Company, New York, 1953.

31. Moise, S., PARAMETRIC AND PRELIMINARY DESIGN STUDIES OF CRUISE-FAN PROPULSION SYSTEMS, Pratt and Whitney Aircraft Division, United Aircraft Corporation, May 1965.

APPENDIX I.

REVIEW OF THE AVAILABLE THEORETICAL ANALYSES FOR VARIOUS PROPULSION SYSTEMS

Presented in this section is a brief review of the available theoretical analyses which is commonly used for performance evaluation of open and ducted propellers and turbofan propulsion systems.

A. OPEN PROPELLER

The analytical methods used for predicting the performance of open propellers are based on a combination of momentum, blade element, and vortex theories. Although these theories are considered to be adequate for performance prediction of lightly loaded propellers operating in axial cruise flight, they have certain limitations as to their applicability to heavily loaded propellers operating in static conditions. The basic deficiency of these analyses is in the assumptions pertaining to propeller inflow distribution and the associated wake structure in determining the blade load distribution. Considerable effort is being expended to better represent the propeller flow field for a more accurate prediction of propeller static performance. The following is a brief synopsis of the available propeller theories:

1. Momentum Theory

The momentum theory, based on the work of Rankine and Froude, is derived from the following fundamental assumptions:

a. Flow through the actuator is a potential flow.

b. Propeller acts as an actuator disc (infinite number of blades).

c. Continuous inflow velocity across propeller disc.

d. Uniform distribution of velocity over the disc.

e. Zero slipstream rotation.

Referring to Figure 27, the actuator disc thrust can be expressed as the change of axial momentum of the air passing through the disc in unit time; thus,

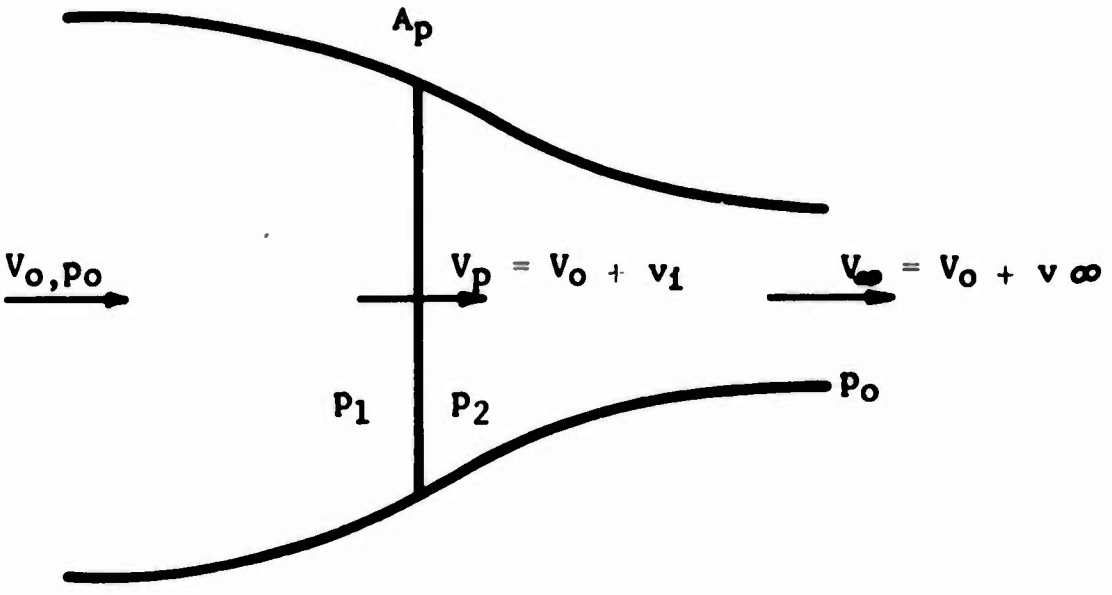

Figure 27. Schematic Representation of the Flow Through an Actuator Disc.

$$T_p = \rho A_p V_p (V_\infty - V_o) \tag{41}$$

From Bernoulli's equation, the increase in pressure across the disc Δ_p is

$$p = p_2 - p_1 = \tfrac{1}{2} \rho (V_\infty^2 - V_o^2) \tag{42}$$

Also, the thrust of the actuator disc can be expressed as

$$T_p = A_p \Delta_p \tag{43}$$

Substituting equations (41) and (42) into equation (43) yields

$$V_p = \tfrac{1}{2}(V_\infty + V_o) \tag{44}$$

If the velocity increments at the plane of the propeller and in the far wake are defined as v_i and v_∞, respectively, there follows:

$$V_p = V_o + v_i \tag{45}$$

$$V_\infty = V_o + v \tag{46}$$

Substituting equations (45) and (46) into equation (44) yields

$$v_i = \tfrac{1}{2} v_\infty \tag{47}$$

Substituting equations (45), (46), and (47) into equation (41) yields

$$T_p = 2 \rho A_p (V_o + v_i) v_i \tag{48}$$

From equation (48), the induced velocity at the propeller plane can be expressed as follows:

$$v_i = -\frac{V_o}{2} + \sqrt{\left(\frac{V_o}{2}\right)^2 + \frac{T_p}{2\rho A_p}} \tag{49}$$

The ideal power is the work done by the thrust, namely,

$$P_i = T_p V_o \tag{50}$$

The actual power P is the change of kinetic energy per unit time. Thus,

$$P = \tfrac{1}{2}\rho A_p V_p \left[V_\infty^{\,2} - V_o^{\,2} \right] = T_p(V_o + v_i) \tag{51}$$

The ideal efficiency is defined as the ratio of useful work (ideal power) to total work (actual power); thus,

$$\eta_i = \frac{P_i}{P} \tag{52}$$

Substituting equations (50) and (51) into equation (52), the ideal efficiency in cruise becomes

$$\eta_i = \frac{V_o}{V_o + v_i} \tag{53}$$

where v_i is given by equation (9).

Equation (53) is not applicable to static conditions (since $\eta_i = 0$ at $V_o = 0$). The measure of propeller efficiency at static conditions is given by figure of merit, FM, defined as

$$FM = \frac{1}{\sqrt{2}} \frac{T_p}{P} \sqrt{\frac{T_p}{\rho A_p}} \qquad (54)$$

The momentum theory as outlined above yields overall propeller performance results; however, it does not provide the information required for blade detail design.

2. Blade Element Theory

Some information pertaining to blade detail design can be obtained by using the blade element theory outlined below.

Consider a blade element of chord C_x and width dr located at a radius r from the propeller axis as shown in Figure 28. The forces acting on the blade element along and perpendicular to the propeller axis are:

$$dT_p = dL\cos\phi - dD\sin\phi \qquad (55)$$

$$dF = dD\cos\phi + dL\sin\phi \qquad (56)$$

Also, the section lift and drag forces are given by

$$dL = \frac{\rho}{2} BCdrV^2C_L \qquad (57)$$

$$dD = \frac{\rho}{2} BCdrV^2C_D \qquad (58)$$

Defining blade solidity as $\sigma = BC_x/\pi R$ and nondimensional propeller radius as $x = r/R$, equations (57) and (58) can be written as follows:

$$dL = \frac{\rho}{2} A_p\sigma_x C_L V^2 d_x \qquad (59)$$

$$dD = \frac{\rho}{2} A_p\sigma_x C_D V^2 d_x \qquad (60)$$

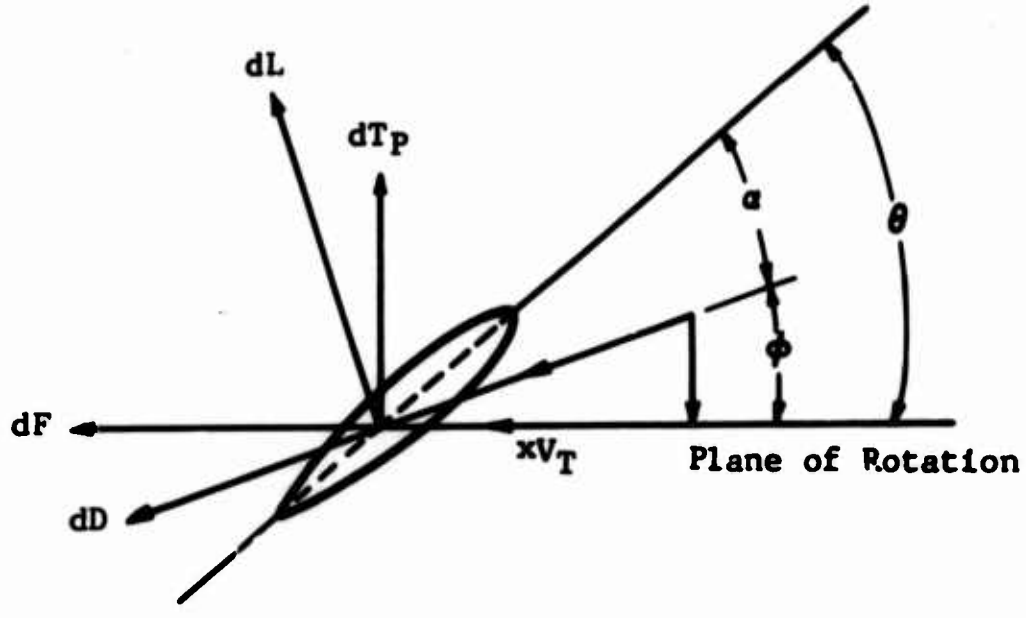

Figure 28. Blade Element at Radius r From Propeller Axis.

Substituting equations (59) and (60) into equations (55) and (56) yields

$$dT_p/dx = \frac{\rho}{2} A_p \sigma_x V^2 (C_L \cos\phi - C_D \sin\phi) \tag{61}$$

$$dF/dx = \frac{\rho}{2} A_p \sigma x\, V^2 (C_D \cos\phi + C_L \sin\phi) \tag{62}$$

Defining $\lambda = (V_o + v_i)/V_T$ and $\delta = C_D/C_L$, equations (61) and (62) become

$$dT_p/dx = \frac{\rho}{2} A_p V_T^2 \sigma_x C_L (\lambda^2 + x^2)^{\frac{1}{2}} (x - \delta\lambda) \tag{63}$$

$$dF/dx = \frac{\rho}{2} A_p V_T^2 \sigma_x C_L (\lambda^2 + x^2) (\delta x + \lambda) \tag{64}$$

The elemental horsepower is given by

$$dHP/dx = \frac{1}{550} dF/dx\, V_T x \tag{65}$$

Substituting equation (64) into (65) yields

$$dHP/dx = \frac{x}{550} \left(\frac{\rho}{2} A_p V_T^3 \sigma_x C_L (\lambda^2 + x^2)^{\frac{1}{2}} (\delta x + \lambda)\right) \tag{66}$$

Equation (48) can be written in differential form as

$$dT_p/dx = 4\rho A_p (V_o + v_i) v_i x \tag{67}$$

Equating equation (67) and equation (63) yields

$$\sigma_x C_L = \frac{8 v_i x (V_o + v_i)}{V_T^2 (\lambda^2 + x^2)^{\frac{1}{2}} (x - \delta\lambda)} \tag{68}$$

Equation (68) expresses the relationship between blade chord, lift and drag coefficient, and inflow velocity at the blade element. This equation can be used for optimization and detail design of the blade section.

3. Vortex Theory

The vortex theory as applied to open propellers considers the propeller wake as a system of trailing vortices which are shed along the rotating blades and which propagate downstream in the form of helical sheets (Figure 29). Due to the complexity of the wake structure, the existing mathematical models representing the flow field utilize a variety of simplifying assumptions. The validity of some of these assumptions, such as rigid wake (no wake contraction), is questionable, especially when applied to heavily loaded propellers operating in static conditions. It is therefore convenient to discuss the vortex theory from the point of view of its applicability to either lightly or heavily loaded propellers.

a. Lightly Loaded Case

By considering the propeller to be lightly loaded and having an infinite number of blades, the helicoidal wake structure can be approximated by a series of cylindrical vortex sheets. With this model, the inflow can be directly related to the circulation distribution at the propeller plane. However, the assumption of an infinite number of blades is considered to be inaccurate for propellers with four or less blades. This is due to the fact that for a low number of blades, the helicoidal trailing vortex system induces an appreciable radial flow near the boundary of the slipstream, thus resulting in a drop of circulation and, hence, loss of lift at the tip of the blades. To account for this loss of lift, Prandtl (Reference 24) developed an approximate correction for the circulation at each radial station. In a modified vortex analysis, Goldstein (Reference 25) obtained a rigorous mathematical solution for two-and four-bladed propellers. This analysis has been extended by

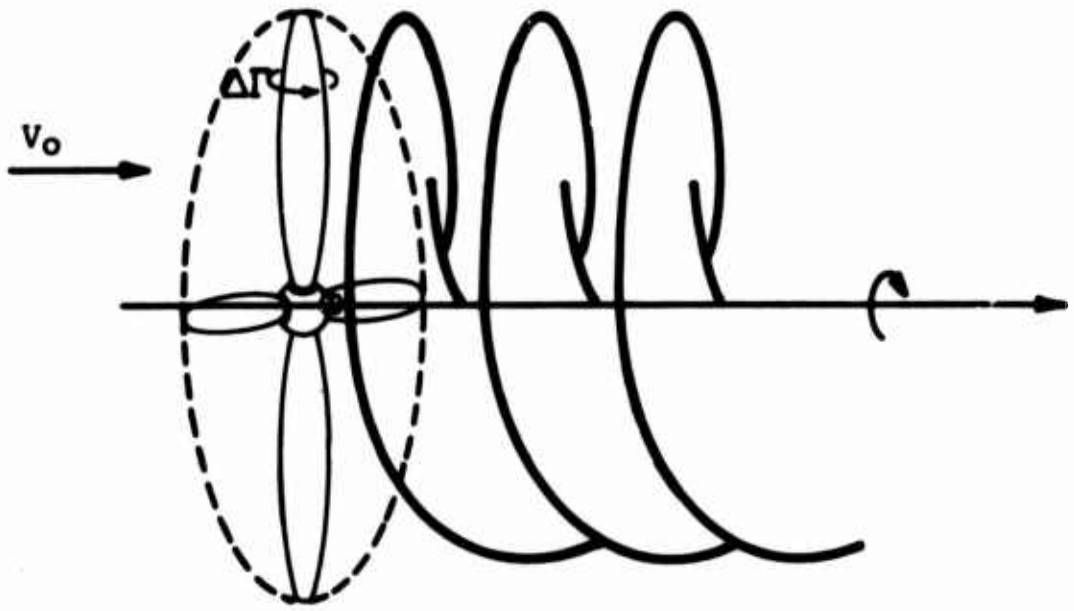

Figure 29. Propeller Wake Represented by a System of Helicoidal Sheets.

Lock (Reference 26) to a general case for n number of blades.

b. Heavily Loaded Propeller

The vortex theory discussed above was extended to heavily loaded propellers by Theodorsen (Reference 27). This was achieved using specially developed circulation functions, K(x), which relate the conditions in the far wake to blade circulation. These functions were determined experimentally using an electrical analogy method.

With the advent of high-speed digital computers, several propeller analyses have been developed which attempt to eliminate the basic assumptions of the classical propeller theories. These analyses, which are summarized in References 15, 28 and 29, differ primarily in details of mathematical representation of the propeller wake structure, and all of them require lengthy iterative computer solutions to obtain propeller performance and stress data. The mathematical representation of the propeller flow field, as shown in Figure 30, consists of a bound vortex line along the blade radius and a system of discrete trailing vortices shed from each section of the blade. In some of the analyses, this model is simplified by considering the trailing vortex system to consist of a strong spiral tip vortex and a central line vortex.

In each case, the strength and the geometry of the trailing vortices are computed from the known blade load distribution (based on blade element and momentum theories) and blade geometry and rotational speed. The induced velocity due to each vortex filament is then computed utilizing the Biot-Savart law. These velocities are then used to compute a better approximation for the blade airload distribution. This iteration cycle is performed until a desired convergence is obtained; i.e., the finally computed velocity distribution at the propeller plane is compatible with the airload distribution.

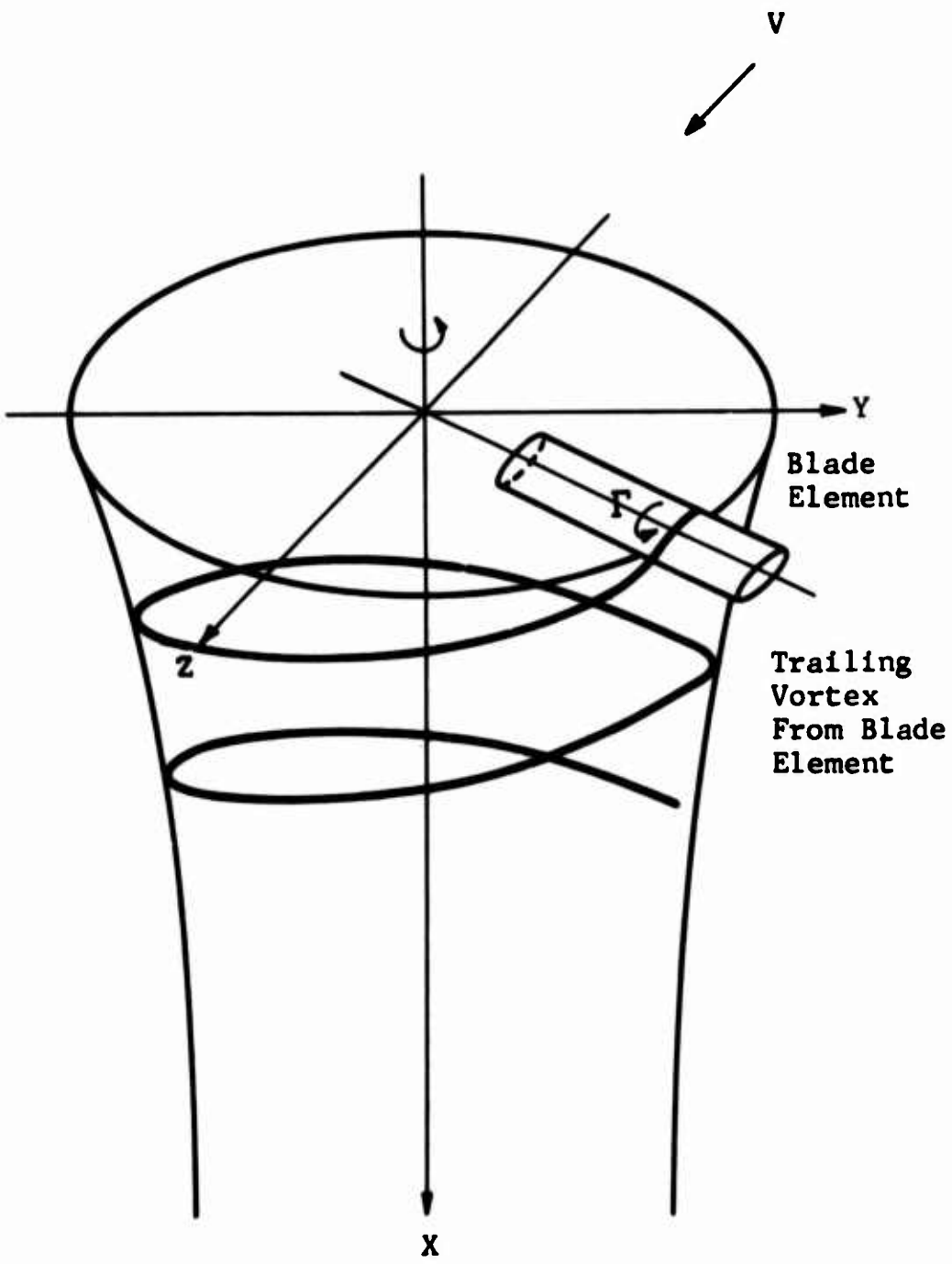

Figure 30. Trailing Vortex Spiral Geometry.

Modern vortex analyses include the effects of slipstream contraction and rotation which are of great importance in predicting static performance of free propellers.

B. DUCTED PROPELLER

The ducted propeller is basically a free propeller which is circumscribed by a shroud. The main purpose of the shroud is to modify the flow field of a free propeller so as to achieve an increase in propeller thrust. The methods for analyzing the performance of ducted propellers are essentially similar to those used for free propellers with the exception that a proper account must be made for the effect of the shroud. These methods are as follows:

1. Momentum theory for basic propeller.

2. Method of singularities for shroud effects.

3. Combination of momentum, blade element, and singularity theories for overall ducted propeller performance.

1. Momentum Theory

In addition to the momentum assumptions applied to free propeller analyses, the ducted propeller analysis utilizes the following assumptions:

a. The flow in the duct wake is cylindrical.

b. The velocity at the duct exit is uniform and is equal to that in the infinite wake.

Using the nomenclature of Figure 31, the total thrust of a ducted propeller can be expressed as change of momentum per unit time; thus,

$$T_T = \rho A_p V_p (V_\infty - V_o) \qquad (69)$$

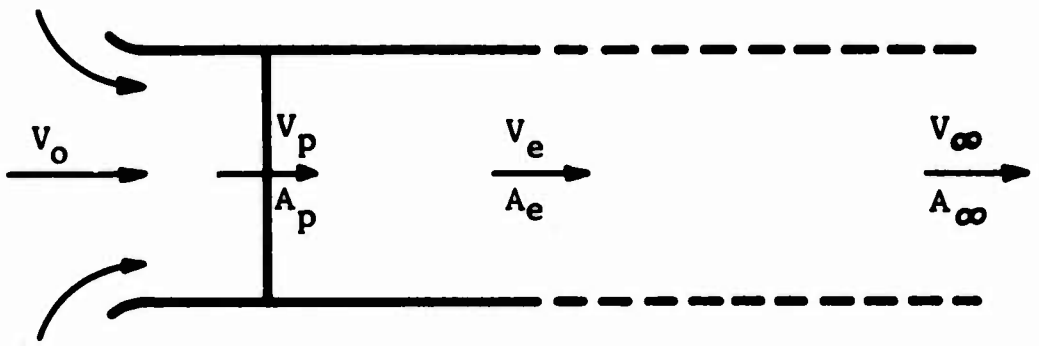

Figure 31. Schematic Representation of the Flow of a Ducted Propeller.

The continuity relationship between the propeller plane and the duct exit requires that

$$A_p V_p = A_e V_e \tag{70}$$

Since $V_e = V_\infty$ (assumption), then

$$V_p = A_e / A_p V \tag{71}$$

The velocity at the propeller plane can be defined in terms of the duct far wake velocity; thus,

$$V_p = (\tfrac{1}{2} + \delta_p) V_\infty \tag{72}$$

where δ_p is the duct local induced velocity coefficient representing the effect of the shroud on propeller flow.

Using equations (71) and (72), the average momentum value of δ_p can be expressed as follows:

$$\delta_p = A_e / A_p - \tfrac{1}{2} \tag{73}$$

Substituting equation (71) into equation (69), the total thrust T_T can be expressed as

$$T_T = \rho A_p V_p (A_p / A_e V_p - V_o) \tag{74}$$

Equation (74) yields the following quadratic in V_p:

$$V_p^2 - (A_e / A_p) V_o V_p - \left(\frac{T_T}{\rho}\right)\left(\frac{A_e}{A_p^2}\right) = 0 \tag{75}$$

Solving equation (75) yields the following relationship for the velocity at the propeller plane:

$$V_p = \frac{1}{2}\left\{ \frac{A_e}{A_p} V_o + \left[\left(\frac{A_e}{A_p} V_o \right)^2 + \left(\frac{4T_T}{\rho} \right) \left(\frac{A_e}{A_p^2} \right) \right]^2 \right\} \qquad (76)$$

The power required (excluding duct drag) can be expressed as the change in kinetic energy per unit time given by

$$P = \frac{1}{2} A_p V_p \rho (V_\infty^2 - V_o^2) \qquad (77)$$

The ideal propulsive efficiency can be defined as

$$\eta_i = \frac{T_T V_o}{P} \qquad (78)$$

Substituting equations (69) and (77(into equation (78) yields

$$\eta_i = \frac{2V_o}{V_o + V_\infty} \qquad (79)$$

Substituting equation (72) into equation (79) yields

$$\eta_i = \frac{2V_o}{V_o + \dfrac{V_p}{\frac{1}{2} + \delta_p}} \qquad (80)$$

It should be noted that in this analysis the duct contribution to the propeller induced velocity δ_p is only a function of the area ration A_e/A_p. This is nearly true only for the

case when the length-to-diameter ratio of the duct is larger than 1.0. For length-to-diameter ratios of less than 1.0, the radial variation of the duct parameter δ_p becomes appreciable, as will be shown in the subsequent analysis.

2. Method of Singularities

A convenient technique of evaluating the duct effect on the propeller flow is provided by the method of singularities. In this approach, both the propeller and the duct are replaced with singularity distributions which mathematically represent the ducted propeller flow field. Although the determination of these singularity distributions is extremely difficult in the general case, the case of the optimum ducted propeller operating at or near its design condition can be readily solved. The optimum propeller produces a uniform velocity in its remote wake and therefore can be represented by a combination of a sink disc and a semi-infinite parallel flow, as shown in Figure 32(a). This in turn can be equivalently represented by a uniform semi-infinite vortex cylinder. The duct can be replaced by a distribution of vortex rings of unknown strength, γ_D, as indicated in Figure 32(b). The unknown strength, γ_D, can be determined by first representing it as a series of Birnbaum standard functions, and then by satisfying the duct boundary condition; namely, the duct is coincident with the streamline of the resultant flow. This boundary condition can be represented by the following equation:

$$dR/dx = \frac{Vr}{V_o + V_x} \tag{81}$$

Once the vorticity distribution is determined, the velocities, $V_D(x)$, induced along the propeller plane by the duct can be calculated using the tables in Reference 30.

Since the velocity, $V(x)$, induced at the propeller plane is the sum of the duct induced velocity, $V_D(x)$, plus the propeller induced velocity, V_p, and since $V_p = \frac{1}{2} V_\infty$, then the induced velocity, $V(x)$, can be written as

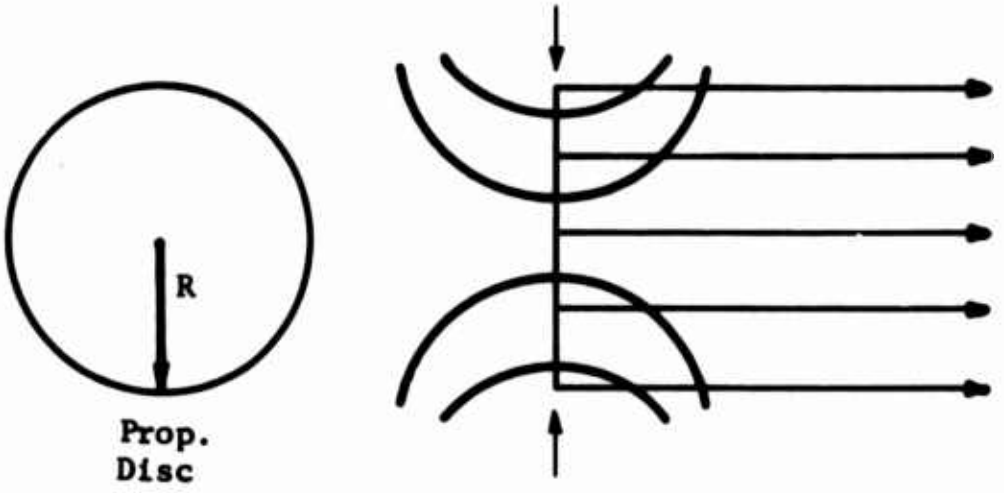

(a) Uniform Sink Disc and Parallel Flow Representing Propeller.

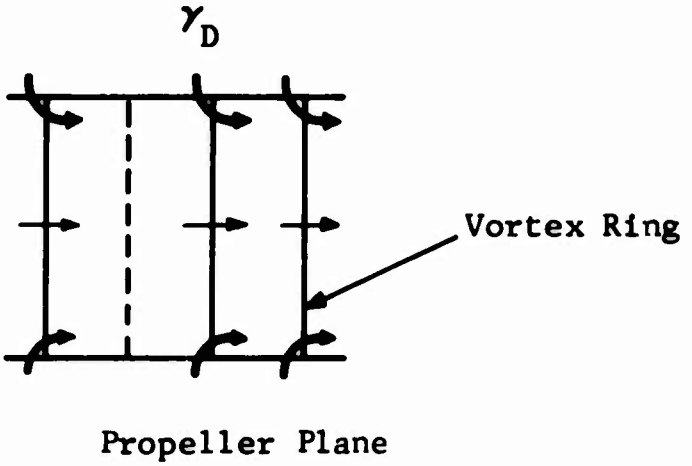

(b) Distribution of Vortex Rings Representing Duct.

Figure 32. Mathematical Model of the Ducted Propeller Flow Field.

$$V(x) = \left(\frac{V_D(x)}{V_\infty} + \frac{1}{2} \right) V_\infty \tag{82}$$

Substituting equation (72) into equation (82) yields

$$\delta_p = \frac{V_D(x)}{V_\infty} \tag{83}$$

Equation (83) gives the δ_p distribution along the propeller plane. For length of duct/diameter of propeller values less than 1.0, δ_p will vary appreciably along the propeller radius. For length-to-diameter ratio greater than 1.0, δ_p can be taken as a constant.

3. Combination of Momentum, Blade Element, and Singularities

The combination of momentum, blade element, and singularity theories can be used to obtain a detailed geometry of a propeller within a given shroud.

Consider a ducted propeller in axial flight as illustrated in Figure 33. The differential thrust of an annular element is given by momentum theory as

$$dT_T = 2\pi r \, dr \, \rho V_p (V_\infty - V_o) \tag{84}$$

The velocity at the propeller plane is defined as

$$V_p = \left(\frac{1}{2} + \delta_p \right) V_\infty \tag{85}$$

Using equations (84) and (85), there follows:

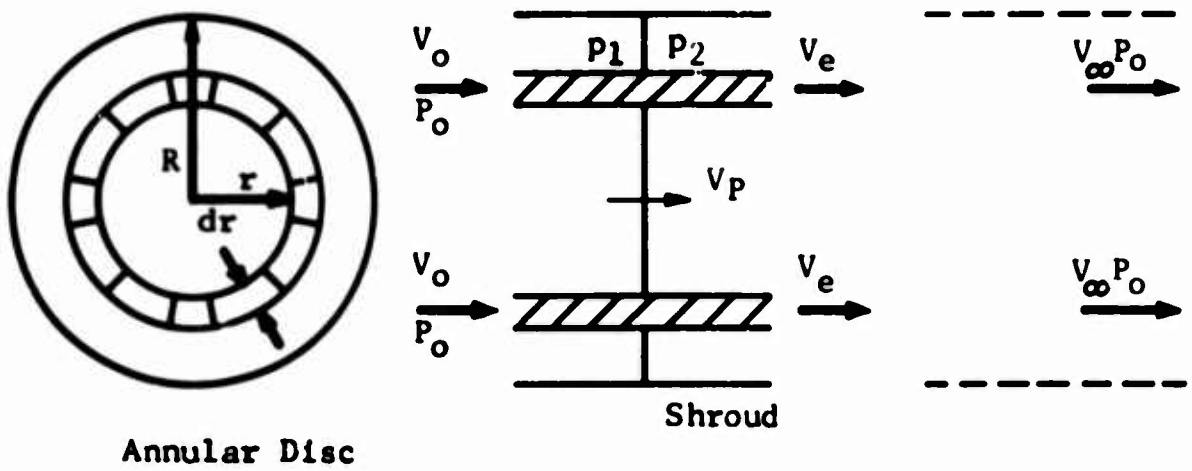

Figure 33. Flow Through an Annular Element of a Shrouded Propeller.

$$dT_p/dx = 4\rho A_p x\left[\frac{V_p^2}{\frac{1}{2}+\delta_p} - V_o V_p\right] \tag{86}$$

where

$$A_p = \pi R^2, \quad x = r/R$$

Writing Bernoulli's equation ahead of and behind the disc yields

$$p_o + \frac{1}{2}\rho V_o^2 = p_1 + \frac{\rho}{2} V_p^2 \tag{87}$$

$$p_2 + \frac{1}{2}\rho V_p^2 = p_o + \frac{1}{2}\rho V_\infty^2 \tag{88}$$

$$\therefore\ p_2 - p_1 = \frac{1}{2}\rho\left(V_\infty^2 - V_o^2\right) \tag{89}$$

The elemental propeller thrust can be expressed as

$$dT_p = (p_2-p_1)dA_p = \rho A_p(p_2-p_1)2\pi r dr = \rho A_p x(V_\infty^2 - V_o^2) \tag{90}$$

Using equations (85) and (90), there results

$$dT_p/dx = \rho A_p\left[\frac{V_p^2}{\left(\frac{1}{2}+\delta_p\right)^2} - V_o^2\right] x \tag{91}$$

Substituting equation (63) into equation (90) yields

$$\sigma_x C_L = \frac{\left[\frac{V_p^2}{\left(\frac{1}{2} + \delta_p\right)^2} - V_o^2\right] 2x}{V_T^2 \left(\lambda^2 + x^2\right)^{\frac{1}{2}} \left(x - \delta\lambda\right)} \qquad (92)$$

Equation (92) can be used for a detailed design of a shrouded propeller once the δ_p parameter and the inflow velocity are established. The δ_p parameter can be determined by using the method of singularities as outlined in paragraph 2, and the inflow velocity σ is usually obtained from momentum theory discussed previously.

More rigorous analyses which can be applied for design optimization and performance evaluation of ducted propellers are presented in References 16 and 17. In Reference 16, the ducted propeller is assumed to operate in axial flight in a uniform, unbounded stream of inviscid, incompressible fluid. The shroud, blade, and hub thicknesses are assumed to be zero, and the shroud camber as well as ratio of the blade chord to the shroud chord is considered to be small. The mathematical model consists of a cylindrical surface of distributed vortices representing the duct, and the propeller blades are introduced as individual, radial vortex lines of varying circulation with trailing helical vortex sheets. Reference 17 presents a similar analysis for ducted propellers operating in static conditions.

C. TURBOFAN

The theoretical analyses utilized for performance prediction of turbofan propulsion systems are in principle similar to those applied to open or ducted propellers. However, the turbofan analyses are more completed since they must take into account not only aerodynamic but also thermodynamic effects associated with each component of the system. These analyses are generally comprised of a combination of momentum vortex, blade cascade, and heat transient theories which are augmented by suitable test data.

A good summary of modern turbofan analyses is presented in References 8, 14, and 31. These investigations contain recent turbofan performance data which have been utilized in the present program. Table XIII shows the range of the most pertinent turbofan parameters cosidered.

Table XIII

TURBOFAN PARAMETERS INVESTIGATED

Source	Turbine Inlet Temp.	Gas Generator Pressure Ratio	Bypass Ratio	Fan Pressure Ratio
Reference 8	1700°F 2300°F	13:1	2.73-10	1.2 - 1.6
Reference 14	1800°F 2400°F	8:1-20:1	3 - 12	
Reference 31	1900°F	10:1	2.0-12.5	1.2 - 2.0

The turbofan parameters presented in the above table apply to a hypothetical fan-engine design which reflects the 1970 state-of-the-art turbofan technology.

APPENDIX II

PERFORMANCE AND WEIGHT DATA

Tables XIV through XVI present a summary of the performance results obtained from the comparative study of the three propulsion systems considered.

TABLE XIV

OPEN PROPELLER PROPULSION SYSTEM
PERFORMANCE AND WEIGHT DATA
W_G = 20,000 lb.
(a) Range = 100 Nautical Miles

AF	d-ft.	V_C-kt.	w_F-lb.	W_{UL}-lb.	W_E-lb.	W_{PL}/W_G	$W_{PL}V_C/W_E$
140	18.5	208.7	917.2	7417	12583	0.297	98.7
		260.9	967.6	7415	12585	0.294	122.2
		347.9	1222.4	7403	12597	0.281	155.5
130		208.7	905.7	7502	12498	0.302	101.0
		260.9	949.9	7500	12500	0.300	125.2
		347.9	1192.6	7489	12511	0.287	159.8
120		208.7	921.1	7589	12411	0.305	102.9
		260.9	938.9	7588	12412	0.305	128.2
		347.9	1183.3	7577	12423	0.292	163.6
120	19.0	200.7	896.1	7498	12502	0.302	101.0
		260.9	942.5	7496	12504	0.300	125.2
		347.9	1191.4	7484	12516	0.287	159.6
110		208.7	887.7	7593	12407	0.307	103.5
		260.9	930.3	7591	12409	0.305	128.4
		347.9	1182.2	7579	12421	0.292	163.7
100		208.7	882.5	7691	12309	0.312	106.1
		260.9	915.4	7689	12311	0.311	132.0
		347.9	1172.1	7678	12322	0.297	168.1
100	19.5	208.7	876.8	7602	12398	0.308	103.9
		260.9	914.1	7600	12400	0.306	129.1
		347.9	1171.8	7588	12412	0.293	164.4
90		208.7	868.9	7709	12291	0.314	106.8
		260.9	904.4	7707	12293	0.312	132.7
		347.9	1161.5	7695	12305	0.299	169.1
85		208.7	868.9	7764	12236	0.317	108.2
		260.9	902.3	7762	12238	0.315	134.5
		347.9	1141.4	7751	12249	0.303	172.1

TABLE XIV (Continued)
(b) Range = 300 Nautical Miles

AF	d-ft.	V_C-kt.	w_F-lb.	W_{UL}-lb.	W_E-lb.	W_{PL}/W_G	$W_{PL}V_C/W_E$
140	18.5	208.7	2242.3	7356	12644	0.228	75.3
		260.9	2382.8	7350	12650	0.220	91.1
		347.9	3086.6	7317	12683	0.184	100.9
130		208.7	2203.4	7443	12557	0.234	77.9
		260.9	2327.6	7437	12563	0.228	94.6
		347.9	3008.4	7406	12594	0.192	106.2
120		208.7	2176.3	7531	12469	0.240	80.4
		260.9	2297.7	7526	12474	0.233	97.8
		347.9	2973.9	7495	12505	0.198	110.4
120	19.0	208.7	2187.3	7438	12562	0.235	78.1
		260.9	2316.1	7432	12568	0.228	94.8
		347.9	3006.6	7401	12599	0.192	106.1
110		208.7	2157.4	7534	12466	0.241	80.8
		260.9	2274.7	7529	12471	0.235	98.4
		347.9	2973.9	7496	12504	0.198	110.5
100		208.7	2127.5	7633	12367	0.247	83.6
		260.9	2219.5	7629	12371	0.243	102.5
		347.9	2938.2	7596	12404	0.205	115.2
100	19.5	208.7	2134.9	7544	12456	0.2430	81.4
		260.9	2242.5	7539	12461	0.2373	99.3
		347.9	2980.8	7505	12495	0.1987	110.6
90		208.7	2096.9	7652	12348	0.250	84.6
		260.9	2198.8	7647	12353	0.244	106.4
		347.9	2893.9	7615	12385	0.208	120.9
85		208.7	2084.3	7707	12293	0.253	86.1
		260.9	2183.8	7703	12297	0.248	105.4
		347.9	2847.9	7672	12328	0.213	120.6

TABLE XIV (Continued)
(c) Range = 500 Nautical Miles

AF	d-ft.	V_C-kt.	w_F-lb.	W_{UL}-lb.	W_E-lb.	W_{PL}/W_G	$W_{PL}V_C/W$
140	18.5	208.7	3486.8	7299	12701	0.163	53.6
		260.9	3703.0	7982	12711	0.151	62.3
		347.9	4793.2	7238	12762	0.094	51.6
130		208.7	3394.8	7388	12612	0.172	56.9
		260.9	3569.6	7380	12620	0.163	67.4
		347.9	4669.0	7329	12671	0.105	57.9
120		208.7	3314.3	7479	12521	0.180	60.2
		260.9	3569.6	7467	12533	0.167	69.6
		347.9	4620.7	7419	12581	0.112	62.1
120	19.0	208.7	3403.8	7382	12618	0.171	56.7
		260.9	3599.5	7373	12627	0.161	66.6
		347.9	4671.3	7324	12676	0.105	57.7
110		208.7	3430.9	7475	12525	0.174	58.2
		260.9	3541.5	7470	12530	0.168	70.3
		347.9	4627.6	7420	12580	0.112	62.0
100		208.7	3302.8	7574	12426	0.180	60.5
		260.9	3449.8	7572	12428	0.178	75.0
		347.9	4363.1	7530	12470	0.130	73.0
100	19.5	208.7	3323.7	7489	12511	0.180	60.3
		260.9	3491.4	7481	12519	0.172	71.7
		347.9	4638.8	7428	12572	0.112	61.9
90		208.7	3254.5	7599	12401	0.189	63.8
		260.9	3443.6	7590	12410	0.179	75.6
		347.9	4494.2	7541	12459	0.124	69.7
85		208.7	3238.9	7654	12346	0.193	65.3
		260.9	3384.9	7647	12353	0.185	78.4
		347.9	4416.0	7600	12400	0.131	73.8

TABLE XV

DUCTED PROPELLER PROPULSION SYSTEM
PERFORMANCE AND WEIGHT DATA
W_G = 20,000 lb.
(a) Range = 100 Nautical Miles

AF	d-ft.	V_C-kt.	W_F-lb.	W_{UL}-lb.	W_E-lb.	W_{PL}/W_G	$W_{PL}V_C/W_E$
500	11.5	208.7	901.6	7661	12338	0.310	105.0
600		208.7	897.3	7564	12435	0.306	102.6
700		208.7	922.8	7472	12527	0.300	99.9
500	11.5	260.9	982.0	7658	12341	0.306	129.5
600		260.9	986.2	7560	12439	0.301	126.3
700		260.9	973.5	7469	12530	0.297	123.8
500	11.5	330.1	1168.0	7649	12350	0.297	158.5
600		330.1	1151.4	7553	12446	0.293	155.2
700		330.1	1159.7	7461	12538	0.288	151.4
400	12	208.7	946.1	7666	12333	0.308	104.0
600		208.7	882.5	7449	12551	0.301	100.0
500		208.7	910.1	7553	12446	0.305	102.2
400	12	260.9	937.6	7666	12333	0.310	130.7
600		260.9	1005.3	7443	12556	0.294	122.3
500		260.9	994.9	7549	12450	0.300	125.8
400	12	330.1	1103.5	7656	12340	0.300	158.2
600		330.1	1105.6	7438	12561	0.289	149.7
500		330.1	1100.4	7545	12454	0.295	153.9
400	12	363.2	1363.1	7647	12352	0.287	168.6
400	13	208.7	927.0	7491	12508	0.301	100.3
500		208.7	882.5	7361	12638	0.296	99.9
600		208.7	880.3	7239	12760	0.290	95.0

TABLE XV (Continued)

(a) Range = 100 Nautical Miles

AF	d-ft.	V_C-kt.	W_F-lb.	W_{UL}-lb.	W_E-lb.	W_{PL}/W_G	$W_{PL}V_C/W_E$
400	13	260.9	981.1	7488	12511	0.298	124.1
500		260.9	982.0	7356	12643	0.291	120.2
600		260.9	986.2	7234	12765	0.285	116.4
400	13	330.1	1130.6	7482	12518	0.290	153.0
500		330.1	1147.2	7348	12651	0.283	147.5
600		330.1	1157.6	7226	12773	0.276	142.6

(b) Range = 300 Nautical Miles

AF	d-ft.	V_C-kt.	W_F-lb.	W_{UL}-lb.	W_E-lb.	W_{PL}/W_G	$W_{PL}V_C/W_E$
500	11.5	208.7	2202.4	7601	12398	0.242	81.6
600		208.7	2194.9	7504	12495	0.238	79.5
700		208.7	2260.6	7410	12589	0.230	76.2
500	11.5	260.9	2427.5	7591	12408	0.231	97.0
600		260.9	2442.2	7493	12506	0.225	93.9
700		260.9	2447.7	7401	12598	0.220	91.2
500	11.5	330.1	2947.7	7567	12432	0.203	108.0
600		330.1	2898.6	7472	12527	0.201	106.0
700		330.1	2930.2	7279	12720	0.190	98.6
400	12	208.7	2258.7	6605	12394	0.240	80.7
600		208.7	2157.2	7390	12609	0.234	77.5
500		208.7	2240.0	7492	12507	0.235	78.4
400	12	260.9	2288.6	7604	12395	0.238	100.3
600		260.9	2500.9	7374	12625	0.216	89.3
500		260.9	2455.1	7482	12517	0.224	93.3
400	12	330.1	2748.1	7583	12416	0.214	112.2
600		330.1	2783.7	7361	12638	0.201	103.6
500		330.1	2758.8	7468	12531	0.208	107.9

TABLE XV (Continued)

(b) Range = 300 Nautical Miles

AF	d-ft.	V_C-kt.	w_F-lb.	W_{UL}-lb.	W_E-lb.	W_{PL}/W_G	$W_{PL}V_C/W_E$
400	13	208.7	2194.9	7421	12579	0.234	77.59
500		208.7	2187.4	7300	12699	0.228	75.0
600		208.7	2176.1	7179	12820	0.222	72.51
400	13	260.9	2464.2	7420	12579	0.220	91.3
500		260.9	2469.7	7287	12712	0.213	87.6
600		260.9	2482.6	7165	12834	0.207	84.0
400	13	330.1	2868.7	7401	12598	0.199	104.4
500		330.1	2912.6	7267	12732	0.190	98.6
600		330.1	2965.1	7142	12807	0.181	93.1

(c) Range = 500 Nautical Miles

AF	d-ft.	V_C-kt.	w_F-lb.	W_{UL}-lb.	W_E-lb.	W_{PL}/W_G	$W_{PL}V_C/W_E$
500	11.5	208.7	3425.5	7545	12454	0.178	59.8
600		208.7	3420.5	7448	12551	0.174	57.8
700		208.7	3524.9	7352	12647	0.164	54.0
500	11.5	260.9	3769.2	7529	12470	0.161	67.7
600		260.9	3801.3	7430	12569	0.154	63.9
700		260.9	3809.3	7338	12661	0.149	61.4
500	11.5	330.1	4563.1	7492	12507	0.119	62.8
600		330.1	4514.2	7398	12602	0.117	61.1
700		330.1	4573.4	7303	12696	0.109	56.7
400	12	208.7	3500.2	7548	12451	0.175	58.6
600		208.7	3367.0	7334	12665	0.171	56.3
500		208.7	3483.6	7435	12564	0.170	56.5
400	12	260.9	3557.9	7545	12452	0.172	72.0
600		260.9	3904.9	7309	12690	0.143	58.7
500		260.9	3817.3	7419	12580	0.153	63.3

TABLE XV (Continued)

(c) Range = 500 Nautical Miles

AF	d-ft.	V_C-kt.	w_F-lb.	W_{UL}-lb.	W_E-lb.	W_{PL}/W_G	$W_{PL}V_C/W_E$
400	12	330.1	4255.1	7513	12486	0.135	70.5
600		330.1	4331.8	7290	12710	0.120	61.6
500		330.1	4300.8	7397	12602	0.127	65.7
400	13	208.7	3425.5	7376	12623	0.170	56.2
500		208.7	3423.8	7243	12756	0.163	53.5
600		208.7	3408.8	7122	12877	0.158	51.2
400	13	260.9	3841.3	7356	12643	0.148	61.2
500		260.9	3849.3	7224	12775	0.141	57.7
600		260.9	3862.0	7101	12898	0.134	54.4
400	13	330.1	4481.3	7327	12672	0.115	59.8
500		330.1	4540.9	7192	12807	0.105	54.1
600		330.1	4600.0	7067	12932	0.096	48.9

TABLE XVI

TURBOFAN PROPULSION SYSTEM
PERFORMANCE AND WEIGHT DATA
W_G = 20,000 lb.
(a) Range = 100 Nautical Miles

Fan P_r	Bypass Ratio	V_C-kt.	W_F-lb.	W_{UL}-lb	W_E- lb.	W_{PL}/W_G	$W_{PL}V_e/W_E$
1.6	5.31	195.3	1743.0	7371	12628	0.254	78.5
1.6	3.31	195.3	1928.0	7714	12285	0.262	83.2
1.6	2.73	195.3	2041.3	7614	12385	0.251	79.2
1.4	6.78	195.3	1664.2	6897	13102	0.234	69.8
1.4	4.36	195.3	1879.7	7494	12505	0.253	79.0
1.4	3.59	195.3	1968.5	7681	12318	0.258	81.8
1.3	9.79	195.3	1544.8	6891	13109	0.240	71.4
1.3	6.43	195.3	1743.0	7204	12795	0.246	74.9
1.3	5.29	195.3	1879.7	7345	12654	0.246	75.8
1.6	5.31	292.1	1840.8	7367	12632	0.249	115.0
1.6	3.31	292.1	1879.7	7716	12283	0.264	125.7
1.6	2.73	292.1	1935.8	7619	12380	0.257	121.1
1.4	6.78	292.1	1756.9	6893	13106	0.229	102.2
1.4	4.36	292.1	1805.7	7497	12502	0.257	120.1
1.4	3.59	292.1	1762.7	7691	12308	0.269	127.8
1.3	9.79	292.1	1456.3	6895	13104	0.244	108.9
1.3	6.43	292.1	1664.2	7207	12792	0.250	114.0
1.3	5.29	292.1	1762.7	7350	12649	0.252	116.3
1.6	5.31	390.5	1899.0	7364	12635	0.246	151.9
1.6	3.31	390.5	1801.8	7719	12280	0.268	170.7
1.6	2.73	390.5	2071.8	7613	12386	0.250	157.3
1.4	6.78	390.5	1844.8	6889	13110	0.224	133.8
1.4	4.36	390.5	1930.0	7491	12508	0.251	156.4
1.4	3.59	390.5	1926.1	7683	12316	0.260	165.1
1.3	9.79	390.5	1683.9	6894	13105	0.230	138.8
1.3	6.43	390.5	1811.6	7201	12798	0.242	147.6
1.3	5.29	390.5	1895.2	7344	12655	0.242	151.1

TABLE XVI (Continued)

(a) Range = 100 Nautical Miles

Fan P_r	Bypass Ratio	V_C-kt.	w_F-lb.	W_{UL}-lb.	W_E-lb.	W_{PL}/W_G	$W_{PL}V_C/W_E$
1.6	5.31	585.8	2877.5	7319	12680	0.195	179.7
1.6	3.31	585.8	3017.6	7663	12336	0.205	194.4
1.6	2.73	585.8	3086.6	7566	12433	0.196	185.1
1.4	6.78	585.8	2789.2	6845	13154	0.175	156.2
1.4	4.36	585.8	2930.2	7445	12554	0.198	185.0
1.4	3.59	585.8	3017.6	7633	12366	0.203	192.5
1.3	9.79	585.8	2717.9	5674	14325	0.120	98.3
1.3	6.43	585.8	2965.1	7147	12852	0.182	165.5
1.3	5.29	585.8	2965.1	7295	12704	0.189	174.2

(b) Range = 300 Nautical Miles

Fan P_r	Bypass Ratio	V_C-kt.	w_F-lb.	W_{UL}-lb	W_E-lb.	W_{PL}/W_G	$W_{PL}V_C/W_E$
1.6	5.31	195.3	3753.1	7278	12721	0.149	45.6
1.6	3.31	195.3	4038.7	7616	12383	0.151	47.7
1.6	2.73	195.3	4224.5	7513	12486	0.137	42.8
1.4	6.78	195.3	3615.3	6807	13192	0.132	39.1
1.4	4.36	195.3	3912.8	7400	12599	0.147	45.5
1.4	3.59	195.3	4101.0	7583	12416	0.147	46.1
1.3	9.79	195.3	3442.1	6803	13196	0.141	41.6
1.3	6.43	195.3	3801.3	7109	12890	0.138	41.7
1.3	5.29	195.3	4023.1	7246	12753	0.134	40.9
1.6	5.31	292.1	4023.1	7266	12733	0.135	61.8
1.6	3.31	292.1	3897.0	7623	12376	0.159	74.9
1.6	2.73	292.1	3928.7	6537	12472	0.152	71.4
1.4	6.78	292.1	3912.9	6793	13206	0.116	51.5
1.4	4.36	292.1	3769.2	7406	12593	0.154	71.6
1.4	3.59	292.1	3541.4	7609	12390	0.176	83.1
1.3	9.79	292.1	3206.5	6794	13185	0.153	67.3
1.3	6.43	292.1	3507.9	7120	12879	0.151	68.3
1.3	5.29	292.1	3704.7	7261	12738	0.50	68.9

TABLE XVI (Continued)

(b) Range = 300 Nautical Miles

Fan P_r	Bypass Ratio	V_C-kt.	w_F-lb.	W_{UL}-lb.	W_E-lb.	W_{PL}/W_G	$W_{PL}V_C/W_E$
1.6	5.31	390.5	4161.4	7260	12739	0.127	78.1
1.6	3.31	390.5	4209.1	7608	12391	0.142	89.8
1.6	2.73	390.5	4300.8	7510	12489	0.133	83.1
1.4	6.78	390.5	4093.3	6785	13214	0.107	63.2
1.4	4.36	390.5	4116.5	7390	12609	0.136	84.3
1.4	3.59	390.5	3991.7	7588	12411	0.152	95.8
1.3	9.79	390.5	3833.3	6785	13214	0.120	70.9
1.3	6.43	390.5	3952.3	7102	12897	0.130	78.7
1.3	5.29	390.5	4054.3	7244	12755	0.132	80.8
1.6	5.31	585.8	7459.5	7107	12892	-0.045	-40.9
1.6	3.31	585.8	6802.9	7489	12510	0.007	6.3
1.6	2.73	585.8	6882.2	7391	12608	-0.002	-1.8
1.4	6.78	585.8	6548.1	6671	13328	-0.021	-18.7
1.4	4.36	585.8	6688.1	7272	12727	0.001	1.5
1.4	3.59	585.8	6757.1	7461	12539	0.007	7.1
1.3	9.79	585.8	6500.7	5499	14500	-0.078	-62.6
1.3	6.43	585.8	6904.8	6966	13033	-0.024	-26.4
1.3	5.29	585.8	6802.9	7118	12881	-0.012	-10.6

(c) Range = 500 Nautical Miles

Fan P_r	Bypass Ratio	V_C-kt.	w_F-lb.	W_{UL}-lb.	W_E-lb.	W_{PL}/W_G	$W_{PL}V_C/W_E$
1.6	5.31	195.3	5588.9	7194	12805	0.053	16.0
1.6	3.31	195.3	5936.4	7529	12470	0.052	16.3
1.6	2.73	195.3	6174.8	7423	12576	0.035	10.8
1.4	6.78	195.3	6088.3	6693	13306	0.003	0.8
1.4	4.36	195.3	5771.5	7314	12685	0.05	15.2
1.4	3.59	195.3	6013.3	7495	12504	0.047	14.5
1.3	9.79	195.3	5170.5	6723	13276	0.050	14.7
1.3	6.43	195.3	5654.6	7023	12976	0.041	12.3
1.3	5.29	195.3	5937.7	7158	12841	0.034	10.1

TABLE XVI (Continued)
(c) Range = 500 Nautical Miles

Fan P_r	Bypass Ratio	V_C-kt.	W_F-lb.	W_{UL}-lb.	W_E-lb.	W_{PL}/W_G	$W_{PL}V_C/W_E$
1.6	5.31	292.1	5962.9	7176	12823	0.033	15.3
1.6	3.31	292.1	5732.7	7538	12461	0.063	29.9
1.6	2.73	292.1	5758.6	7442	12557	0.057	26.8
1.4	6.78	292.1	5745.8	6708	13291	0.021	9.2
1.4	4.36	292.1	5562.5	7324	12675	0.061	28.4
1.4	3.59	292.1	5177.4	7533	12466	0.09	43.0
1.3	9.79	292.1	5273.6	6718	13281	0.045	20.0
1.3	6.43	292.1	5273.6	7041	12958	0.061	27.9
1.3	5.29	292.1	5456.1	7180	12819	0.059	27.2
1.6	5.31	390.5	6187.1	7166	12833	0.021	13.0
1.6	3.31	390.5	6211.6	7516	12483	0.038	23.6
1.6	2.73	390.5	6309.1	7417	12582	0.028	17.3
1.4	6.78	390.5	6088.3	6693	13306	0.003	1.5
1.4	4.36	390.5	6088.2	7299	12700	0.033	20.3
1.4	3.59	390.5	5861.4	7502	12497	0.055	34.0
1.3	9.79	390.5	5758.6	6696	13303	0.019	11.3
1.3	6.43	390.5	5874.1	7013	12986	0.029	17.7
1.3	5.29	390.5	6013.3	7154	12845	0.030	17.9

Unclassified

Security Classification

DOCUMENT CONTROL DATA - R & D

(Security classification of title, body of abstract and indexing annotation must be entered when the overall report is classified)

1. ORIGINATING ACTIVITY (Corporate author)
Dynasciences Corporation
Blue Bell, Pennsylvania

2a. REPORT SECURITY CLASSIFICATION
Unclassified

2b. GROUP

3. REPORT TITLE
COMPARATIVE PERFORMANCE STUDY OF PROPELLER, DUCTED PROPELLER, AND TURBOFAN PROPULSION SYSTEMS

4. DESCRIPTIVE NOTES (Type of report and inclusive dates)
Final Report

5. AUTHOR(S) (First name, middle initial, last name)
Douglas, D. S.
Mills, S.
Kisielowski, E.

6. REPORT DATE
June 1968

7a. TOTAL NO. OF PAGES
167

7b. NO. OF REFS
31

8a. CONTRACT OR GRANT NO.
DA 44-177-AMC-437(T)

b. PROJECT NO.
Task 1M121401D14415

c.

d.

9a. ORIGINATOR'S REPORT NUMBER(S)
USAAVLABS Technical Report 68-21

9b. OTHER REPORT NO(S) (Any other numbers that may be assigned this report)
Dynasciences Report No. DCR-248

10. DISTRIBUTION STATEMENT
This document has been approved for public release and sale; its distribution is unlimited.

11. SUPPLEMENTARY NOTES

12. SPONSORING MILITARY ACTIVITY
U.S. Army Aviation Materiel Laboratories, Fort Eustis, Virginia

13. ABSTRACT

Presented in this investigation are analytical methods for evaluating performance of open propellers, ducted propellers, and turbofans for the purpose of selecting the most suitable propulsion system for Army aircraft mission requirements. Techniques are presented for tradeoff analyses and optimization of the basic design parameters of each propulsion system. These techniques utilize specially developed nomographs, which can be effectively applied for preliminary design purposes. The nomographs and other numerical results presented in this report are based on the available performance data for the three propulsion systems.

DD FORM 1 NOV 68 1473 REPLACES DD FORM 1473, 1 JAN 64, WHICH IS OBSOLETE FOR ARMY USE.

Unclassified

Security Classification

14. KEY WORDS	LINK A		LINK B		LINK C	
	ROLE	WT	ROLE	WT	ROLE	WT
Propulsion System Propeller Ducted Propeller Turbofan Weight Trend						